ULTRA-STRONG, DOUBLE NETWORK HYDROGELS FOR IMPLANTABLE GLUCOSE BIOSENSORS AND SYNTHETIC CARTILAGE

A Dissertation

by

ANNA KRISTEN MEANS

Submitted to the Office of Graduate and Professional Studies of
Texas A&M University
in partial fulfillment of the requirements for the degree of

DOCTOR OF PHILOSOPHY

Chair of Committee,	Melissa A. Grunlan
Committee Members,	Daniel L. Alge
	Akhilesh K. Gaharwar
	Michael J. McShane
Head of Department,	Ibrahim Karaman

May 2019

Major Subject: Materials Science and Engineering

ABSTRACT

Hydrogels, crosslinked hydrophilic polymer networks, are widely used as biomaterials because of their similarity to soft biological tissues; however, their poor mechanical properties greatly limit their utility. This work focuses on enhancing the mechanical robustness of hydrogels without diminishing their numerous favorable characteristics such as hydration, biocompatibility, diffusivity and lubricity. Double network (DN) hydrogels, consisting of two independent and asymmetrically crosslinked polymer networks, have been previously shown to achieve notable mechanical properties such as ultra-high strength. Herein, by utilizing a DN hydrogel design and tailoring the composition of each network, mechanically robust hydrogel biomaterials have been developed towards two distinct applications: subcutaneous glucose biosensor membranes and synthetic cartilage.

Current transcutaneous continuous glucose monitors (CGMs) have limited lifetimes due to biofouling on the implant surface which leads to an increase in local metabolism of glucose and a reduction in glucose diffusion. To minimize this foreign body reaction, a thermoresponsive, DN hydrogel membrane was designed to enhance biocompatibility through the removal of adhered cells via cyclical deswelling/reswelling, induced by natural body temperature fluctuations. The first generation of the "self-cleaning" membrane consisted of two thermoresponsive poly(*N*-isopropylacrylamide) (PNIPAAm) networks with embedded polysiloxane nanoparticles for increased thermosensitivity. Although this membrane demonstrated excellent biocompatibility,

improved mechanical properties would enhance long-term durability. Therefore, the second generation self-cleaning membrane incorporated an anionic copolymer into the 1st network, enhancing both the swelling kinetics and the mechanical properties. These anionic DNs exhibited remarkable strength (~25x stronger than conventional hydrogels) as well as biocompatibility up to 90 days.

There is tremendous need for synthetic, off-the-shelf replacements for articular cartilage to avoid limitations of current chondral defect treatments such as donor site morbidity in autografting and mechanical mismatch in focal resurfacing. Towards a load-bearing application, the strength and stiffness of these PNIPAAm-based DNs were increased significantly without diminishing their hydration and lubricity. By tuning the polymer compositions and concentrations, hydrophobic and/or electrostatic secondary interactions were introduced between the polymer chains as sacrificial, reversible bonds. Ultimately, two ultra-strong DNs, thermoresponsive (PAMPS/P(NIPAAm-*co*-MEDSAH)) and non-thermoresponsive at body temperature (PAMPS/P(NIPAAm-*co*-AAm)), were developed with cartilage-mimetic properties, including strength, stiffness, hydration and lubricity, never before achieved in literature.

To Duong

Thank you for your unwavering support throughout my doctoral degree. You have the kindest heart, the calmest spirit and always encouraged me to follow my dreams, no matter how big. I am so grateful to have you by my side during this journey and could not imagine it any other way.

ACKNOWLEDGEMENTS

I would first like to thank my committee chair, Prof. Melissa Grunlan, for her guidance throughout the course of this research. Prof. Grunlan has been my most influential mentor since I joined her lab as an undergraduate student, and I would not be where I am today if it was not for her support. Her encouragement has inspired me to pursue a career in academia, a path I never imagined possible five years ago. I would also like to thank my committee members, Prof. Daniel Alge for his expertise in hydrogel biomaterials, Prof. Akhilesh Gaharwar for his assistance with graphics design and Prof. Michael McShane for his knowledge of biosensors and getting a product to market.

Thanks also go to my friends and colleagues and the department faculty and staff for making my time at Texas A&M University a great experience. The Grunlan lab has always felt like family, and I deeply appreciate the support of both alumni, Raymond Fei, Marc Rufin, Melissa Hawkins and Lindsay Woodard, as well as current students, Bryan Ngo, Ping Dong, Michaela Pfau, Mike Frassica, Felipe Beltran, Alec Marmo, Connor Demott and Dr. Jakkrit Suriboot. Additionally, I would like to thank each of the undergraduate students who assisted in conducting this work, including Alex Herrick, Ala Tobeh, Erica Gacasan, Daniel Ehrhardt, Lauren Whitney and Courtney Shrode.

Finally, thanks to my family for their encouragement along the way. Their positive words have given me the confidence to persevere. And a special thanks goes to Duong Mai for his inspiring creativity, patience and love that have kept me motivated and brought me so much joy over the years.

CONTRIBUTORS AND FUNDING SOURCES

Contributors

This work was supervised by a dissertation committee consisting of Professor Melissa Grunlan [advisor] of the Department of Materials Science and Engineering, Department of Biomedical Engineering and Department of Chemical Engineering and Professors Daniel Alge, Akhilesh Gaharwar and Michael McShane of the Department of Materials Science and Engineering and Department of Biomedical Engineering.

The data analyzed in Chapter II was conducted in part by Alex Abraham under the advisement of Professor Gerard Coté in the Department of Biomedical Engineering at Texas A&M University. Analyses in Chapters II and III were supported by Professor Fred Clubb, DVM, DACLAM in the Cardiovascular Pathology Laboratory (CVP) in the College of Veterinary Medicine & Biomedical Sciences at Texas A&M University. Data depicted in Figure 5-6d within Chapter V was facilitated by students Wei Dai and Yan Chen under the advisement of Professor Han Liang in the Department of Mechanical Engineering at Texas A&M University. Figures 1-1, 3-1 and 5-1 were graphically designed in part by Don Mai at DM Visual Studio.

All work for the dissertation was completed by the student, under the advisement of Professor Melissa Grunlan of the Department of Materials Science & Engineering.

Funding Sources

Graduate study was supported by the Doctoral Graduate Diversity Fellowship from Texas A&M University and the Graduate Research Fellowship Program (GRFP M1703014) from the National Science Foundation (NSF).

This work was made possible in part by National Institutes of Health (NIH) National Institute of Diabetes and Digestive and Kidney Diseases (NIDDK) under Grant Number 1R01DK095101-01A1, the NSF Engineering Research Center for Precise Advanced Technologies and Health Systems for Underserved Populations (PATHS-UP) under Award Number 1648451, the Robert J. Kleberg, Jr. and Helen C. Kleberg Foundation and the Texas A&M Engineering Experiment Station (TEES). Its contents are solely the responsibility of the authors and do not necessarily represent the official views of the institutions.

TABLE OF CONTENTS

Page

LIST OF FIGURES

Page

LIST OF TABLES

Page

CHAPTER I

INTRODUCTION

1.1 Overview

Hydrogels are frequently used biomaterials due to their similarity in hydration and structure to biological tissues. However, their utility is limited by poor mechanical properties, namely a lack of strength and stiffness that mimic that of tissues, particularly load bearing tissues. Thus, numerous recent strategies have sought to enhance and tune these properties in hydrogels, including interpenetrating networks (IPNs), macromolecular crosslinking, composites, thermal conditioning, polyampholytes and dual crosslinking. Individually, these approaches have achieved hydrogels with either high strength (σ_f > 10 MPa), high stiffness (E > 1 MPa) or, less commonly, both high strength and stiffness (σ_f > 10 MPa and E > 1 MPa). However, only certain unique combinations of these approaches have been able to synergistically achieve retention of a high, tissue-like water content as well as high strength and stiffness. Applying such methods to stimuli-responsive hydrogels have also produced robust, smart biomaterials. Overall, methods to achieve hydrogels that simultaneously mimic the hydration, strength and stiffness of soft and load bearing tissues have the potential to be used in a much broader range of biomedical applications.

1.2 Introduction

Although hydrogels have been extensively studied for decades, the enhancement of their mechanical properties to permit their use in broader applications, particularly biological tissue replacement, remains a challenge. Due to their high equilibrium water content (EWC) (up to > 90%), most hydrogels exhibit strengths and moduli on the order of kPa's,[1] similar to that of soft tissues such as vasculature,[2, 3] skin[4, 5] or muscle[6] (**Figure 1-1**). This tissue-like hydration of hydrogels promotes their biocompatibility and, thus, their frequent use as tissue-contacting biomaterials. Currently, hydrogels are utilized in a multitude of biomedical applications,[7] including drug delivery,[8, 9] wound dressings,[10, 11] soft contact lenses[12] and tissue engineering.[13, 14] However, replacement of load bearing tissues, such as cartilage, tendons and ligaments, requires hydrogels whose fracture strengths (σ_f) and moduli (E) are in the MPa range (**Figure 1-1**).[15-18] In addition, other existing biomaterials could benefit from an enhancement in mechanical properties of hydrogels, such as vascular grafts,[19, 20] artificial muscles,[21, 22] flexible electronics,[23, 24] soft machines[25] and implantable biosensors.[26, 27] For many biomedical devices, maintaining high hydration while withstanding daily mechanical stresses, as well as potentially high peak stresses experienced during implantation and/or accidental impact, is essential.

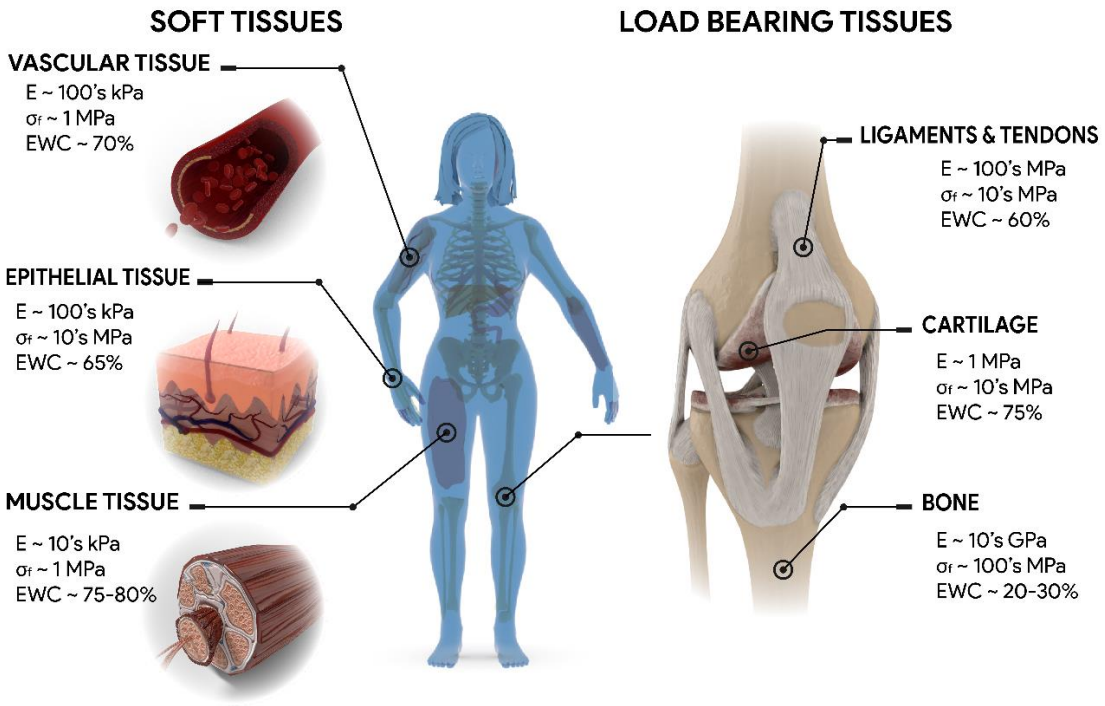

Figure 1-1. Summary of the modulus (E), fracture strength (σ_f) and equilibrium water content (EWC) values of biological tissues.[2-6, 15-18, 28-30]

Many factors can influence the mechanical properties of conventional hydrogels (i.e. single network (SN) hydrogels prepared with common crosslinkers and no fillers), including crosslink density, monomer concentration, homopolymer properties (e.g. hydrophilicity, electrostatic charge, backbone mobility, etc.) and copolymerization (**Figure 1-2**).[1] In general, hydrogel networks can be physically or covalently crosslinked, with the latter typically exhibiting superior mechanical robustness. The direct correlation between increasing crosslink density and/or monomer concentration to an increase in stiffness is well-established.[1] However, by creating a denser polymer network, the water content is inherently decreased. Alternatively, electrostatic charge has

been shown to enhance modulus through chain stiffening due to repulsive forces. Unlike the decrease in water content seen with increasing crosslink density or monomer concentration, the hydration of electrostatic hydrogels is increased with greater ionic content.[31, 32] However, the excessive chain stiffening will produce an extremely brittle polymer network due to the highly extended state of the polymer chains which lack the ability to undergo deformation before fracture.[32] Other inherent polymer properties, such as hydrophilicity and molecular mobility, can also influence the hydration and strength of hydrogels. Copolymerization can be utilized to combine desired attributes of more than one polymer to greatly broaden the properties of conventional hydrogels.[33-35]

More recently, several strategies have been reported to improve the mechanical properties of hydrogels, including the use of interpenetrating networks (IPNs),[31, 36-43] macromolecular crosslinking,[44-46] composites,[47-54] thermal conditioning,[55-59] polyampholytes[60-62] and dual crosslinking.[63-67] Hydrogels produced from these methods can generally be categorized by their mechanical properties into the following groups: "conventional hydrogels" (sub-MPa σ_f and E), "ultra-strong hydrogels" (σ_f > 10 MPa), "ultra-stiff hydrogels" (E > 1 MPa) and "ultra-strong & stiff hydrogels" (σ_f > 10 MPa and E > 1 MPa) (**Figure 1-2**). Although progress has been made towards enhancing hydrogel modulus and strength, it has proven difficult to concurrently maintain a high water content (> 70%) (**Figure 1-3**).[31, 45, 46, 59, 68-72] Most high stiffness hydrogels exhibit moderate (~60-70%) or, more commonly, low water contents (< 60%). However, combinations of the aforementioned strategies have been successful in producing ultra-

strong and stiff hydrogels with tissue-like hydration making them candidates for load bearing applications.[43, 73-75] Herein, modern strategies to individually as well as simultaneously tune hydrogel hydration and mechanical properties are discussed. Additionally, examples of highly robust, stimuli-responsive hydrogels are highlighted to demonstrate the utility of these strategies to produce robust, smart biomaterials that can further broaden the use of hydrogels in biomedical applications.

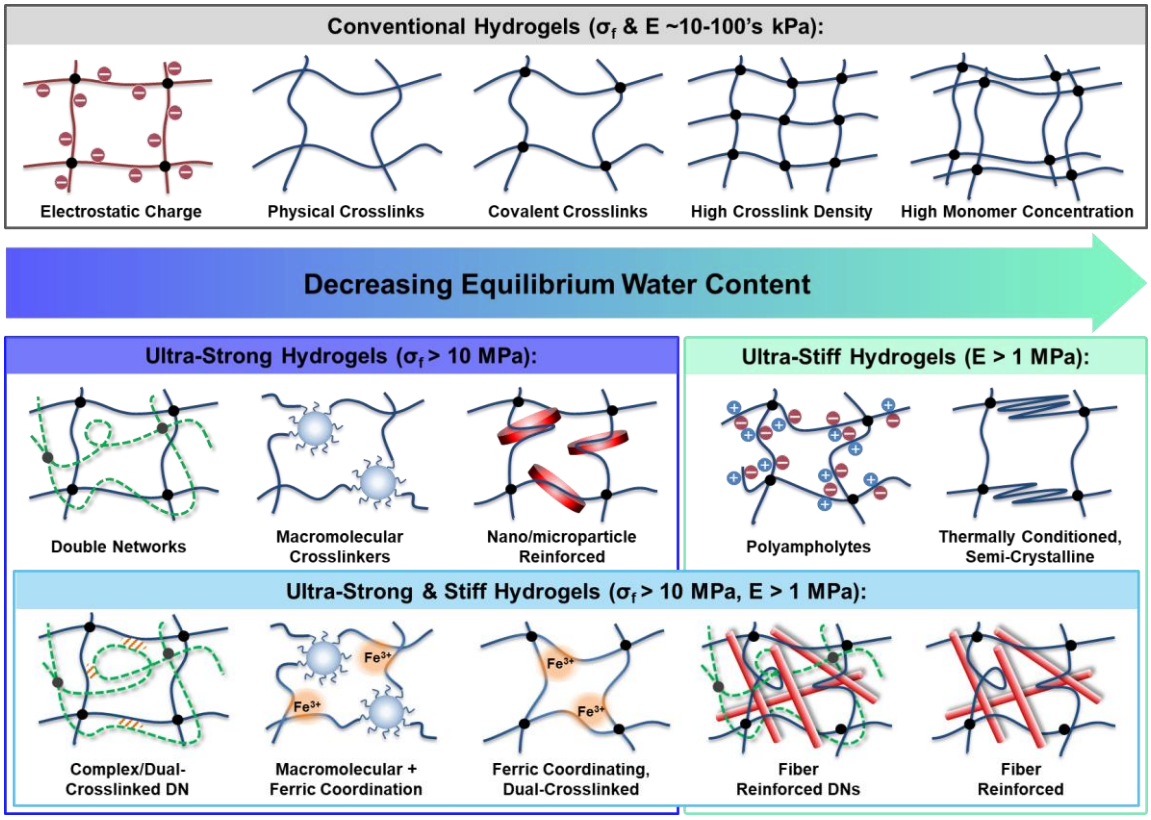

Figure 1-2. Strategies to enhance mechanical properties of hydrogels categorized by fracture strength (σ_f) and modulus (E) [denoted in boxes] and by decreasing equilibrium water content (EWC) [from left to right].

1.3 Ultra-Strong Hydrogels

1.3.1 DN Hydrogels

One of the most studied methods to enhance hydrogel mechanical properties is the use of IPN designs. IPNs can be formed as either a non-crosslinked (i.e. thermoplastic) polymer cured within a crosslinked network (i.e. semi-IPNs) or as two interwoven, independently crosslinked networks (i.e. double networks, DNs). DN hydrogels were first reported by Gong *et al.* in which a tightly crosslinked, anionic network of poly(2-acrylamido-2-methylpropanesulfonic acid) (PAMPS) was combined with a loosely crosslinked, neutral network of poly(acrylamide) (PAAm).[31] This hydrogel and a variety of other DN hydrogels can withstand high strains (> 98%) and reach remarkable fracture strengths (~10's MPa, **Figure 1-2**) while maintaining high water contents (> 80%).[31, 39, 69, 70, 76-78] However, their moduli are typically only in the 100's kPa range, similar to that of soft tissues (**Figure 1-1**). DN hydrogels are most commonly fabricated sequentially in which a SN hydrogel is soaked in a 2nd precursor solution then cured to form the 2nd polymer network within the pre-existing 1st network.[37] Alternatively, two independent networks can be formed simultaneously if non-competing crosslinking chemistries are used.[78] For sequential DNs, the main contributing factors to their notable mechanical properties include the ratio of monomer concentration of the 1st to 2nd network, crosslink density of each network and ionic charge.[37] For instance, it has been shown that the strength of PAMPS/PAAm DN hydrogels increases when the molar ratio of the 2nd network to the 1st network increases.[31] Additionally, the crosslinking density of the 1st network is typically greater than the 2nd network to impart

an asymmetric structure of extended and coiled polymer chains. Finally, the incorporation of a polyelectrolyte produces charge-charge repulsion and exaggerates the chain extension resulting in chain stiffening. Thus, the tightly crosslinked 1st network is commonly charged while the loosely crosslinked 2nd network is neutral to remain relaxed and mobile.[37] Ultimately, the asymmetric crosslinking structure of DN hydrogels permits stress dissipation through the fracture of the brittle 1st network while the ductile 2nd network remains intact.[79] The effects of additional independent networks have been evaluated as well from triple networks (TNs) to up to five individual networks.[80] However, the benefits in mechanical properties achieved with more than two interpenetrating networks are typically due to the associated decrease in water content as overall polymer concentration increases. In general, versus conventional hydrogels, IPNs exhibit greatly improved fracture strength without diminishing their tissue-like water content, but their moduli remains limited to the sub-MPa range.

1.3.2 Macromolecular Crosslinked Hydrogels

Macromolecular crosslinking also utilizes the regulation of polymer network structure to enhance hydrogel mechanical properties.[44] Most conventional, synthetic hydrogels use low molecular weight, difunctional crosslinkers or difunctional pre-polymers (i.e. macromers) to form a covalently crosslinked network with many inhomogeneities, such as kinks and loops, within a ladder type architecture. However, by using alternative macromolecular crosslinkers, network architectures with greater homogeneities can be achieved to improve their strength. A wide range of macromolecular crosslinkers have been developed, including complex pre-polymers,[81] micelles,[82]

polymer microspheres[46] and microgels.[83] By forming defined pre-polymers before crosslinking, the distance between crosslinks and the number of branches stemming from each crosslinking point can be highly controlled. Multi-arm, star-shaped pre-polymers are predominantly used to enhance homogeneity via their highly symmetrical structure. Larger macromolecular crosslinkers, such as self-assembled micelles, polymer microspheres and microgels, are less restrictive compared to typically rigid and brittle chemical crosslinks. While the use of macromolecular crosslinkers provides a means of stress dissipation and enhances the strength of resulting hydrogels (~10's MPa) while retaining high water contents (> 70%) (**Figure 1-2**), their moduli are generally lower than most DN hydrogels (~10's kPa).[46, 82, 83]

1.3.3 Nanocomposite Hydrogels

Rather than altering network architecture and/or composition, a nanocomposite approach may be utilized in which inorganic fillers are used to reinforce the hydrogel matrix. Some of the most commonly used fillers range from nano- to microscale for clays,[47, 84, 85] silicates[86-88] and carbon nanotubes.[54, 68] Many key factors determine their effects on the hydrogel properties, including size, charge, hydrophobicity and surface functionality. These nanofillers typically serve as macro-crosslinkers through either covalent bonding or physical adsorption of polymer chains. Similar to organic macromolecular crosslinkers, nanocomposite hydrogels exhibit improved structural homogeneity and high fracture strengths (> 10 MPa) without diminishing high water contents (> 70%) (**Figure 1-2**).[54, 68, 85, 88] Additionally, the reversible adsorption/desorption of polymer chains during deformation allows for stress dissipation

without permanently damaging the hydrogel network, greatly enhancing their fatigue resistance.[86] In instances when fillers were incorporated within DN hydrogels,[68, 85] exceptional compressive strengths (> 50 MPa) were achieved. However, little enhancement in modulus was observed and thus, remained low (~100's kPa).

1.4 Ultra-Stiff Hydrogels

1.4.1 Thermally Conditioned Hydrogels

Although a number of hydrogels have achieved significant strengths, their low moduli limit their use in many load bearing tissues (**Figure 1-1**). In attempts to increase stiffness in hydrogels, methods have been developed to incorporate crystalline domains within hydrogel networks. Those involving rigid, hydrophobic polymers typically require the use of surfactants[89] or organic solvents[58] to reduce phase separation, making them less desirable for most biomedical applications due to the concern of cytotoxicity. Furthermore, the hydrophobicity of the crystalline domains decreases hydrogel water content to as low as 50%.[58] Alternatively, some hydrophilic polymers (e.g. poly(vinyl alcohol), PVA) can form crystallites through thermal conditioning methods (e.g. dry-annealing[56, 90] and freeze-thawing[55, 59]) that serve as physical crosslinks. Although dry-annealing can produce hydrogels with moduli in the MPa range, their water contents are greatly diminished (~40-60%).[56, 90] On the other hand, freeze-thawing can maintain hydration levels similar to cartilage and tendon/ligament tissues (60-80%) while exhibiting high moduli (> 1 MPa) (**Figure 1-2**) and moderate fracture strengths (~1-2 MPa).[55, 59, 91] Additionally, the degree of crystallite formation can be highly controlled by the freezing temperature and rate, number of cycles and direction of

freezing,[55] allowing for high tunability of their mechanical and hydration properties. Thus, freeze-thawed PVA hydrogels have been utilized in low impact connective tissues. For example, Cartiva® is a PVA hydrogel that is an FDA approved cartilage replacement for the first metatarsophalangeal joint. These implants have notable moduli ~1 MPa; however, their compressive fracture strength is relatively low (~2 MPa), limiting them to non-loading bearing joints.[59] In general, the incorporation of crystalline domains into hydrogels has the ability to enhance their stiffness, but water content or strength are diminished in return.

1.4.2 Polyampholytes and Polyion Complexes (PICs)

Polyampholytes, polymers with both anionic and cationic charges, have the potential to impart stiffness in hydrogels due to intra- and inter-chain electrostatic interactions that produce ionic complexes that serve as crosslinking points.[62, 92] Likewise, two oppositely charged polymers, one anionic and one cationic, can form polyion complexes (PICs).[60, 61] Despite being physically crosslinked hydrogels, polyampholyte and PIC hydrogels simultaneously exhibit high moduli (up to ~8 MPa) and moderately high strengths (up to ~5 MPa) (**Figure 1-2**).[60-62] It has been shown that strong ionic complexing can serve as pseudo-permanent crosslinks at most strains, whereas weaker ionic interactions serve as reversible sacrificial bonds allowing for stress dissipation.[61] However, the excellent mechanical properties of these types of hydrogels are primarily associated with their low water contents (~40 to ~60%).[60-62] In summary, similar to thermally conditioned hydrogels, polyampholyte and PIC hydrogels have

demonstrated remarkably high moduli, but lack the proper hydration and/or high strength to serve as load bearing tissue replacements.

1.5 Ultra-Strong & Stiff Hydrogels

1.5.1 Dual-Crosslinked Hydrogels

To obtain hydrogels with both high strength and stiffness, the combination of multiple crosslinking types appears key. Particularly effective are dual-crosslinked hydrogels that utilize permanent covalent crosslinks combined with reversible physical crosslinks which act as sacrificial bonds to dissipate stress. These reversible crosslinks can be formed through a variety of physical interactions such as hydrogen bonding,[57, 65] hydrophobic interactions,[58, 89] host-guest interactions[67] and ionic interactions.[33, 63, 64, 66] During deformation, these sacrificial physical bonds provide the rigidity of a highly crosslinked network under low strains without imparting the brittleness typically seen at high strains due to their ability to break and reform repeatedly.[93] This unique character has produced hydrogels with both high strength and high stiffness as well as good self-healing.[63, 66, 89] However, these mechanical properties are directly related to their low water contents (~40-60%) stemming from their high apparent crosslink densities and/or increased hydrophobicity.[57, 58, 63-66, 89] One of the most predominant dual-crosslinking mechanisms used in recent literature utilizes ferric coordination with a covalently crosslinked, ionic polymer network to form secondary, non-covalent crosslinks. Lin *et al.* has pioneered the use of Fe^{3+} coordination with a covalently crosslinked poly(acrylic acid) (PAAc) network through which mechanically robust hydrogels with excellent strengths (~10's MPa) and moduli (~10's MPa) (**Figure**

1-2); however, these exhibit low water contents (<~60%).[63, 64] Despite lacking proper hydration, this dual-crosslinking strategy is one of the most promising approaches to enhancing hydrogel mechanical properties towards load bearing biomaterials, such as cartilage, ligaments and tendons.

1.5.2 Fiber Reinforced Hydrogels

Another method to enhance both the strength and modulus of hydrogels involves their reinforcement with rigid, non-hydrated fibers. Typically, these fibers are highly organized through electrospinning,[94, 95] 3D printing[53, 96, 97] or standard weaving techniques (e.g. gauze and fabrics)[50, 98] to enhance their durability. Others have utilized naturally occurring fibers such as silk[51] and nanocellulose[99] which are evenly dispersed in the hydrogel precursor solution before curing. Many studies have demonstrated an increase in hydrogel stiffness with the incorporation of fibers; however, most exhibit low fracture strengths (<~2 MPa) due to the poor hydrogel-fiber interactions.[51, 94, 96, 97] Recently, advancements have been made in fiber-reinforced hydrogels through their combination with additional strengthening methods, including DNs,[100, 101] thermal conditioning[99] and polyampholyte interactions.[50] For example, Yang *et al.* produced cellulose nanofiber/PVA composite hydrogels with a high modulus (~50 MPa) and high fracture strength (~16 MPa) through the formation of strong hydrogen bonds between the cellulose nanofibers and PVA during dry-annealing.[99] Still, while similar to epithelial tissue (~65%), the hydration of these hydrogels was not particularly high. Arguably the strongest and stiffest fiber-reinforced hydrogels have been developed by King *et al.*, in which polyampholyte hydrogels were formed around woven

glass fibers.[50] Inter- and intra-chain ionic bonding interactions force the polyampholyte hydrogel to deswell onto the glass fibers, producing an exceptional modulus (~600 MPa) and high fracture strength (~17 MPa). Yet, this deswelling produces hydrogels with low water contents (~50%). In addition, fiber-reinforced hydrogels show extremely high tear resistance and the ability to exhibit anisotropic properties, making them highly desirable for many biological applications. Such hydrogels could serve as synthetic tendons and ligaments (strength ~10's MPa, moduli ~100's MPa, water contents ~60%) (**Figure 1-1**).

1.5.3 Complex/Dual-Crosslinked DNs & Other Hydrogels Formed with Combined Strategies

Several combinations of strategies have been successfully used to form a wide range of complex hydrogels with exceptional mechanical properties. For example, two physically crosslinked hydrogels, through the use of reversible crosslinking mechanisms, have attained strength and moduli in MPa range. Li *et al.* applied thermal conditioning to a dual-crosslinked network to form a physical PVA/hyaluronic acid-Fe^{3+} DN hydrogel.[56] Zhang *et al.* reported DNs that employed hydrogen bonding and hydrophobic interactions as secondary, reversible interactions to attain a physically crosslinked DN hydrogel from an amphiphilic triblock copolymer and linear PAAm.[102] Although both hydrogel systems exhibited impressive moduli (~1's MPa) and strengths (~10 MPa), their water content values remained relatively low (~45%).[56, 102] Additional studies have paired ferric coordination with macromolecular crosslinking[45, 103] or DN[72, 104] structures to achieve strong, rigid hydrogels (σ_f > 10 MPa and E > 1 MPa) (**Figure 1-2**) with slightly higher water contents (~50-65%) on average versus

purely dual-crosslinked hydrogels (~40-60%). While these complex/dual-crosslinked hydrogels exhibit mechanical properties on the same order as connective tissues, their water contents typically remain < 70%.

1.5.4 Maintaining Hydration in Strong and Stiff Hydrogels

Hydrogels with high water contents (> 70%) that also possess the high strength (> ~10 MPa) and high rigidity (> ~1 MPa) of load bearing tissues are challenging to produce due to the inverse relationship of these properties. However, a few hydrogel systems have achieved this through unique combinations of strategies (**Figure 1-3**). Huang *et al.* reported a chemically crosslinked P(AAm-*co*-AAc) hydrogel with embedded cellulose nanofibers wherein the nanofibers formed ionic complexes with AAc blocks through ferric coordination. With a minimal fiber content (~0.6%), these hydrogels exhibited a high tensile strength (~10 MPa) and high modulus (~3 MPa) as well as retained a high water content, near that of cartilage (~70-80%).[73] While interactions between stiff fibers and soft, hydrated networks are typically poor, this Fe^{3+} dual-crosslinking strategy was able to overcome this challenge. Other hydrogels that have achieved high strength, rigidity and hydration have all been based on DNs that incorporated secondary reversible interactions to serve as sacrificial bonds that increased apparent crosslinking density at low strains but provided stress dissipation at high strains. For instance, Argun *et al.* reported a non-ionic TN hydrogel composed of a chemically crosslinked poly(*N*,*N*-dimethylacrylamide) (PDMA) 1^{st} network and linear, non-crosslinked PDMA 2^{nd} and 3^{rd} networks. These high water content hydrogels (~90%) exhibited both high fracture strengths (~20 MPa) and high moduli (~2 MPa). Their exceptional mechanical properties were attributed to the

hydrophobic interactions between sequential network components allowing for a high molar ratio of the 2nd & 3rd networks to the 1st network.[43] Similarly, work in our group has combined the commonly used anionic PAMPS 1st network with a PNIPAAm 2nd network to impart hydrophobic interactions between the latter's isopropyl groups to enhance their modulus.[74] This stiffening phenomenon has been demonstrated previously in AAm-based semi-IPN hydrogels, in which physical interactions between the PNIPAAm chains were shown to increase the apparent crosslink density and thus, stiffness at all temperature ranges (i.e. above and below the volume phase transition temperature, VPTT).[105] In addition to utilizing hydrophobic secondary interactions, a zwitterionic comonomer, [2-(methacryloyloxy)ethyl] dimethyl-(3-sulfopropyl) ammonium hydroxide (MEDSAH), was introduced to the PNIPAAm 2nd network at low concentrations to induce inter- and intra-network ionic interactions with itself and the PAMPS 1st network. By linking the two networks with sacrificial, reversible bonds, the modulus (~1.5 MPa) and compressive fracture strength (~23 MPa) were increased without diminishing water content (~83%).[74] Alternatively, by tailoring the amount of hydrophobic interactions through the addition of a hydrophilic, neutral comonomer, AAm, to the PNIPAAm 2nd network, a slight decrease in modulus (~1.1 MPa) afforded for an increase in strength (~26 MPa) while maintaining similar water content (~84%).[75] These studies demonstrated the ability of complex structured hydrogels to achieve robust mechanical properties with excellent hydration as well as ways to tailor their properties by regulating the amount of secondary bonding present. Thus, these complex crosslinking strategies permit the use of

hydrogels in load bearing tissue applications that require high water contents, stiffness and strength simultaneously.

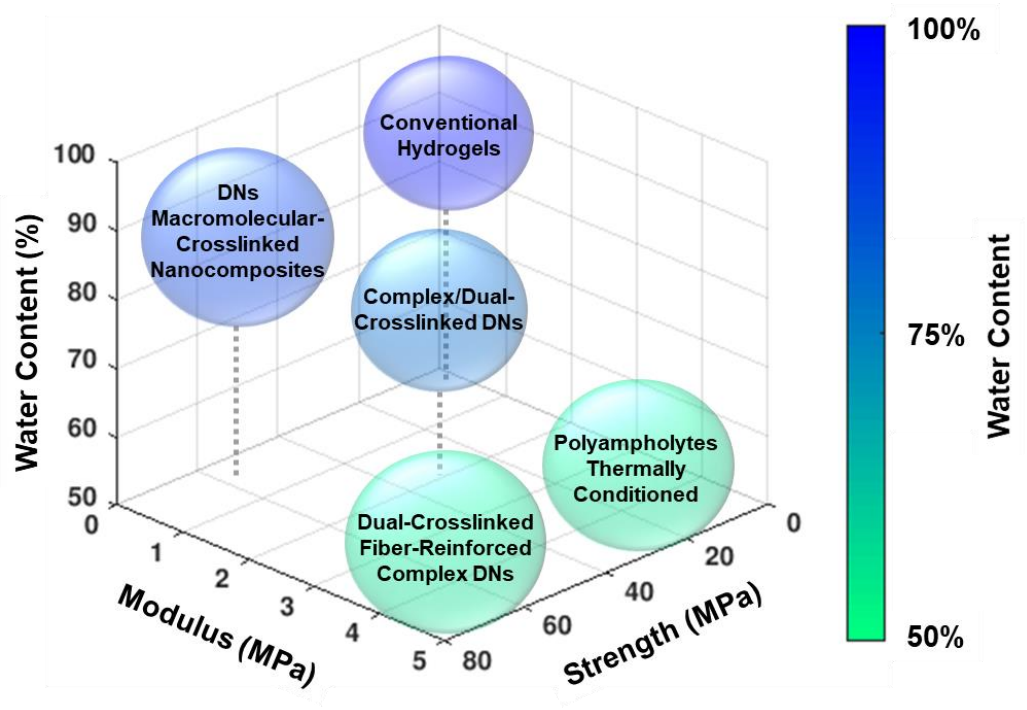

Figure 1-3. A visual comparison of the fracture strength (σ_f), modulus (E) and equilibrium water content (EWC) of hydrogels produced with different strategies, demonstrating the rarity of enhancing all three simultaneously.

1.6 Incorporating Stimuli-Responsiveness

1.6.1 Stimuli-Responsive, Robust Hydrogels

These modern strategies to obtain mechanically robust hydrogels have been applied to stimuli-responsive materials to permit their use in a variety of biomedical applications, such as artificial muscles,[21, 106] soft robotics,[107, 108] drug delivery[109, 110] and regulation of cell adhesion/detachment.[27, 111] A range of robust, smart hydrogels have been reported, including thermoresponsive,[74, 112-114] pH-

responsive,[83, 115-117] photo-responsive[111, 118] and others[106, 110] (**Figure 1-4**). Nanocomposite reinforcement and macromolecular crosslinking are frequently utilized in stimuli-responsive hydrogels due to their exceptional swelling kinetics. Their rapid swelling rates are attributed to their less restrictive crosslinking mechanisms versus more rigid, chemical crosslinks, allowing the network chains to behave similar to that of linear polymers.[84, 113-115, 119, 120] Other complex crosslinked hydrogels including polyampholytes,[83, 121] DNs[74, 76, 117, 119] and dual-crosslinked[107, 111, 112, 116, 118] hydrogels have been developed as robust, stimuli-responsive membranes. In our group, various thermoresponsive, DN hydrogels have been designed with polysiloxane nanoparticles to enhance swelling kinetics[120] and polyampholyte copolymers to enhance mechanical properties without diminishing thermosensitivity[74]. Thus, by combining unique strengthening approaches to stimuli-responsive hydrogels, these smart, tissue-mimetic materials could be used in a broad range of load bearing applications that require a response to their external environment.

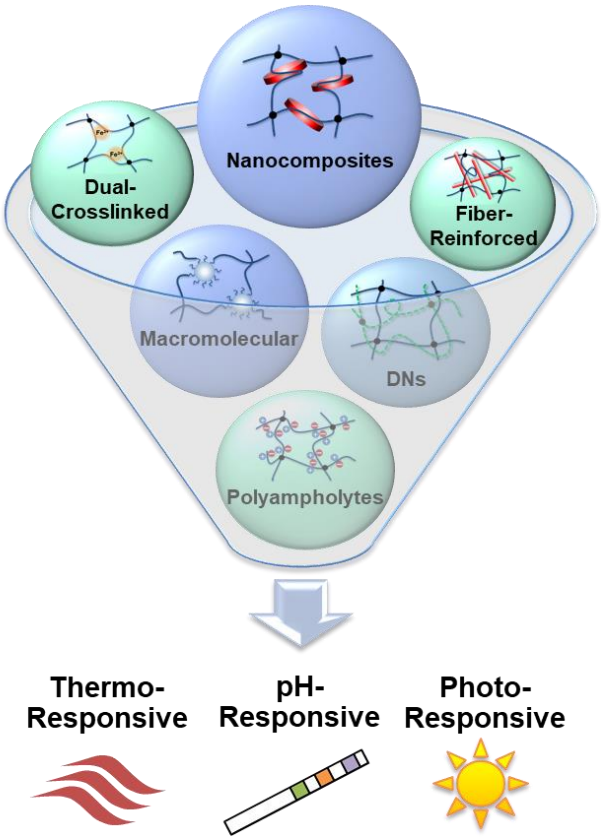

Figure 1-4. Robust, stimuli-responsive hydrogels can be developed through the application of modern strategies to enhance the mechanical properties on conventional stimuli-responsive hydrogels.

1.7 Conclusions

In summary, the development of numerous complex crosslinking structures has progressed hydrogel biomaterials towards mimicking both the mechanics and hydration of tissues. Compared to conventional hydrogels with sub-MPa moduli and strengths, these membranes have achieved ultra-high strength (σ_f > 10 MPa), high stiffness (E > 1 MPa) and even ultra-high strength and stiffness together (σ_f > 10 MPa and E > 1 MPa) in some; although, many suffer from a reduction in water content. In general, most DN,

macromolecular crosslinked and nanocomposite hydrogels are able to withstand high strains and reach ultra-high fracture strengths while maintaining > 70% water content, but exhibit sub-MPa moduli. On the other hand, thermally conditioned and polyampholyte hydrogels have shown high stiffness, but typically suffer from moderately-low fracture strengths and poor hydration. Dual-crosslinked and fiber-reinforced hydrogels have been able to simultaneously achieve high fracture strengths and moduli, but are limited to ~40-60% water content. Thus far, few hydrogels have been able to retain tissue-mimetic hydration while enhancing both their stiffness and strength. By using a combination of synergistic strategies, such as dual-crosslinking incorporated into a DN structure, exceptional strengths, moduli and water contents can be attained concurrently in a single hydrogel. Finally, these crosslinking structures can be applied to stimuli-responsive hydrogels (i.e. thermoresponsive, pH-responsive, photo-responsive and others) to produce smart hydrogels with exceptional mechanical properties. By employing these complex crosslinking strategies to match the hydration and mechanics of tissues, the utility of hydrogels can be greatly expanded, even to load bearing regions of the body.

CHAPTER II

FOREIGN BODY REACTION TO A SUBCUTANEOUSLY IMPLANTED SELF-CLEANING, THERMORESPONSIVE HYDROGEL MEMBRANE FOR GLUCOSE BIOSENSORS*

2.1 Overview

Towards achieveing a subcutaneously implanted glucose biosensor with long-term functionality, a thermoresponsive membrane previously shown to have potential to house a glucose sensing assay was evaluated herein for its ability to minimize the foriegn body reaction (FBR) and the resulting fibrous capsule. The severity of the FBR proportionally reduces diffusion of glucose to the sensor and hence sensor lifetime. However, efforts to reduce the FBR have largedly focused on anti-fouling materials that passively inhibit cellular attachment, particularly poly(ethylene glycol) (PEG). Herein, the extent of the FBR of a subcutaneously implanted "self-cleaning" cylindrical membrane was analyzed in rodents. This membrane represents an "actively anti-fouling" approach to reduce cellular adhesion. It is a thermoresponsive double network nanocomposite hydrogel (DNNC) comprised of poly(*N*-isopropylacrylamide) (PNIPAAm) and embedded polysiloxane nanoparticles. The membrane's cyclical deswelling/reswelling response to

*Reprinted with permission from "Foreign body reaction to a subcutaneously implanted self-cleaning, thermoresponsive hydrogel membrane for glucose biosensors" by Abraham, A.A.[†]; Means, A.K. [†]; Clubb, F.J.; Fei, R.; Locke, A.K.; Gacasan, E.G.; Coté, G.L. and Grunlan, M.A., *ACS Biomat. Sci. Eng.*, 2018, 4, 4104-4111. ([†]Contributed equally) Copyright [2018] American Chemical Society.

local body temperature fluctuations was anticipated to limit cellular accumulation. Indeed, after 30 days, the self-cleaning membrane exhibited a notably thin fibrous capsule (~30 μm) and increased microvascular density within 1 mm of the implant surface in comparison to a non-thermoresponsive, benchmark biocompatible control (PEG diacrylate, PEG-DA).

2.2 Introduction

Thermoresponsive poly(*N*-isopropylacrylamide) (PNIPAAm) hydrogels undergo cyclical deswelling and reswelling at temperatures above and below, respectively, their volume phase transition temperature (VPTT).[122-127] This dynamic nature of PNIPAAm has been utilized in various biomedical applications such as drug delivery[8, 128] and cell sheet engineering[127, 129]. We hypothesized that this mechanism could be used by membranes surrounding subcutaneously implanted glucose biosensors to control biofouling, a leading cause of device failure. Specifically, such a thermoresponsive membrane could house a liquid glucose sensing assay[130] as an electronics-free, subcutanteously implantable glucose biosensor that could be accompanied with a wearable, optical detection method. Previously, we reported a glucose biosensor membrane candidate, a thermoresponsive double network nanocomposite (DNNC) hydrogel composed of an interpenetrating, asymmetrically cross-linked PNIPAAm matrix with polysiloxane nanoparticles (~200 nm diameter) embedded during the formation of the 1st network.[120] Cyclical deswelling/reswelling with heating/cooling around its VPTT was shown to effectively cause the detachment of cultured cells. Furthermore, this membrane did not limit glucose diffusion (D ~2.7x10^{-6} cm^{2}s^{-1})[131] and also provided

robust mechanical strength (strength ~0.4 MPa)[120] versus conventional hydrogels (~1-100s kPa)[31] necessary for long-term durability. Moreover, its modulus (E ~0.2 MPa)[120] remained similar to that of the native subcutaneous and dermis tissues (E ~0.01-0.25 MPa)[4, 132, 133], avoiding adverse shear stresses often experienced by tissues surrounding current metallic, transdermal CGM electrodes.[134] However, the ability of this thermoresponsive DNNC membrane to limit the foreign body reaction (FBR) has yet to be established and represents a primary challenge in the development of subcutaneously implanted glucose and other biosensors that possess lifetimes of months rather than only days. For an implanted biosensor to remain functional long-term, sufficient diffusion of the analyte (e.g. glucose) to the sensor must be maintained throughout the initial (acute) host response, FBR and healing processes that are triggered by implantation. The FBR particularly leads to the formation of a dense, avascular fibrous capsule comprised of fibroblasts, fibrocytes and collagenous tissue.[135] Depending on the extent of the FBR, this compact fibrous capsule may vary from 30 to >200 μm in thickness and may lack nearby vascularization, thereby limiting analyte diffusion.[136-139] Moreover, the FBR and resulting fibrous capsule, once formed, remain present for the lifespan of the implanted device.[135] Therefore, to ensure analyte diffusion to the biosensor, measures must be taken to minimize the FBR as well as to encourage healing so as to reduce the formation of this dense tissue barrier and increase nearby microvascularization.

After the subcutaneous implantation of a membrane-coated glucose biosensor or other device, a series of sequential, innate host responses occur, including: injury, humeral

interactions (proteins, complements, kinins, etc.), acute inflammatory response, chronic inflammatory response, FBR, granulation tissue formation (admixture of lymphocytes, macrophages, fibroblast and neovascular buds) and fibrous capsule formation.[140] Acute inflammation, chronic inflammation and FBR are often investigated in tandem as these stages are closely related and provide insight into the host response to a biomaterial.[140] The acute inflammatory response is primarily impacted by local damage to the surrounding tissue where a greater implantation trauma will result in a more amplified acute response.[135] Therefore, minimizing injury during implantation is essential. In the case of subcutaneous biosensors, this can be accomplished with injection, but does limit the implant's geometry and size. Additionally, the chemical and physical properties of the implant can potentially lead to chronic inflammation and a heightened FBR. In order to minimize the FBR, numerous groups have concentrated on "passively anti-fouling" polymeric materials that reduce protein and cellular adhesion, including: poly(tetrafluoro-ethylene) (PTFE),[136, 141-143] poly(vinyl alcohol) (PVA)[142, 143] and poly(ethylene glycol) diacrylate (PEG-DA).[144-146] However, *in vivo* investigations with each of these materials have shown the presence of a fibrous capsule surrounding the implant of up to >100 μm,[136, 141, 143] with PEG-DA exhibiting the thinnest capsule, ~30 μm.[146] Currently, most commercialized transcutaneous continuous glucose monitoring (CGM) sensors (i.e. Dexcom Seven®, Guardian™) use stiff metal electrodes, such as platinum,[147] which have limited lifetimes of days due to the host response.[148] To enhance biocompatibility and lifetime, many transcutaneous electrodes and optical fibers have been coated with non-fouling polymers including Nafion,[149-151]

polyurethanes[152, 153] and PEG-DA.[145, 154, 155] Although transcutaneous CGMs have improved significantly over recent years, the lifetime of these devices remain limited to < ~2 weeks.[148, 156-158]

In contrast to these passively anti-fouling approaches, the thermoresponsive DNNC hydrogel membrane described herein relies on an "actively anti-fouling" or "self-cleaning" approach to physically detach adsorbed cells from its surface and also to limit initial cellular attachment strength and stability.[120, 122, 123, 131] Having previously confirmed glucose diffusion, mechanical properties, swelling kinetics and cytocompatibility,[120, 131] the DNNC membrane's thermally-driven self-cleaning behavior was then demonstrated *in vitro* by the reduction of cellular adhesion and successful cell-release when thermally cycled with an external heating system.[131] In this work, a rodent animal model was utilized to evaluate the extent of the FBR elicited by this self-cleaning membrane in a biological enviroment. Time points of seven and 30 days were utilized as these represent early- and mid-stages of healing. Here, we relied on local body temperature fluctuations around the membrane to drive cell detachmant in contrast to using an external heating source to remove cultured cells. The DNNC hydrogels were prepared as cylinders (diameter ~1.5 mm, length ~5 mm) and implanted into the dorsal subcutaneous tissue of rats via injection with a trocar needle. This represents a plausbile geometry for a membrane-based glucose biosensor and an implantaion method that minimizes injury. Passively anti-fouling PEG-DA implants were evaluated in parallel to represent a benchmark response as a hydrophilic (**Figure A-1a**), biocompatible control with high dimensional stability (i.e. non-thermoresponsive to the

temperature range of the subcutaneous tissue of rats). While the PEG-DA implants exhibited a higher modulus than the DNNC membranes (**Figure A-1b**), their stiffness remained much lower than most metallic CGM electrodes (moduli ~GPa). Thus, the objective of this work is to assess the extent of the FBR around the DNNC membrane implants *in vivo* under normal local body temperature fluctuations without the need for an external transdermal heating system.

2.3 Experimental Section

2.3.1 Materials

N-Isopropylacrylamide (NIPAAm, 97%), *N*-vinylpyrrolidone, and poly(ethylene glycol) diacrylate (PEG-DA, MW 575 g/mol) were purchased from Sigma-Aldrich (St. Louis, MO). *N*,*N*'-methylenebisacrylamide (BIS, 99%) was purchased from Acros Organics (Geel, Belgium). 2-Hydroxy-2-methyl-1-phenyl-1-propanone (Darocur 1173) and 1-[4-(2-Hydroxy)-phenyl]-2-hydroxy-2-methyl-1-propane-1-one (Irgacure 2959) was purchased from Ciba Specialty Chemicals (Tarrytown, NY). Octamethylcyclotetrasiloxane (D4) and 1,3,5,7-tetra-methyl-1,3,5,7-tetra¬vinylcyclotetrasiloxane (D4Vi) came from Gelest, Inc. Dodecylbenzene-sulfonic acid (DBSA, BIO-SOFT® S-101) came from Stepan Co. (Northfield, IL). For hydrogel fabrication and other experiments, deionized water (DI) with a resistance of 18 MΩ·cm (Millipore, Billerica, MA) was used.

2.3.2 Polysiloxane Nanoparticle Preparation

Polysiloxane colloidal nanoparticles with an average diameter of ~200 nm were prepared via emulsion polymerization and purified via dialysis as previously reported.[123] The final emulsion was 4.8 wt% solids.

2.3.3 DNNC Hydrogel Preparation

DNNC hydrogels were prepared by sequential formation of a relatively tightly crosslinked 1st network containing polysiloxane nanoparticles (2 wt% solid nanoparticles based on NIPAAm weight) and a loosely crosslinked 2nd network.[120] The "1st network precursor solution" was formed by combining NIPAAm monomer (1.0 g), NVP co-monomer (0.16 g), BIS crosslinker (0.04 g), polysiloxane nanoparticle emulsion (0.485 g), Irgacure-2959 photoinitiator (0.08 g) and DI (6.54 g). The "2nd network precursor solution" was formed by combining NIPAAm (6.0 g), NVP (0.96 g), BIS (0.012 g), Irgacure 2959 (0.24 g), and DI (21.0 g). Cylindrical hydrogels (~1.5 mm x 5 mm, diameter x length) were prepared by pipetting the 1st network precursor solution into a cylindrical glass mold (inside diameter = 1.0 mm, length = 15 mm). The mold was immersed in an ice water bath (~7 °C) and exposed for 10 min to longwave UV light. Cylindrical hydrogels were removed from their molds, rinsed with DI, and soaked in a Petri dish containing DI (60 mL) for 2 days at RT with daily water changes. The cylindrical hydrogels were then transferred into a Petri dish containing the 2nd network precursor solution for 24 hr at RT. Each cylindrical hydrogel was then placed into a second cylindrical mold (diameter = 1.5 mm, length = 15 mm), submerged in an ice water bath (~7 °C), exposed for 10 min to longwave UV light and soaked in DI as above. A clean

razor blade was used to trim ends to reduce the cylindrical length to 5 mm. The final diameter was measured via calipers. Similarly, planar sheet hydrogels were formed by injection of the 1st precursor solution between two glass slides separated by 1 mm spacers and UV irradiated for 30 min in an ice water bath (~7 °C). The planar gels were allowed to soak in DI for 2 days and then transferred into the 2nd precursor solution for 2 days. Each planar gel was placed between two glass slides separated by 1 mm spacers, UV irradiated for 30 min in an ice water bath (~7 °C) and soaked in DI as above.

2.3.4 PEG-DA Hydrogel Cylinder Preparation

Precursor solutions were formed by vortexing PEG-DA (100 %v/v) and Darocur 1173 (1% v/v) for 1 min. Cylindrical hydrogels (~1.5 mm x 5 mm, diameter x length per electronic caliper) were prepared by pipetting the precursor solution into a hollow cylindrical glass mold (inside diameter = 1.0 mm, length = 15 mm) with one end sealed by Parafilm. After sealing the other end of the mold, it was exposed to longwave UV light (UV-Transilluminator, 6 mw/cm^2, 365 nm) at room temperature (RT) for 3 sec. The cylindrical hydrogel was removed from the mold, rinsed with DI and immersed in a Petri dish containing DI (60 mL) for 24 hr. A clean razor blade was used to equally trim the ends to reduce the length to 5 mm. Similarly, planar PEG-DA hydrogels were prepared by injecting the precursor solution between two glass slides separated by 1 mm spacers and UV irradiating for 20 sec at RT. The planar gels were removed from the molds and soaked in DI as above.

2.3.5 Implanted DNNC Thermocycling Theoretical Diameter Change

Previously reported DNNC thermosensitivity data [131] was best-fit to a linear function spanning the expected implanted DNNC hydrogel cylinder temperature range (37-38 °C) seen in the subcutaneous tissue due to innate body temperature fluctuations of rats.[159, 160] This linear function was then used to determine the theoretical dimensional change with respect to ~1 °C oscillations of the implanted DNNC hydrogel cylinder temperature.

2.3.6 Mesh Size of DNNC Hydrogel.

Due to the complex structure of DN hydrogels, the mesh size is unable to be determined through standard calculations that typically require the molecular weight between crosslinks[161, 162] which is difficult to estimate with two interpenetrating, assymetrically crosslinked networks. Thus, in this study, DNNC mesh size was characterized via a series of dextran diffusion experiments, similar to as previously reported.[163] Hydrogel discs (~13 x 1.2 mm, diameter x thickness) were punched from hydrogel sheets and each were soaked in 1 mL of 0.01 mg mL^{-1} concentrated FITC-dextran DI solutions (4, 10, 20, 40, 70, 150 or 250 kDa, 3 discs for each mol. wt.). After 24 h at RT, the hydrogel discs were removed, gently rinsed with DI and blotted dry before transfering to 1 mL of fresh DI on a shaker table at 150 rpm. The dye was allowed to diffuse out of the hydrogels and the fluroescence of the surrounding solution was measured at 0 h and after 24 h at ex/em 480/520 nm. Standard calibration curves for each FITC-dextran size were used to convert fluorescence intensity to concentration. When the difference in concentration from 0 h to 24 h fell to negligible levels, it was assumed that

diffusion was inhibited and therefore the mesh size could be correlated to a size range between that of the FITC-dextrans at this point.

2.3.7 Implantation & Histological Evaluation

PEG-DA and DNNC cylindrical hydrogels (diameter ~1.5 mm, length ~5 mm) were sterilized by exposure to 80% ethanol for 45 min. Hydrogels were then washed three times for 30 min with sterile Dulbecco's phosphate buffer solution (PBS). Disposable, sterile trocar needles (13G; inner diameter = 1.804 mm, Avid Identification Systems, Inc.) were utilized to inject a single cylindrical hydrogel into the subcutaneous tissue (2~3 mm in depth) within the panniculus muscle (**Figure 2-1**) in the dorsal of CD® Hairless rats (N = 20, male, 8 weeks old, Charles River Laboratories). The CD® Hairless rat species encompasses a normal immune response despite its abnormal, reduced hair growth. The rat's hairless characteristic is ideal to facilitate the membrane implantation without unwarranted skin irritation commonly associated with shaving and nairing. Using isoflurane by inhalation, animals were anesthetized and anesthesia depth was tested by foot pinch reaction. Following implantation, the injection site was closed with surgical adhesive (3M Vetbond™ Tissue Adhesive, No. 1469SB). Material composition and dorsal placement were recorded for each rat/implant. All animals were immediately returned to individual cages and monitored every 12 hr. A custom designed LabView program (National Instruments) recorded cage temperatures every 5 min. After either 7 or 30 days post-implantation, 10 animals were euthanized by CO_2 asphyxiation, photographed, evaluated for gross changes and immediately fixed in 10% neutral buffered formalin for one week. Finally, implants and their surrounding tissue were removed and processed for

histology by serial dehydration, paraffin embedding, sectioning, and staining (hematoxylin and eosin (H&E)).

All morphometric analysis was performed in the Cardiovascular Pathology Laboratory (CVP) in the College of Veterinary Medicine & Biomedical Sciences at Texas A&M University by a board certified pathologist (Dr. Fred Clubb, DVM) that remained blinded throughout the study. Each tissue cross-section was scanned to enable consistent viewing at 100x using OlyVIA Olympus slide-viewing software during analysis to provide a standard field of view (~50 μm x ~70 μm, height x width). Each cross-section was divided into 4 sectors (**Figure A-2**) and 100 cells per sector were identified manually by established morphometric parameters as neutrophils, eosinophils, lymphocytes, erythrophagocytosis, hemosiderin-laden macrophages, macrophages, fibroblasts, fibrocytes, multi-nucleated giant cells (MNGCs) or plasma cells. The percentages of each cell type were calculated for each sector and averaged giving an average cellular presence around each implant type per animal. These values were then averaged over all animals for each implant type to get the final reported percentages at each time point. Additionally, in each sector the presence of capillaries, fibrin, loose collagen and dense collagen was recorded as (-) indicating little to no presence, (+/-) indicating low presence and (+) indicating high presence. To further evaluate microvascular density, blood vessels (10-100 μm in diameter) within 1 mm of the superficial half of the polymer interface were manually counted. Finally, a healing score was assigned to each sector utilizing a criteria (**Table A-1**) previously established in the CVP lab[164] to determine the healing stage at each time point. Fibrous capsule thickness was measured at 8 distinct locations, 12:00

corresponding to the most superior point of the capsule nearest the dermis and 6:00 corresponding to the most inferior point of the capsule (**Figure A-2**). The depth of the implant was determined from the outermost edge of the dermis to the interface of the hydrogel with the tissue at the 12:00 position. Furthermore, the diameter of each hydrogel cylinder was measured from the 12:00 to 6:00 position (perpendicular to the dermis) and the 3:00 to 9:00 position (parallel to the dermis) as shown in **Figure A-2**. All capsule measurements were performed blinded to avoid potential bias. Multiple student's T-tests with the Holm-Sidak correction were applied to determine significance ($p < 0.05$) in all histological analysis. *IACUC Approval*. NIH guidelines for the care and use of laboratory animals (NIH Publication #85-23 Rev. 1985) have been observed. All animal investigations conducted were approved by the Texas A&M University Institutional Animal Care and Use Committee and fell under the Animal Use Protocol #2012-191.

2.4 Results and Discussion

2.4.1 DNNC Hydrogel Fabrication and Characterization

The thermoresponsive DNNC membrane fabrication has been previously described[131] to obtain a cylindrical geometry for ease of implantation via trocar needle. Although these do not contain macropores, all hydrogels inherently have a mesh-like network that can be tuned through factors such as crosslink density and/or monomer concentration, thereby tailoring diffusion rates and swelling properties. Due to the multi-network design of these DNNC membranes, the traditional models used to calculate mesh size from equilibrium swelling ratios[161, 162] could not be easily adopted. Therefore, in this study a size exclusion experiment was performed via diffusion of varying sizes of

FITC-dextran (4, 10, 20, 40, 70, 150, and 250 kDa MW) to estimate the mesh size. The mesh size of the DNNC hydrogels at RT was determined to be between 6.5 and 9.6 nm (**Figure A-3**), corresponding to the hydrodynamic diameters (D_h) of 20 and 40 kDa FITC-dextran respectively.[165] As a result, glucose (D_h ~1 nm) would be expected to diffuse freely through this membrane, with a diffusion coefficient of $2.73 \pm 0.01 \times 10^{-6}$ cm^2s^{-1} (at RT) and 1.88 ± 0.001 (at 35 °C) as was reported previously.[131] This nicely matches the diffusion coefficient of the surrounding dermis tissue, reported as $2.64 \pm 0.42 \times 10^{-6}$ cm^2s^{-1}.[166] With their comparable glucose diffusivity, the DNNC hydrogels show great potential as self-cleaning, biosensor membranes that would not severely limit analyte diffusion.

2.4.2 Deswelling/Reswelling Behavior of Thermoresponsive DNNC Hydrogel Cylinder

By undergoing cyclical deswelling/reswelling, implanted thermoresponsive membranes were expected to actively inhibit cellular attachment and/or facilitate cellular detachment, and so potentially reduce the severity of the FBR. The core body temperature oscillations in normal male rats have been reported in literature to range from ~37.0-38.0 °C over a 24 hr period.[159, 160] Additionally, studies comparing body temperatures measured rectally (core) to temperatures measured by subcutaneously implanted monitors have confirmed that the core body temperature of rats is approximately equal to that of the subcutaneous tissue.[167] However, the VPTT of conventional crosslinked PNIPAAm hydrogels is ~33-35 °C and would so render such an implanted membrane in a fully deswollen, "static" state not conducive for cell-release or for maximum glucose diffusivity. Thus, the VPTT of the DNNC hydrogel was tuned to

36.5 °C (onset temperature, T_o) and 39.5 °C (maximum temperature,T_{max}) by incorporation of a hydrophilic comonomer (NVP).[131] Previously reported DNNC thermosensitivity data[131] was best-fit to a linear function spanning the expected implanted DNNC hydrogel cylinder temperature range (37-38 °C) to quantify the corresponding diameter change. The theoretical maximum diameter change of a cylindrical hydrogel (~1.5 mm x 5 mm, diameter x length) over this estimated 1.0 °C temperature oscillation from 37 to 38 °C was calculated to be ~9 μm. During a 24 hr period, the DNNC hydrogel cylinder would undergo constant dimensional alterations while still remaining in a hydrated, swollen state well below its VPTT (T_{max} = 39.5 ºC) but slightly over the onset temperature of the transition (T_o = 36.5 ºC).[131] This consistent, localized change at the implant-tissue interface could potentially decrease cell adhesion on the DNNC surface, inhibiting the formation of a dense fibrous capsule around the biosensor. For the non-thermoresponsive PEG-DA implant, it was previously shown to exhibit dimensional stability over a broad range of temperatures (25-40 ºC).[131]

2.4.3 Implantation of PEG-DA and Self-Cleaning DNNC Hydrogel Implants

Using a trocar needle, one sterile cylindrical (diameters ~1.5 mm, length ~5 mm) thermoresponsive DNNC hydrogel and one PEG-DA (non-thermoresponsive control) were implanted into the dorsal panniculus muscle (1~3 mm in depth, **Figure 2-1**, **Figure A-4a**) lateral to the spine of CD® Hairless rats (N = 20, male, 8 weeks old). This location was chosen for the higher vascular density compared to that of the adipose tissue of the subcutaneous region.[168] A greater amount of vascularization is desired to reduce the lag time between blood glucose to interstitial glucose levels in the tissue surrounding the

biosensor membrane. One potential drawback of implanting into a more vascularized tissue is the greater initial injury imparted by the trocar needle, which may lead to a more intense acute inflammatory response. However, by evaluating the cellular response at 7 and 30 days, we were able to determine the extent of acute inflammation after 1 week and to monitor its resolution over time to ensure that proper healing was achieved. At each time point after explantation, the implant diameters of both implant types remained similar to the original implant geometry (diameters ~1.5 mm, **Figure A-4b**).

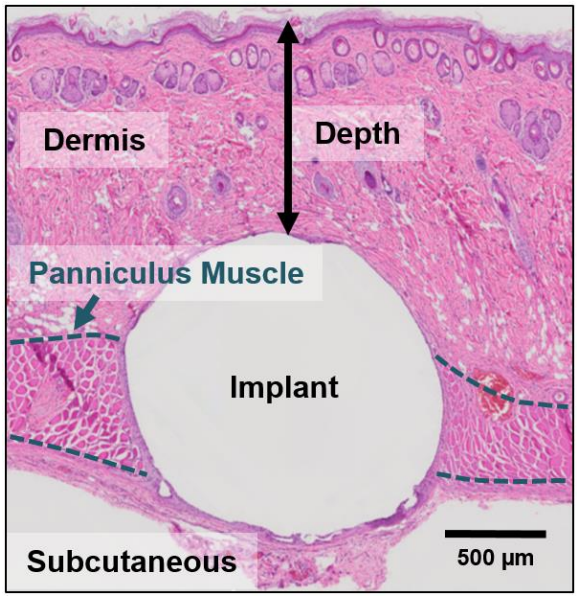

Figure 2-1. Representative histological image of cylindrical hydrogel implant cross-section, showing the location of implantation within the panniculus muscle and the typical depth (~1-3 mm).

2.4.4 Cellular Response

To evaluate the host response induced by the thermoresponsive DNNC membranes, the presence of dominant cellular components related to inflammation and

healing was determined at 7 and 30 days to investigate the early- and mid-stages of healing (**Figure A-5**). As a benchmark biocompatible material, dimensionally stable PEG-DA was utilized as a positive control to establish a favorable cellular response. During early-healing (~3-10 days), the acute inflammation caused by the minimal trauma incurring from implantation should begin to recede. At 7 days, cellular presence around both material compositions consisted mainly of macrophages with small numbers of fibroblasts, lymphocytes, neutrophils and multi-nucleated giant cells (MNGCs), as shown in **Figure 2-2**. Macrophages are strongly recruited to the site of injury during acute inflammation;[169, 170] therefore, this result was expected. Notably, a slightly lower amount of macrophages was present surrounding the thermoresponsive DNNC membrane compared to the PEG-DA implant. We hypothesize that the lower modulus (**Figure A-1b**), similar to that of the surrounding tissue, as well as the dimensional instability of the self-cleaning membranes produced a slightly milder acute inflammatory response. The clearing of red blood cells generated from vascular injury is confirmed by the reduction in erythrophagocytosis seen from 7 to 30 days (**Figure A-6**). Furthermore, the number of inflammatory cells, including macrophages and MNGCs, were seen to significantly decrease at the 30 day time point, indicating resolution of the acute inflammatory response into mid-stage healing. Additionally, the presence of fibroblasts and fibrocytes increased after 30 days, indicating the formation of fibrous capsule tissue and a typical healing response. From the types of cells observed and the notable progression towards healing, the DNNC membranes demonstrated high biocompatibility and did not elicit any substantial adverse reactions by the body.

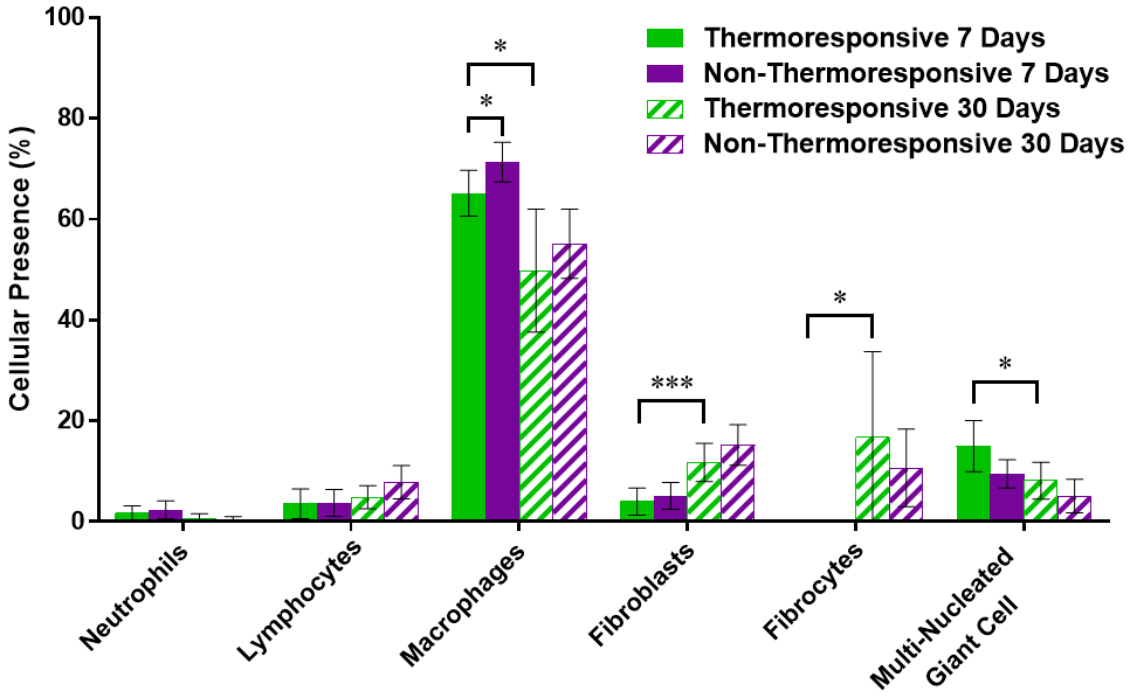

Figure 2-2. Cellular response surrounding thermoresponsive DNNC and non-thermoresponsive PEG-DA implants. Graphical analysis displaying the various cell types and their approximate percentage adjacent to DNNC and PEG-DA implants after 7 (solid) and 30 days (striped), where * indicates a significant difference of $p < 0.05$ and *** indicates a significant difference of $p < 0.005$.

2.4.5 Fibrous Capsule Formation

The formation of a dense avascular fibrous capsule around the biosensor will inhibit the rate of glucose diffusion from the surrounding interstitial fluid. This reduction in rate can be directly correlated with the thickness of the capsule (i.e. increased thickness, increased sensor lag time). Fibrosis occurs in the later stages of the FBR (weeks rather than days).[171] Thus, at 7 days the tissue capsule around the implant was an unorganized cellular layer without significant fibrous tissue. The width of this unorganized cellular tissue surrounding the thermoresponsive DNNC was measured at multiple points (**Figure**

A-2) that resulted in 37.5 ± 11.0 μm (**Figure 2-3**) across all animals. The high deviation in the measured thickness at 7 days could be explained by the high cellularity resulting in a poorly defined tissue capsule. However, as resolution proceeded for 30 days, the capsule around the DNNC implants became more fibrous and well-defined. This organized, collagenous tissue capsule exhibited an average thickness of 33.2 ± 6.1 μm, nearing the minimum thickness typically reported in literature, ~30 μm.[136-139] and slightly thinner than the passively anti-fouling PEG-DA control with a thickness of 45.9 ± 13.4 μm (**Figure 2-3**). By inhibiting the fibrous capsule formation, this self-cleaning membrane may reduce sensor lag time in a potential implantable biosensor.

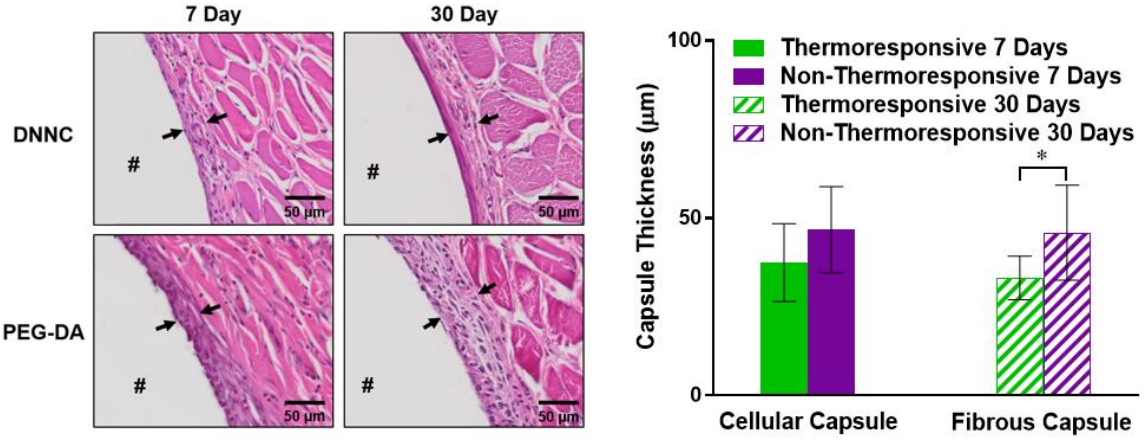

Figure 2-3. Representative histological images showing the cross-section of the thermoresponsive DNNC (top) and non-thermoresponsive PEG-DA (bottom) implants indicated by (#) and the surrounding tissue at 7 and 30 days, highlighting the fibrous capsule thickness indicated by the double arrows. The graph shows the quantitative tissue capsule thickness surrounding the thermoresponsive and non-thermoresponsive membranes at 7 days (solid, cellular capsule) and 30 days (striped, fibrous capsule), where * indicates a significant difference of $p < 0.05$ and *** indicates a significant difference of $p < 0.005$.

Additionally, the composition of the capsule around the implant is important in determining the extent of healing. Thus, the fibrotic tissue presence, including fibrin and collagen, was evaluated qualitatively over 7 and 30 day time points with (-) indicating little to no presence, (+/-) indicating low presence and (+) indicating high presence (**Table A-2**). Fibrin is released from the blood during initial injury, thus is more prevalent at the earlier time point of 7 days. Activated fibroblasts produce collagen, which densifies as healing matures. Due to the relatively low number of fibroblasts seen near the implants at 7 days (**Figure 2-2**), only small regions of loose collagen were found at this time point. With the recruitment of more fibroblasts at 30 days, an increase in loose collagen was observed as well as trace amounts of dense collagen. This progression from loose fibrin to a dense collagenous capsule demonstrates normal resolution during the FBR.

Although a dense fibrous capsule indicates appropriate healing, it can potentially inhibit glucose diffusion to the biosensor. Therefore, microvascular presence within the capsular tissue is important to carry glucose closer to the implant surface. Around both implant types, as expected due to a lack of macroporosity, a greater amount of vascularization was found in the outer regions of the tissue capsule than in the tissue nearest the implant surface (**Table A-2**). To quantify microvascular presence, blood vessels (10-100 μm in diameter) within 1 mm of the superficial half of the hydrogel interface were counted. It was determined that DNNC hydrogels had a significantly higher vascular density (vessels per mm^2) than the benchmark biocompatible PEG-DA implants post 30 days (**Figure 2-4**). We hypothesize that the dynamic nature at the DNNC hydrogel

surface may promote a less organized extracellular matrix and promote neovascularization.

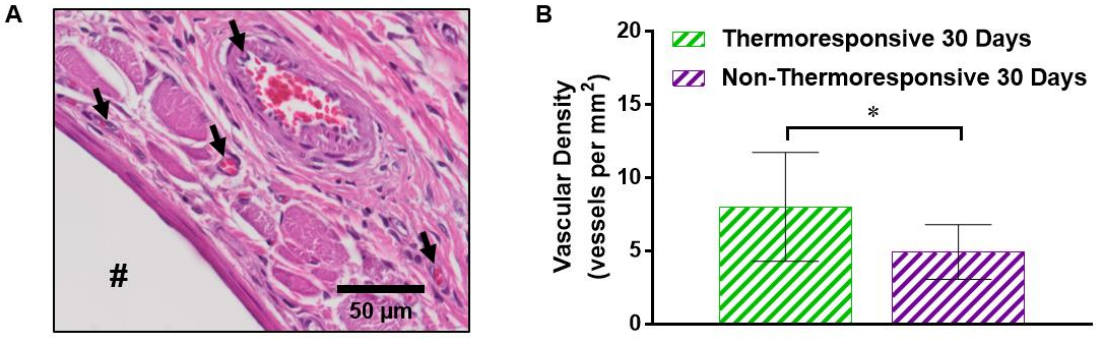

Figure 2-4. A) Representative histological image showing the cross-section of a thermoresponsive DNNC implant indicated by (#) and the surrounding tissue at 30 days, highlighting the microvasculature presence indicated by arrows. B) The average vascular density within 1 mm of the implants after 30 days of implantation. For statistics, * indicates a significant difference of $p < 0.05$.

As an overall confirmation of proper resolution around the implants, the dominant substrate and cellular components were evaluated and compiled into a healing score, rated from 0 to 6 from initial implantation to end-stage healing as defined in **Table A-1**. This criteria used for determining the stage of healing has been well established by the Cardiovascular Pathology Laboratory. In **Figure A-7**, the expected progression of healing from early-stage at 7 days to mid-stage at 30 days was confirmed for the DNNC implants.

2.5 Conclusions

Towards establishing its utility to house a subcutaneous glucose biosensor with long-term functionality, the biocompatibility of a thermoresponsive DNNC hydrogel membrane was evaluated in a rodent model in terms of its ability to minimize the FBR.

This membrane was previously shown to effectively release culture cells with thermal cycling around its VPTT. Herein, the implanted membrane relied on an "actively anti-fouling" or "self-cleaning" mechanism to limit cell adhesion and the subsequent FBR. Having tuned its VPTT **(**T_o **=** 36.5 °C; T_{max} = 39.5 °C**),** the implanted cylindrical membrane (diameter ~1.5 mm, length ~5 mm) was expected to remain in a largely swollen state but undergo small diameter changes (~9 μm) due to normal body temperature fluctuations (~37-38 °C). DNNC hydrogel cylinders were implanted subcutaneously (via injection) for 7 and 30 days to observe the FBR at both early- and mid-stages of healing, respectively. "Passively anti-fouling" PEG-DA implants were evaluated in parallel as a non-thermoresponsive, benchmark biocompatible control. Notably, after 30 days, the fibrous capsule surrounding the thermoresponsive membranes was remarkably thin (~33 μm) versus those typically reported in literature (~30 to >100 μm) and slightly thinner than that of the passively anti-fouling PEG-DA implants (~46 μm). Moreover, the microvascular density around the DNNC implant was greater than that surrounding the non-thermoresponsive PEG-DA. By minimizing the fibrous capsule thickness and enhancing local vascularization, the self-cleaning DNNC membrane provides a potential solution to avoid reductions in analyte (glucose) diffusion to implanted biosensors. By utilizing an actively anti-fouling or self-cleaning approach rather than a passively anti-fouling approach, the DNNC membranes demonstrate an alternative method to control the FBR through constant dimensional change at the implant surface inhibiting cell accumulation and stability. Overall, the thermoresponsive DNNC membrane's high biocompatibility combined with previously established *in vitro* properties (e.g. glucose

diffusion and mechanical strength), make it a desirable candidate for a long-term, implantable glucose biosensor.

CHAPTER III

A SELF-CLEANING, MECHANICALLY ROBUST MEMBRANE FOR MINIMIZING THE FOREIGN BODY REACTION: TOWARDS EXTENDING THE LIFETIME OF SUB-Q GLUCOSE BIOSENSORS

3.1 Overview

Towards Long-term, subcutaneously implanted continuous glucose biosensors have the potential to improve diabetes management and reduce associated complications. However, the innate foreign body reaction (FBR) both alters the local glucose concentrations in the surrounding tissues and compromises glucose diffusion to the biosensor due to the recruitment of high-metabolizing inflammatory cells and the formation of a dense, collagenous fibrous capsule. Minimizing the FBR has mainly focused on "passively antifouling" materials that reduce initial cellular attachment, including poly(ethylene glycol) (PEG). Instead, the membrane reported herein utilizes an "actively antifouling" or "self-cleaning" mechanism to inhibit cellular attachment through continuous, cyclic deswelling/reswelling in response to normal temperature fluctuations of the subcutaneous tissue (**Figure 3-1**). This thermoresponsive double network (DN) membrane is based on *N*-isopropylacrylamide (NIPAAm) and 2-acrylamido-2-methylpropane sulfonic acid (AMPS) (75:25 and 100:0 NIPAAm:AMPS in the 1st and 2nd networks, respectively; "*DN-25%*"). The extent of the FBR reaction of a subcutaneously implanted *DN-25%* cylindrical membrane was evaluated in rodents in parallel with a PEG-diacrylate (PEG-DA) hydrogel as an established benchmark biocompatible control.

Notably, the *DN-25%* implants were more than 25x stronger and tougher than the *PEG-DA* implants while maintaining a modulus similar to that of subcutaneous tissue. From examining the FBR at 7, 30 and 90 days after implantation, the thermoresponsive *DN-25%* implants demonstrated a rapid healing response and a minimal fibrous capsule (~20-25 µm), similar to the *PEG-DA* implants. Thus, the dynamic self-cleaning mechanism of the *DN-25%* membranes represents a new approach to limit the FBR while achieving the durability necessary for long-term implantable glucose biosensors.

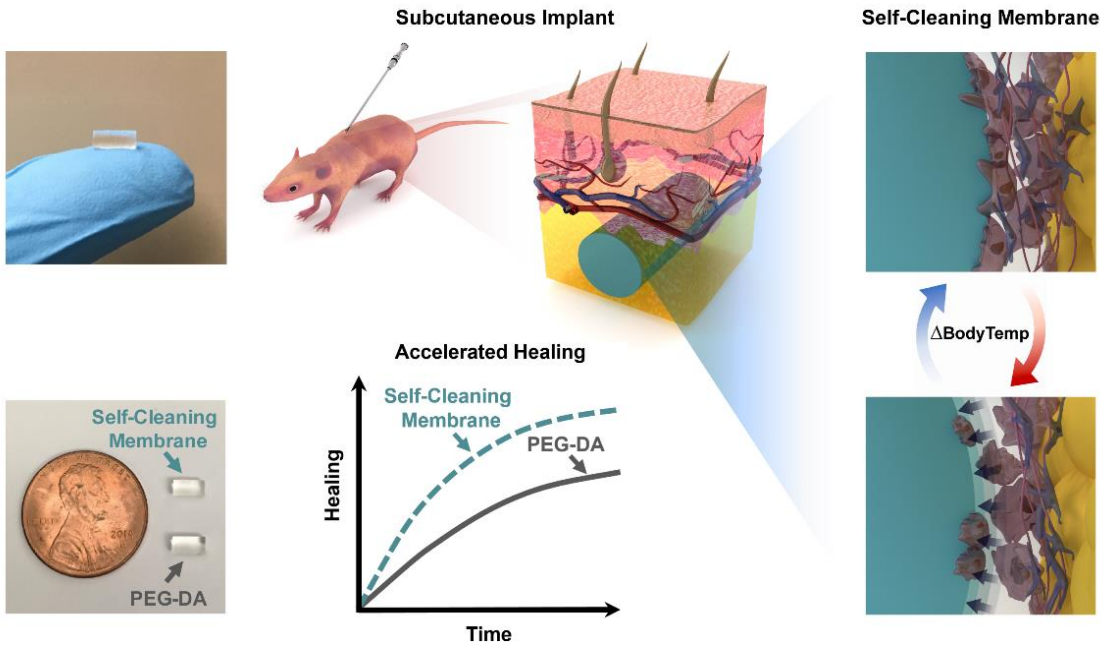

Figure 3-1. Overview of self-cleaning DN hydrogels highlighting their small size and actively anti-fouling mechanism after subcutaneous implantation.

3.2 Introduction

Current commercial continuous glucose monitors (CGMs) are limited to ~7-14 days of use before replacement of the transcutaneous electrode is required due to a combination of biofouling, fluctuations in local analyte levels via metabolic reactions and irritation/infection at the implant site.[148, 169, 172, 173] The first fully subcutaneous CGM, using fluorescent-based glucose detection, has recently received FDA approval but must be replaced after three months or less.[174] To extend the lifetime of transcutaneous and subcutaneous biosensors, it is essential to minimize the innate inflammatory response and foreign body reaction (FBR) while also maintaining requisite mechanical properties for long-term durability. Broadly, the normal progression seen immediately after implantation includes the recruitment of proteins and cells to the implant site during acute inflammation (days to weeks) which resolves through the encapsulation of the foreign material with dense, avascular collagenous tissue that may be 30 to >200 μm thick [138, 139, 175] (weeks to months).[140, 176] Thicker fibrous capsules can significantly inhibit analyte diffusion to the biosensor, ultimately diminishing its function.[139, 169, 177] Furthermore, the local glucose concentrations are influenced by high-metabolizing inflammatory cells, primarily macrophages, which are recruited during acute inflammation and persist throughout the FBR.[169, 173, 178] Therefore, a method to reduce the extent of fibrous encapsulation and accelerate the clearance of inflammatory cells could significantly improve the longevity of implantable glucose biosensors.

To overcome these challenges, most prior efforts have focused on “passively antifouling” membranes that use a hydration layer to minimize initial protein and cell

adhesion, including hydrogel coatings (i.e. PEG[179, 180] and PHEMA[181, 182]), surface functionalization[183] and biomimetic coatings.[184, 185] However, *in vivo* results have been inconsistent, possibly due to the inability to prevent non-specific protein adhesion and thus cellular adhesion long-term as well as their lack of durability (i.e. coating degradation or de-lamination).[170] Alternatively, porous materials have been utilized to encourage ingrowth of the surrounding tissue and to promote neovascularization to decrease the lag time of interstitial tissue analytes to the biosensor.[170, 186, 187] Although these porous implants have shown promising results for increasing the rate of transport of small molecules to biosensors, the continued presence of macrophages and other high-metabolizing cells could potentially impact glucose sensor functionality.[186]

While multiple studies utilized passively antifouling materials to minimize the FBR around subcutaneous implants,[179-185] none to our knowledge have explored a dynamic "self-cleaning" strategy. Thus, we have reported self-cleaning membranes based on thermoresponsive poly(*N*-isopropylacrylamide) (PNIPAAm) hydrogels whose cyclical deswelling/reswelling at temperatures above and below, respectively, their volume phase transition temperature (VPTT) may minimize biofouling and the FBR of subcutaneously implanted glucose biosensors.[26, 27] Moreover, we anticipate that such membranes could be used to contain a liquid glucose sensing assay[130, 188] to form an electronics-free, subcutanteously implantable glucose biosensor that could be used with a wearable, optical detection method. In our previous study,[26] we demonstrated the ability of a cylindrical thermoresponsive, nanocomposite membrane to minimize the fibrous capsule

formation when implanted into the subcutaneous tissue of a rodent model. These double network nanocomposite (DNNC) hydrogels were composed of two asymmetrically crosslinked, PNIPAAm-*co*-poly(*N*-vinylpyrrolidone) [P(NIPAAm-*co*-NVP)] networks with polysiloxane nanoparticles embedded within the 1st network to enhance swelling kinetics. By precisely tuning the DNNC membrane's VPTT [onset (T_{onset}) ~36.5 °C, maximum (T_{max}) ~39.5 °C], dynamic self-cleaning based on cyclic deswelling and reswelling would be triggered by natural body temperature fluctuations of rats (T_{rat} ~37-38 °C [159, 160, 167]). This resulted in a favorably thin fibrous capsule (~30 μm) and an increase in local vascularization compared to a stiff PEG-DA control (i.e. prepared from low molecular weight PEG-DA, 575 g/mol, 100%).[26] However, this DNNC membrane also displayed low mechanical strength (~0.4 MPa)[120] which could potentially lead to poor long-term durability. In our later studies, to enhance membrane mechanical properties for improved biosensor longevity, an electrostatic comonomer was incorporated into the 1st network of a PNIPAAm-based DN hydrogel.[76] Denoted as *DN-25%*, these membranes were composed of a tightly crosslinked 1st network of NIPAAm copolymerized with 2-acrylamido-2-methylpropane sulfonic acid (AMPS) at a wt% ratio of 75:25 (NIPAAm:AMPS) and a loosely crosslinked 2nd network of NIPAAm copolymerized with NVP to tune the VPTT.[27] These *in vitro* studies on *DN-25%* planar hydrogels confirmed the simultaneous enhancement of mechanical strength and hydration due to the incorporation of the negatively charged AMPS comonomer as well as cytocompatibility and successful thermally-driven release of cultured fibroblasts.[27, 76]

Herein, we sought to examine the effect of a *DN-25%* membrane implant on the FBR and fibrous capsule formation when implanted in a subcutaneous rodent model experiencing normal local body temperature fluctuations (i.e. without an external transdermal heating device). As for our earlier study,[26] the *DN-25%*'s VPTT was precisely tuned (T_{onset} ~36.5 °C; T_{max} of ~41 °C) such that, throughout the cyclical deswelling/reswelling in response to body temperature fluctuations, the membrane would change in diameter ~20-25 μm (~1% of total diameter) while primarily remaining in a hydrated, swollen state, thereby maximizing the potential for glucose diffusion. A conventional PEG-DA hydrogel (3.4 kDa, 10 wt%) was implanted in parallel to provide a benchmark tissue response to a passively antifouling hydrogel with well-established biocompatibility. Since both the *DN-25%* and *PEG-DA* hydrogels displayed moduli similar to the native subcutaneous and dermis tissues (E ~0.01-0.25 MPa)[4, 132, 133], adverse contributions due to shear stresses were avoided. Both hydrogels were fabricated as small, cylindrical membranes (~2.5 × 5 mm, diameter × length), representing a plausible geometry for a membrane-coated glucose biosensor that permits implantation via injection to minimize local injury. The mechanical integrity, including the modulus, strength and toughness, of both *DN-25%* and *PEG-DA* implants were evaluated prior to implantation. To examine overall biocompatibility, both types of implants were injected subcutaneously via trocar needle into the dorsal of CD® Hairless rats (N = 33, male, ~8 weeks old, Charles River Laboratories). Histological analysis was performed at three well-established time points of 7, 30 and 90 days post-implantation to determine the intensity of the FBR and extent of fibrous encapsulation during the acute inflammatory response (7

days), early-to-mid stage healing (30 days) and late-stage healing (90 days). Primarily, the rate of progression from initial inflammation to complete healing as well as tissue organization were evaluated to assess the potential of the self-cleaning *DN-25%* as a long-term, subcutaneously implantable glucose biosensor membrane.

3.3 Experimental Section

3.3.1 Materials

N-isopropylacrylamide (NIPAAm, 97%), 2-acrylamido-2-methylpropane sulfonic acid (AMPS, 97%), 1-vinyl-2-pyrrolidinone (NVP), *N*,*N*'-methylenebisacrylamide crosslinker (BIS, 99%), acryloyl chloride, triethylamine (Et3N), K_2CO_3, $MgSO_4$, poly(ethylene glycol) (PEG; PEG-3400, MW = 3000 - 3700 g/mol per manufacturers specifications) and 2,2-di-methyl-2-phenyl-acetophenone (DMAP) were obtained from Sigma Aldrich. 1-[4-(2-Hydroxyethoxy)-phenyl]-2-hydroxy-2-methyl-1-propane-1-one (Irgacure® 2959) was purchased from BASF. Ethyl ether anhydrous was acquired from Fisher Scientific. For hydrogel fabrication, deionized water (DI) with a resistance of 18 MΩ·cm (Cascada LS MK2, Pall) was used. Phosphate-buffered saline (PBS, 1X, pH 7.4, without calcium and magnesium) was obtained from Corning®.

3.3.2 Preparation of Thermoresponsive DN Hydrogels ("DN-25%")

The thermoresponsive DN hydrogels were formed through a sequential, two step UV-cure process. The 1st network precursor solution consisted of NIPAAm monomer (0.75 g), AMPS monomer (0.25 g, 75:25 wt% NIPAAm:AMPS), BIS crosslinker (0.04 g), Irgacure-2959 photoinitiator (0.08 g) and DI water (7.0 mL). The 2nd network precursor solution was formed by combining NIPAAm (6.0 g), NVP (0.96 g), BIS (0.012 g),

Irgacure 2959 (0.24 g), and DI H_2O (21.0 mL). The thermoresponsive DN hydrogels are denoted as "*DN-25%*" where *25%* equals the wt% of AMPS in the 1st network's NIPAAm:AMPS wt% ratio. Cylindrical hydrogels (~2.5 × 5 mm, diameter × length) were prepared by pipetting the 1st network precursor solution into a cylindrical glass mold (inside diameter = ~1 mm, length = 10 mm) and sealing the open ends with Parafilm®. The mold was immersed in an ice water bath and exposed for 30 min to longwave UV light. Cylindrical hydrogels were removed from their molds, rinsed with DI, and soaked in a Petri dish containing DI for 2 days at RT with daily water changes. The resulting single network (SN) cylindrical hydrogels were then transferred into a Petri dish containing the 2nd network precursor solution for 48 hr at 2 °C. Next, the cylindrical hydrogel was wrapped in Saran wrap, submerged in an ice water bath, exposed for 10 min to longwave UV light, and soaked in DI as above. The final swollen diameter was ~2.5 mm and a clean razor blade was lastly used to trim ends to achieve a cylindrical length of 5 mm.

3.3.3 Preparation of Non-Thermoresponsive PEG-DA Hydrogels ("PEG-DA")

The conventional PEG-DA hydrogels were formed through a one-step UV-cure process. The precursor solution consisted of PEG-DA (0.1 g, 3.4k g/mol, synthesized as previously reported)[189, 190], 30 wt% DMAP in NVP (10 µL) and DI water (1.0 mL). The PEG-DA hydrogels are denoted as "PEG-DA". Cylindrical hydrogels (~2.5 × 5 mm, diameter × length) were prepared by pipetting the 1st network precursor solution into a cylindrical glass mold (inside diameter = ~2.4 mm, length = 10 mm) and sealing the open ends with Parafilm®. The mold was exposed for 2 min at RT to longwave UV light.

Cylindrical hydrogels were removed from their molds, rinsed with DI, and soaked in a Petri dish containing DI for 2 days at RT with daily water changes. The final swollen diameter was ~2.5 mm and a clean razor blade was used to trim ends to achieve a cylindrical length of 5 mm.

3.3.4 Mechanical Testing of Hydrogel Implants

The mechanical properties of the *DN-25%* and *PEG-DA* hydrogel cylindrical rods were analyzed with an Instron 3340 at RT under static compression at a rate of 1 mm min^{-1} until fracture. The as-prepared implants were sliced into cylindrical cross-sections (~2.5 x 2 mm, diameter x length) and tested in replicate (N = 4). The elastic compressive modulus (E) was obtained from the slope of the linear portion of the stress–strain curve from 0% to 10% strain. The ultimate compressive strength (σ_f) and the % strain at break (ε_f) were defined, respectfully, as the stress and strain values at the point of fracture. Finally, the toughness was obtained from the integration of the stress-strain curve. GraphpadPrism was used to analyze statistical significance ($p < 0.05$) between the *DN-25%* and *PEG-DA* implants through student's *t* tests using Welch's correction.

3.3.5 Implantation

For each time point (7, 30 and 90 days), each animal (N = 11) were implanted with one thermoresponsive *DN-25%* and one conventional *PEG-DA* hydrogels (~2.5 × 5 mm, diameter × length). Prior to implantation, all cylindrical hydrogels were sterilized by soaking in 70% ethanol for 45 min, then transferring into sterile PBS for three consecutive 30 min washes, followed by two overnight soaks in fresh PBS. Using isoflurane by inhalation, animals were anesthetized and anesthesia depth was tested by foot pinch

reaction. Sterile trocar needles (10G; inner diameter = ~2.7 mm, Innovative Research of America) were utilized to inject one *DN-25%* and one *PEG-DA* cylindrical hydrogel into the subcutaneous tissue (2~3 mm in depth) in the dorsal side of CD® Hairless rats (N = 33, male, ~8 weeks old, Charles River Laboratories). For animals designated for the 90 day studies, a cellophane tape debridement method followed by a small incision was utilized prior to injection via trocar needle. The CD® Hairless rats were chosen to avoid shaving of the implant site that commonly results in undesirable skin irritation. Following implantation, the injection site was closed with surgical adhesive (3M Vetbond™ Tissue Adhesive, No. 1469SB). Material composition and dorsal placement were recorded for each rat/implant. Portable temperature monitors (RC-5 USB Temperature Data Logger, Elitech®) recorded the temperature of the room every 5 min in three different locations. *IACUC Approval*: NIH guidelines for the care and use of laboratory animals (NIH Publication #85-23 Rev. 1985) have been observed. All animal investigations conducted were approved by the Texas A&M University Institutional Animal Care and Use Committee and fell under the Animal Use Protocol #2015-0287.

3.3.6 Histological Evaluation

At 7, 30 or 90 days post-implantation, the designated 11 animals were euthanized by CO_2 asphyxiation, photographed, evaluated for gross changes and immediately fixed in 10% neutral buffered formalin for two weeks. Implants and their surrounding tissue were removed and processed for histology by serial dehydration, paraffin embedding, sectioning, and staining (hematoxylin and eosin (H&E), Masson's trichrome). All morphometric analysis was performed in the Cardiovascular Pathology Laboratory (CVP)

in the College of Veterinary Medicine & Biomedical Sciences at Texas A&M University by a board certified pathologist (Dr. Fred Clubb, DVM) that remained blinded throughout the study. Each tissue cross-section was scanned to enable consistent viewing at 100x using OlyVIA Olympus slide-viewing software during analysis to provide a standard field of view. To quantify the cell types and fibrotic tissue present in the capsule surrounding the hydrogel cylinders, the tissue cross-sections were divided into 4 sectors (**Figure A-8**). To examine cellular response, 100 cells per sector were identified manually by established morphometric parameters as neutrophils, eosinophils, lymphocytes, erythrophagocytosis, hemosiderin-laden macrophages, macrophages, fibroblasts, fibrocytes or multi-nucleated giant cells (MNGCs). The percentages of each cell type were calculated for each sector and averaged, giving an average cellular presence around each implant type per animal. These values were then averaged over all animals for each implant type to get the final reported percentages at each time point. Additionally, in each sector the presence of capillaries, fibrin, loose collagen and dense collagen was recorded as (-) indicating little to no presence, (+/-) indicating low presence or (+) indicating high presence. Finally, a healing score was assigned to each sector utilizing a criteria (**Table A-1**) previously established in the CVP lab[26] as a rating of overall healing in each region.

Fibrous capsule thickness was measured at 8 distinct locations, 12:00 corresponding to the most superior point of the capsule nearest the dermis and 6:00 corresponding to the most inferior point of the capsule (**Figure A-8**). The depth of the implant (2~3 mm, **Figure A-9**) was determined from the outermost edge of the dermis to the interface of the implant with the tissue at the 12:00 position. Furthermore, the diameter

of each hydrogel cylinder was measured from the 12:00 to 6:00 position (perpendicular to the dermis) and the 3:00 to 9:00 position (parallel to the dermis). All capsule measurements were performed blinded to avoid potential bias. GraphpadPrism was used to analyze statistical significance ($p < 0.05$) between the *DN-25%* and *PEG-DA* implants through multiple *t* tests or one-way ANOVA (Sidak's multiple comparisons test) for all histological analyses.

3.4 Results and Discussion

3.4.1 Mechanical Properties

The mechanical properties of a membrane for an implantable glucose biosensor are of critical importance to performance and longevity. A narrow, cylindrical geometry affords simple implantation via injection and also minimizes injury to the surrounding tissue. Thus, the membrane must withstand the forces of initial implantation as well as those of everyday activities which may vary depending on implant location. For instance, the wrist represents a potentially desirable location of a subcutaneous glucose biosensor as it could be coupled with a wearable "watch-like" detection device. While many variables may contribute to the impact forces experienced by a subcutaneously implanted biosensor, we hypothesized that a compressive strength of >1 MPa could ensure integrity during most common activities. For example, the force of impact due to a short fall onto outstretched hands has been reported to produce a stress of up to ~0.8 MPa on the palm.[191] To evaluate the compressive strength of the implants, the cylindrical membrane implants were prepared then cut cross-sectionally into discs (~2.5 mm x ~1 mm, diameter x thickness) and compressed until fracture. Notably, the *DN-25%*

membranes exhibited high strength (3.34 MPa) and toughness (446.8 kJ m^{-3}), greater than 25x that of the *PEG-DA* membranes (0.13 MPa and 14.8 kJ m^{-3}, respectively) (**Figure 3-2**). This enhancement in strength and toughness compared to a conventional hydrogel is expected to provide improved durability. However, it is also important that the membrane stiffness does not greatly exceed that of the local subcutaneous and dermis tissues (E ~0.01-0.25 MPa)[4, 132, 133] in order to minimize local shear stress that can lead to a more severe FBR.[134] As such, studies have demonstrated that decreasing the modulus of hydrogel implants can improve the FBR and even reduce fibrous capsule formation.[192] In our study, both types of membranes displayed moduli similar to that of the surrounding tissue, with *DN-25%* having a modulus (~0.50 MPa) somewhat higher than that of *PEG-DA* (~0.22 MPa) (**Figure 3-2c**). Further, these moduli values are much lower than that of transcutaneous metallic CGM electrodes (~GPa). Thus, the *DN-25%* membrane maintains an elastic modulus similar to the surrounding subcutaneous tissue while providing a significantly higher strength and toughness than most standard hydrogels with established biocompatibilities, including the *PEG-DA* implants.

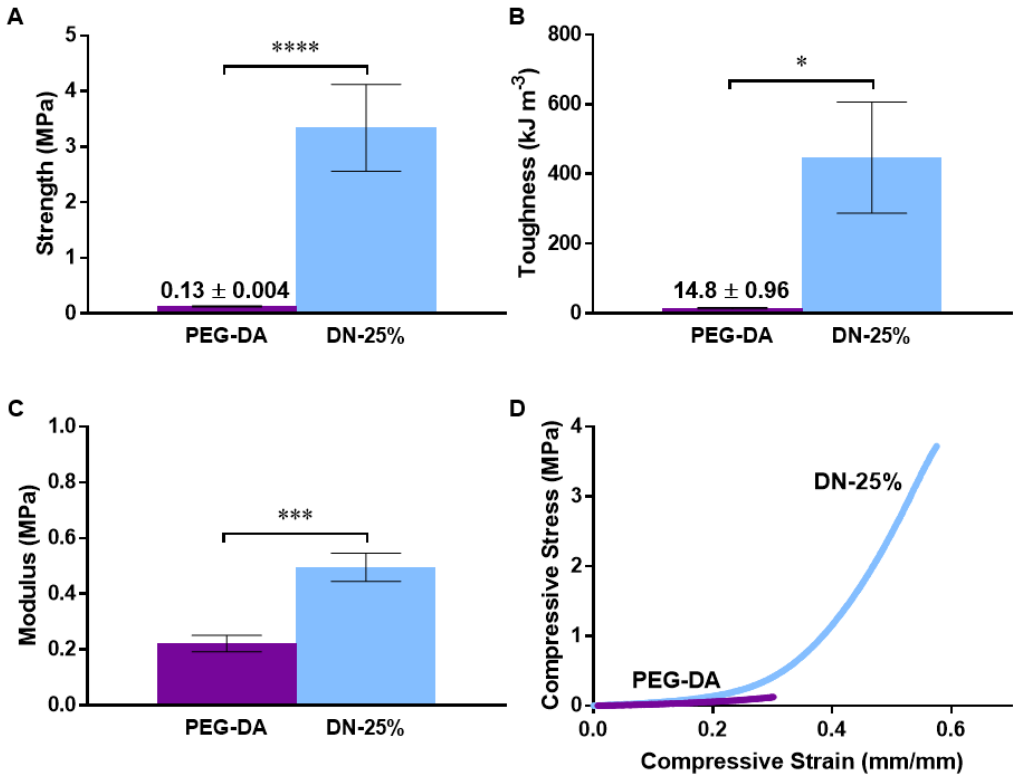

Figure 3-2. Compressive mechanical properties of thermoresponsive *DN-25%* and conventional *PEG-DA* implants, including (A) strength, (B) toughness, (C) elastic modulus and (D) a representative stress vs. strain curve, where * indicates a significant difference of $p < 0.05$, *** indicates a significant difference of $p < 0.001$ and **** indicates a significant difference of $p < 0.0001$.

3.4.2 Implantation

Implantation of the 7 & 30 day time points resulted in small amounts of keratin debris within the subcutaneous tissue that was pulled in alongside the trocar needle during insertion. Due to its inflammatory nature, this keratin was thought to have produced the observed localized pyogranulomas surrounding the debris. These keratin pyogranulomas were shown to be independent of capsular fibrosis, capsular inflammation and gel

composition at both 7 and 30 days. To avoid this in later studies (i.e. the 90 day time point), a cellophane tape debridement method was used to remove any loose keratin on the dermis before making a small incision to allow for easy insertion of the trocar needle into the dorsal subcutaneous tissue of the rats. No keratin debris was observed at the 90 day time points. The observed depth of implantation at each time point was not significantly different between implant types and their diameters remained similar to the initial implant diameters (~2.5 mm) across all time points (**Figure A-9**).

3.4.3 Cellular Response

The cell types present in the capsular tissue surrounding the hydrogel implants are a major indicator for the overall implant biocompatibility and the stage of healing. For a biocompatible implant, a standard wound healing response (**Figure 3-3**) will inevitably occur due to acute injury caused during implantation.[171, 193, 194] Any cellular presence other than what is recruited in this natural response would suggest that the implant could be intensifying or prolonging the normal inflammatory reaction. Typically, at 7 days, it is expected that most neutrophils will have been cleared and macrophages and fibroblasts as well as potentially low numbers of lymphocytes will have been recruited to the area. For a biocompatible implant, as acute inflammation transitions into the early stages of healing at 30 days, macrophages and few lymphocytes will still be present and the ratio of inactive fibrocytes to active fibroblasts will begin to increase as the healing process of fibrosis begins. Progressing into the later stages of healing at 90 days, some macrophages and fibroblasts may remain and the presence of fibrocytes will increase to form a mature fibrous capsule. Herein, this expected cellular response to injury was used

as the basis to evaluate the response in the tissue surrounding the *DN-25%*. Moreover, results were compared to that of the *PEG-DA* membrane as it was anticipated to produce a benchmark, biocompatible response. As described below, the quantification of each major cell type, including neutrophils, macrophages, fibroblasts and fibrocytes, was utilized to evaluate the overall progression towards resolution of the capsular tissue adjacent to the thermoresponsive implant surfaces.

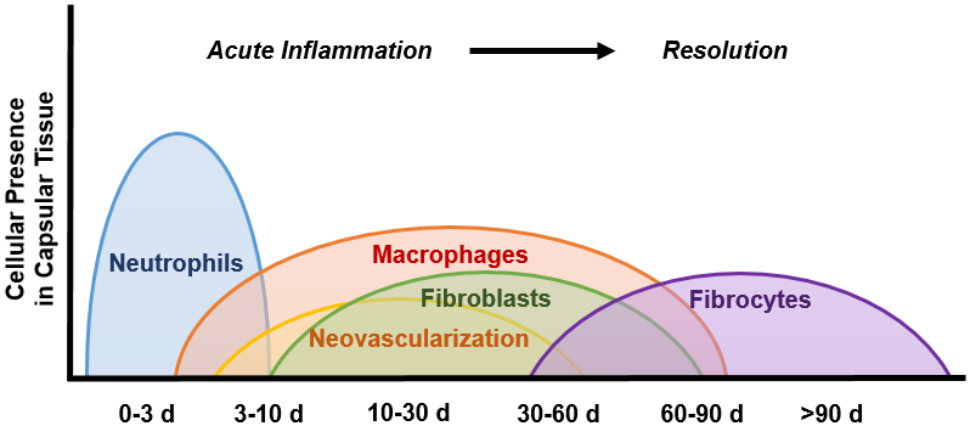

Figure 3-3. Schematic timeline showing the typical changes in cellular presence in the tissue surrounding a biocompatible implant during the progression of acute inflammation and healing after injury (i.e. implantation).

At 7 days, we found <5% neutrophils around the thermoresponsive *DN*-25% cylindrical membranes and no presence of neutrophils at both 30 and 90 days (**Figure 3-4**). This indicated normal resolution of acute inflammation. Furthermore, if a more chronic inflammatory response had ensued, an increase in lymphocytes and plasma cells would have been observed.[171] Low percentages of lymphocytes (<5%) were observed around the *DN-25%* implants at 7 and 30 days, dropping to <1% by 90 days. Plasma cells and

other inflammatory cells, such as eosinophils, were also absent at all time points in the capsular tissue surrounding the implants. As expected, a similarly mild response was seen around the *PEG-DA* implants. Therefore, the *DN-25%* implants did not elicit observable chronic inflammation but rather a normal wound healing response.

Additionally, macrophages play a major role in inflammation as well as healing. These cells are recruited early to the site of injury and remain present until the later stages of the FBR. Macrophages can interfere with local glucose concentration measurements due to their high metabolism of interstitial glucose. Thus, minimizing these inflammatory cells surrounding the implant is expected to optimize the accuracy of an implantable glucose biosensor. As expected, the largest percentage of macrophages was present at 7 days, decreasing at the later time points (**Figure 3-4**). The reduction of macrophages surrounding the *DN-25%* implants after 30 days demonstrated progression from acute inflammation towards resolution. This was similarly observed in the normal healing response elicited by the *PEG-DA* implants. The apparent increase in macrophage presence around all implants from 30 to 90 days may be due to the qualitatively lower overall cellular density observed at 90 days. Notably, versus the *PEG-DA* implants with well-established biocompatibility, a lower percentage of macrophages were seen surrounding the *DN-25%* implants at both 30 and 90 days. Thus, the self-cleaning *DN-25%* membrane could potentially provide a more effective resolution of inflammation than conventional, passively antifouling hydrogels, such as *PEG-DA* membranes.

The amount of erythrophagocytosis and hemosiderin laden macrophages, macrophages involved in the engulfing and digestion, respectively, of red blood cells

(RBCs) from injured capillaries, were also analyzed. The decrease in erythrophagocytosis from 7 days to 30 days (**Figure 3-4**) indicates healing of the capillaries and clearance of any remaining RBCs from the area. The merging of several macrophages into a multinucleated giant cell (MNGC) that tries to engulf the material is a key indicator of an active FBR.[171] However, MNGCs were scarcely present around the thermoresponsive *DN-25%* implants (<2% at the 30 and 90 day time points) and showed no significant differences from the *PEG-DA* implants, signifying negligible aggravated inflammation as well as little activation of a FBR.

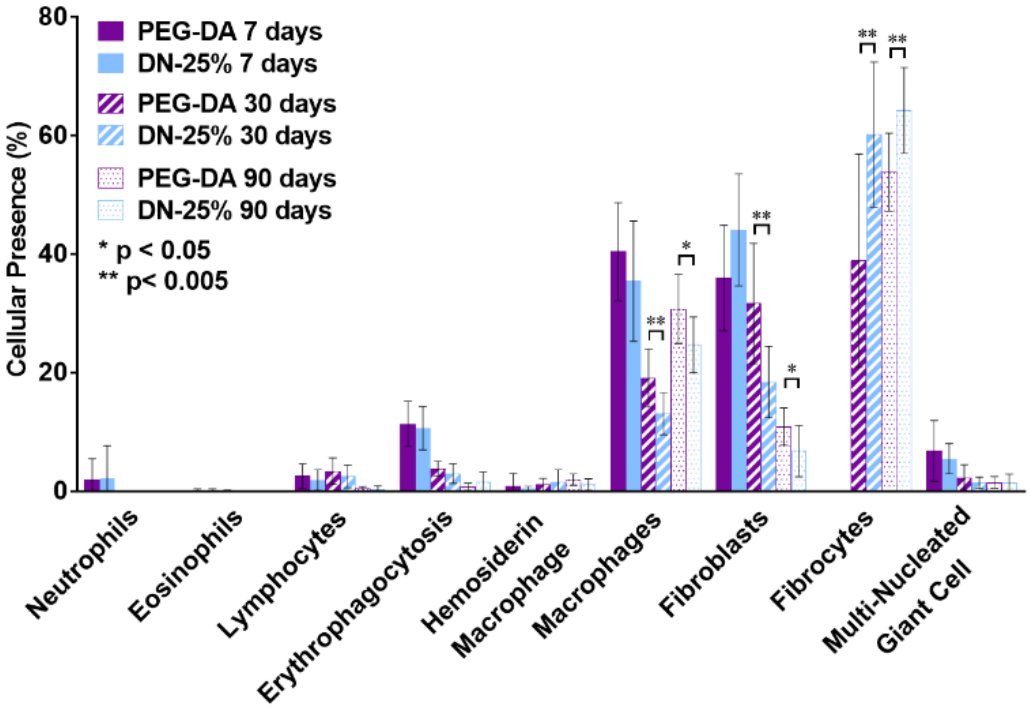

Figure 3-4. Graphical analysis displaying the cellular response surrounding the thermoresponsive *DN-25%* and conventional *PEG-DA* implants through the presence of various cell types after 7 (solid), 30 days (striped) and 90 days (dots), where * indicates a significant difference of $p < 0.05$ and ** indicates a significant difference of $p < 0.01$.

Lastly, the presence of fibroblasts and fibrocytes was observed over these three time points. In normal resolution, fibroblasts will be recruited to the site of injury shortly after macrophages during the early stages of healing to synthesize fibrous matrix proteins such as collagen. As healing progresses, the presence of activated fibroblasts declines as the number of inactive fibrocytes increases to aid in the later stages of healing and fibrosis.[194, 195] At 7 days, the *DN-25%* implants showed an abundance of fibroblasts while no fibrocytes were present (**Figure 3-4**). By 30 days, comparatively more fibrocytes were present than fibroblasts around the *DN-25%* implants. This shift from predominantly fibroblasts to more fibrocytes was expected for normal healing and was similarly seen surrounding the benchmark *PEG-DA* implants. Notably, a greater amount of fibrocytes was observed around the thermoresponsive *DN-25%* implants (~60%) than the *PEG-DA* implants (~40%) at 30 days which could indicate that the self-cleaning hydrogels exhibited a more advanced healing response. This trend continued after 90 days; however, differences were less pronounced as resolution neared completion, with fibrocytes accounting for ~65% of all cells surrounding the *DN-25%* implants and ~55% of the cells around the *PEG-DA* implants (**Figure 3-4**). Generally, a more rapid healing response would be beneficial for an implantable biosensor to reduce fluctuations in the local physiologic environment. Overall, by examining the cellular presence of multiple key cell types of the host response, the *DN-25%* membrane showed the potential to elicit milder inflammation as well as an accelerated healing response when compared to a benchmark biocompatible *PEG-DA* membrane at both the 30 and 90 day time points.

3.4.4 Fibrous Capsule Formation

To evaluate the extent of fibrous capsule formation around the implants, the thickness of the fibrous capsule was measured over eight locations around the cross-section of the membranes and averaged over all animals (**Figure A-8 & A-10**). At each time point, no significant differences in thickness were seen between the *DN-25%* and the highly biocompatible *PEG-DA* implants. For both, the average capsule thickness was extraordinarily thin, never exceeding 25 µm, even after 90 days (**Figure 3-5a & 3-5b**). As reported in our previous study, a rigid PEG-DA cylindrical implant (i.e. prepared from low molecular weight PEG-DA, 575 g/mol, 100%) produced a greater capsule thickness of ~45 µm at just 30 days and that of a nanocomposite thermoresponsive membrane was ~30 µm.[26] Such a capsule thickness of ~30 µm is consistently reported as the thinnest typically seen in most previous literature.[138, 139, 175] The fibrous capsule tissue, due to its dense, avascular nature, could inhibit the rate of glucose diffusion into an enclosed subcutaneous biosensor, with diffusion lag primarily dependent on capsule thickness. Reichert *et al.* estimated the diffusion rate of glucose (D_{eff}) through fibrous capsule tissue to be ~1.87 x 10^{-6} cm^2s^{-1},[196] which is comparable to the diffusion coefficient of the *DN-25%* membrane (~1.99 x 10^{-6} cm^2s^{-1}).[27] The observed capsule thickness (~25 µm) is relatively insignificant compared to the estimated biosensor membrane wall thickness (~800-1000 µm). Thus, no major inhibition of glucose is predicted to be observed due to the remarkably thin fibrous capsule surrounding these implants.

While there were no significant differences in fibrous capsule thickness between the *DN-25%* and *PEG-DA* implants, a distinction was seen in the cellular organization

within the tissue capsule at 7 days. Since fibrosis occurs in the later stages of the FBR (weeks rather than days),[171] the tissue capsule around the implants at 7 days was primarily an unorganized cellular layer without significant fibrous tissue as expected. However, the innermost cells surrounding the *PEG-DA* implant appeared to be more organized than those near the *DN-25%* implant (**Figure 3-5a**). We hypothesize that the cyclical deswelling/reswelling of the thermoresponsive *DN-25%* surface resulted in a less organized tissue capsule initially. However, this trend did not continue after 30 and 90 days as fibrosis progressed at which both implant types resulted in a highly organized fibrous capsule that was easily distinguishable from the surrounding native tissue (**Figure 3-5a**, **Figure A-11**).

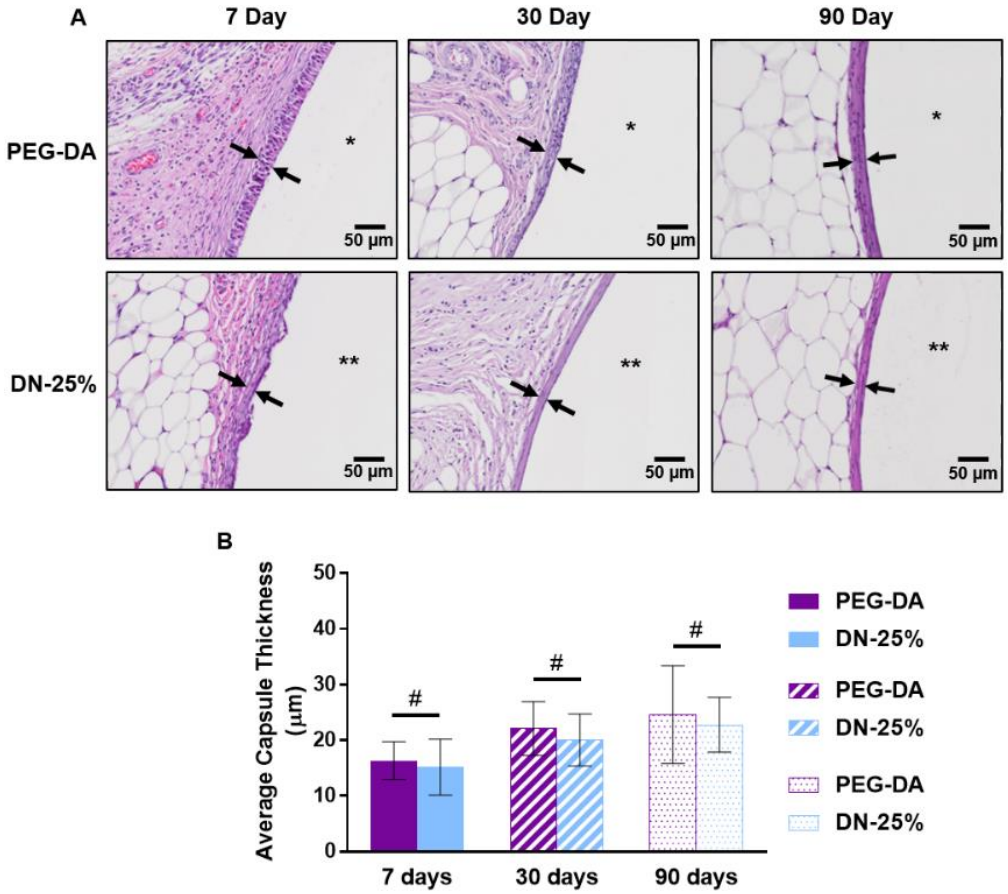

Figure 3-5. Evaluation of fibrous capsule formation around hydrogel implants. (A) H & E stained images representing capsules formed around *PEG-DA* (top, *) and *DN-25%* (bottom, **) implants at 7, 30 and 90 days. Differences in cellular organization near the implants seen only at the 7 day time point. (B) Average fibrous capsule thickness (n = 11) at 7, 30 and 90 days showing statistical similarity (#, $p > 0.05$) between materials at each time point.

To further analyze the composition of the fibrous capsules, the presence of other extracellular matrix (ECM) components was examined, including fibrin and collagen as well as neovascularization. Immediately after implantation, a fibrous scaffolding will begin to develop by the polymerization of fibrinogen into fibrin to aid in healing.[177] Fibrin was observed around the *DN-25%* implants at 7 days and dissipated after 30 and 90 days as expected (**Figure A-12a & A-12c**). Subsequently, activated fibroblasts arriving to

the implant site will produce collagen, which was seen as early as 7 days. Initially, the collagen forms a loose structure that overtime densifies with healing.[171] This densification was observed starting at 30 days (**Figure A-12b & A-12c**) and continued to increase at 90 days (**Figure A-12c**), showing appropriate healing was able to occur around the thermoresponsive *DN-25%* implants, similar to the benchmark *PEG-DA* implants. Moreover, this trend matched the timeline of the cellular response with the highest fibroblast presence at 7 days correlating to a majority of loose collagen and the increase in ratio of fibrocytes to fibroblasts at 30 and 90 days correlating to an increasing presence of dense collagen as fibrosis progresses. Additionally, neovascularization will mainly occur in the early stages of healing and, as the healing proceeds, the amount of vascularization will recede back to the normal levels of the subcutaneous tissue.[177] This expected trend was observed for both *DN-25%* and *PEG-DA* implants, where at 7 days a much higher vascularization was present compared to at 30 and 90 days (**Figure A-12c**). Moreover, as the capsule densified at 30 and 90 days, the tissue was observed to be more avascular nearest the membrane surface around both types of implants (**Figure A-12c**). This low vascular presence confirms the need to minimize the fibrous capsule to avoid inhibition of glucose diffusion.

3.4.5 Healing

Finally, an overall healing score (**Table A-1**), previously established by the CVP lab,[26] was evaluated independently of the aforementioned data as a more general, semi-quantitative analysis of the healing stage at each time point. At 7 days, the *DN-25%* implants scored between a 1 and 2, similar to the *PEG-DA* implants (**Figure 3-6**),

indicating both were undergoing early-stage healing defined by the presence of both fibrin and loose collagen as well as the following dominant cellular components: macrophages, fibroblasts, neutrophils and lymphocytes. No major differences in overall healing were observed between the *DN-25%* implants and the benchmark control at this early time point, possibly due to the acute inflammatory response to injury masking any material-specific differences. However, at 30 days the thermoresponsive *DN-25%* implants showed slightly more advanced healing (score ~5) over the biocompatible *PEG-DA* implants (score ~4). This superior score was mainly due to an increase in dense collagen compared to loose fibrous tissue and a greater presence of fibrocytes compared to fibroblasts surrounding the *DN-25%* implants. Notably, a score of 4 corresponded to a normal healing response seen between days 30-60, whereas a score of 5 represents a mid-stage healing to healed response typically not seen until day 60-90. This indicates that the *DN-25%* membrane showed an enhancement over the expected timeframe for a normal healing response as well as the benchmark biocompatible *PEG-DA* implants. At 90 days, both the *DN-25%* and *PEG-DA* implants reached a nearly healed state, each receiving a similar score of ~5. As expected, at this time point we saw mainly dense collagen with small amounts of loose collagen and mostly fibrocytes along with some remaining macrophages and fibroblasts. Overall, these temporal healing scores agreed well with the qualitative results for fibrous tissue (**Figure A-12c**) and quantitative results for cellular presence (**Figure 3-4**), further confirming the improvement in healing rate seen around the self-cleaning *DN-25%* implants over that of the conventional, passively antifouling *PEG-DA* implants.

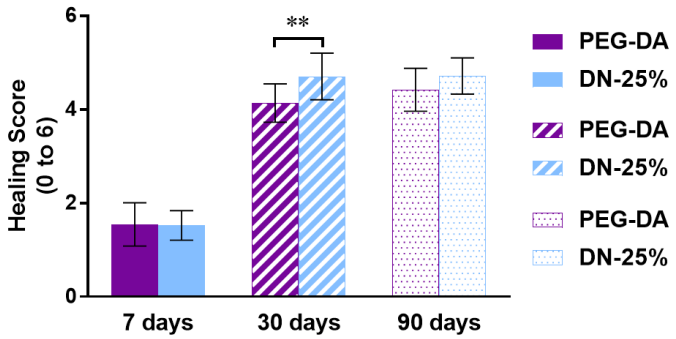

Figure 3-6. Average healing score given to both implant types after 7, 30 and 90 days with a score = 6 indicating fully healed (scores defined in **Table A-1**), where ** indicates a significant difference of $p < 0.01$.

3.5 Conclusions

Towards improving the longevity of subcutaneous glucose biosensors, we have developed a self-cleaning thermoresponsive hydrogel with robust mechanical properties and an ability to minimize the FBR through cyclical deswelling/reswelling stimulated by normal fluctuations in body temperature. Designated as *DN-25%*, this membrane is composed of a tightly crosslinked 1st network of NIPAAm copolymerized with an electrostatic AMPS comonomer at a wt% ratio of 75:25 (NIPAAm:AMPS) and a loosely crosslinked 2nd network of NIPAAm copolymerized with NVP to precisely tune the VPTT. Due to their electrostatic nature and double network structure, *DN-25%* cylindrical implants (~2.5 × 5 mm, diameter × length) achieved substantially higher strength (>25x) and toughness (>30x) than the conventional *PEG-DA* hydrogel implants (i.e. a benchmark biocompatible control) while maintaining the same order of stiffness (i.e. modulus) as both *PEG-DA* and the surrounding subcutaneous tissue. Thus, the *DN-25%* membrane provides durability without increasing the modulus, avoiding increasing the severity of the FBR due to mechanical mismatch with the native tissue. At 30 and 90 days post-implantation

into the subcutaneous tissue of rats, the *DN-25%* implants showed milder inflammation as well as an accelerated healing response versus the well-established biocompatible *PEG-DA* implants. Notably, at these time points, a significantly lower number of macrophages and a higher ratio of fibrocytes to fibroblasts were observed surrounding the *DN-25%* implants. Thus, the self-cleaning *DN-25%* membranes demonstrated the potential to promote more effective resolution of inflammation than current passively antifouling membranes, such as *PEG-DA* implants. By 90 days, an extremely thin fibrous capsule of only ~20-25 μm formed around the *DN-25%* implants, similar to that of the *PEG-DA* implants. This unique combination of a reduction in highly-metabolizing macrophages and the thin surrounding capsule is predicted to better maintain glucose diffusion through the *DN-25%* membrane. In summary, this self-cleaning membrane provides an opportunity to improve subcutaneous glucose biosensor longevity due to its robust mechanical properties and ability to minimize the FBR.

CHAPTER IV

THERMORESPONSIVE DOUBLE NETWORK HYDROGELS WITH EXCEPTIONAL COMPRESSIVE MECHANICAL PROPERTIES*

4.1 Overview

The utility of thermoresponsive hydrogels, such as those based on poly(*N*-isopropylacrylamide) (PNIPAAm), is severely limited by their deficient mechanical properties. In particular, the simultaneous achievement of high strength and stiffness remains unreported. In this work, a thermoresponsive hydrogel is prepared having the unique combination of ultra-high compressive strength (~23 MPa) and excellent compressive modulus (~1.5 MPa) (**Figure 4-1**). This is accomplished by employing a double network (DN) design comprised of a tightly crosslinked, highly negatively charged 1st network based on poly(2-acrylamido-2-methylpropane sulfonic acid (PAMPS) and a loosely crosslinked, zwitterionic 2nd network based on a copolymer of thermoresponsive NIPAAm and zwitterionic [2-(methacryloyloxy)ethyl]dimethyl-(3-sulfopropyl) ammonium hydroxide (MEDSAH). Comparison to other DN designs reveals that this PAMPS/P(NIPAAm-*co*-MEDSAH) DN hydrogel's remarkable properties stem from the intra- and inter-network ionic interactions of the two networks. Finally, this mechanically

*Reprinted with permission from "Thermoresponsive double network hydrogels with exceptional compressive mechanical properties" by Means, A.K.; Ehrhardt D.A.; Whitney L.V.; and Grunlan, M.A., Macromol. Rapid Commun., 2017, 37, 1972-1977, Copyright [2017] by John Wiley and Sons.

robust hydrogel retains the desirable thermosensitivity of PNIPAAm hydrogels, exhibiting a volume phase transition temperature (VPTT) of ~35 °C.

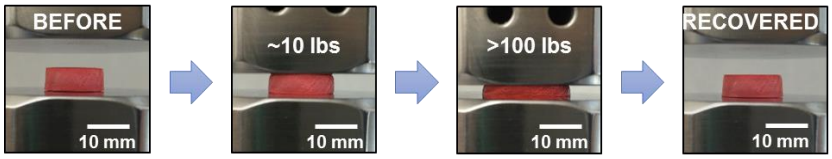

Figure 4-1. Photo series of the compression and recovery of thermoresponsive DN hydrogels under a load of >100 lbs.

4.2 Introduction

The development of thermoresponsive hydrogels with combined stiffness and strength could greatly broaden the utility of hydrogels for applications such as actuators[197-199], soft robotics[25, 200, 201], biosensors[202, 203], drug delivery[8, 204] and tissue engineering[205, 206]. Thermoresponsive hydrogels are 3-dimensional, water swollen polymer networks with the ability to undergo a thermally-triggered, reversible volume change. Poly(*N*-isopropylacrylamide) (PNIPAAm), an extensively studied thermoresponsive polymer, exhibits a lower critical solution temperature (LCST, ~32 °C). Similarly, crosslinked PNIPAAm hydrogels exhibit a volume phase transition temperature (VPTT, ~33-35 °C), above which the hydrogels collapse into a temporary hydrophobic, deswollen state. Subsequently, by cooling below the VPTT, the hydrogels can fully recover their initial hydrophilic, swollen state.[207] Their VPTT near body temperature makes PNIPAAm hydrogels ideal for many biomedical applications.

Currently, PNIPAAm hydrogels are primarily limited by their poor mechanical properties, with modulus and strength values in the sub-MPa range.[47, 105] Many studies have evaluated ways to improve the mechanical properties of hydrogels, including altering the network structure.[31, 77, 78, 208, 209] Specifically, double network (DN) hydrogels, a type of interpenetrating polymer network (IPN), are distinguished by their asymmetrically crosslinked networks.[79] Gong *et al.* first reported non-thermoresponsive DN hydrogels comprised of a tightly crosslinked, highly negatively charged 1st network composed of poly(2-acrylamide-2-methyl-propane sulfonic acid) (PAMPS) and a sparsely crosslinked, neutral 2nd network composed of poly(acrylamide) (PAAm).[31] Such PAMPS/PAAm DNs achieved ultra-high compressive strength due to the ability of the loose 2nd network to dissipate the stress concentrations in the rigid 1st network that would typically lead to early fracture.[79]

A limitation of existing hydrogel designs, including DNs, is the decrease in modulus which typically accompanies an increase in strength and vice versa. For example, the aforementioned PAMPS/PAAm DN hydrogel achieved ultra-high compressive strength (~17 MPa) but its modulus was somewhat low (~0.3 MPa).[31, 210] Non-thermoresponsive bacterial cellulose/polyacrylamide (BC/PAAm) DN hydrogels exhibited a high compressive modulus (~20 MPa), but their strength was limited (~6 MPa).[100] Towards improving the mechanical properties of thermoresponsive PNIPAAm hydrogels, we recently prepared DNs based on a tightly crosslinked, negatively charged 1st network of P(NIPAAm-*co*-AMPS) containing a 25:75 wt% ratio of NIPAAm:AMPS and a loosely crosslinked, interpenetrating 2nd network of PNIPAAm.

While this P(NIPAAm-*co*-AMPS)/PNIPAAm DN hydrogel conveniently maintained a "PNIPAAM-like" VPTT of ~33 °C as well as ultra-high compressive strength (~17 MPa), the modulus was quite low (~0.09 MPa).[76]

Zwitterionic polymers have gained increased interest due to unique properties that arise from monomer units that have both positively and negatively charged functional groups but retain an overall neutral charge.[211] A widely studied zwitterionic polymer, poly([2-(methacryloyloxy)ethyl]dimethyl(3-sulfopropyl)ammonium hydroxide) (PMEDSAH), has monomeric units comprised of a cationic ammonium group and an anionic sulfonate group.[212] Their zwitterionic charge results in not only high hydration,[213, 214] but also the potential to improve mechanical properties through physical intra- and inter-chain electrostatic interactions.[215, 216]

In this work, thermoresponsive DN hydrogels were prepared with a tightly crosslinked, highly negatively charged PAMPS 1st network and a loosely crosslinked, zwitterionic P(NIPAAm-*co*-MEDSAH) 2nd network (**Figure 4-2**). In addition to the aforementioned electrostatic interactions, we hypothesized that such a PAMPS/P(NIPAAm-*co*-MEDSAH) DN hydrogel would yield strong, electrostatic attractive forces between the anionic sulfonate groups of PAMPS and the cationic ammonium groups of MEDSAH (**Figure 4-2: inset**). In fact, a previous report noted that linear polymers comprised of these two functional groups underwent gelation due to such attractive forces.[92] Moreover, while these ionic interactions between the 1st and 2nd network would effectively increase crosslink density, their physical rather than covalent nature was anticipated to avoid mechanical brittleness. Finally, it was predicted that this

type of zwitterionic DN hydrogel would maintain a VPTT near that of PNIPAAm hydrogels if MEDSAH was incorporated into the 2nd network at low levels.[217-219] Ultimately, a PAMPS/P(NIPAAm-*co*-MEDSAH) DN hydrogel reported herein achieved a rare combination of ultra-high compressive strength (~23 MPa) and an excellent modulus (~1.5 MPa) that is nearly triple that of other ultra-strong hydrogels.[31, 77, 209] Additionally, this DN hydrogel was able to undergo appreciable strain (~85%) before fracture and maintained a VPTT of ~35 °C.

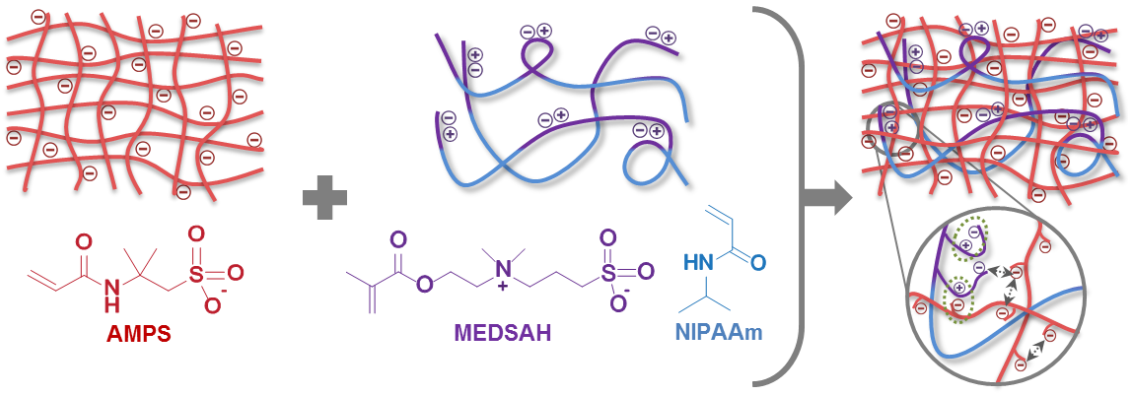

Figure 4-2. Thermoresponsive PAMPS/P(NIPAAm-*co*-MEDSAH) DN hydrogels formed with a tightly crosslinked, anionic PAMPS 1st network and a loosely crosslinked, thermoresponsive 2nd network comprised of NIPAAm copolymerized with MEDSAH. Inset: A variety of ionic interactions exist within and between the 1st and 2nd networks that effectively serve as reversible crosslinks (circled), thereby simultaneously enhancing strength and modulus.

4.3 Experimental Section

4.3.1 Materials

N-Isopropylacrylamide (NIPAAm, 97%), 2-acrylamido-2-methylpropane sulfonic acid (AMPS, 97%), [2-(methacryloyloxy)ethyl]dimethyl-(3-sulfopropyl)ammonium

hydroxide (MEDSAH, 97%), 3-(acrylamidopropy)trimethylammonium chloride solution (AAPTAC, 75 wt% in H_2O). *N*,*N*'-methylenebisacrylamide crosslinker (BIS, 99%) and 2-oxoglutaric acid photo-initiator were obtained from Sigma Aldrich. For hydrogel fabrication, deionized water (DI) with a resistance of 18 MΩ·cm (Cascada LS MK2, Pall) was used.

4.3.2 Preparation of DN hydrogels

DN hydrogels were fabricated through a two-step process. First, a single network (SN) hydrogel was formed via the *in situ* photo-cure of the SN precursor solution. The SN hydrogel was immediately soaked in and swollen with the DN precursor solution. Next, the DN hydrogel was formed by a subsequent photo-cure of the swollen SN hydrogel.

The SN precursor solutions for compositions containing varying AMPS monomer content consisted of AMPS (ranging from 0.5-2.0 M), BIS crosslinker (4 mol%), 2-oxoglutaric acid (0.1 mol%), and DI water. The precursor solution was injected between two glass slides separated by 1 mm thick spacers and exposed to UV light (UV-transilluminator, 6 mW cm^{-2}, 365 nm) for 5 h. The SN hydrogel was removed from the mold and immediately immersed in the DN precursor solution for 48 h at 4 °C. The DN precursor solution consisted of NIPAAm (2.0 M), BIS (0.1 mol%), 2-oxoglutaric acid (0.1 mol%), and DI water. After soaking, the hydrogel was enclosed with two glass slides separated by varying sized spacers depending on extent of swelling of SN hydrogels (1.25-2.5mm) and then exposed to UV light for 5 h while submerged in an ice bath (~7 °C). The resulting DN hydrogels were then removed from the molds and soaked in DI water for 1 week before testing.

DN hydrogels containing zwitterionic comonomer were fabricated similar to above. However, the AMPS concentration in the SN was held constant at 1.5 M and the zwitterionic comonomer, MEDSAH, was incorporated from 5-15 wt% with respect to NIPAAm wt. Specifically, the SN precursor solution consisted of AMPS (1.5 M), BIS (4 mol%), 2-oxoglutaric acid (0.1 mol%), and DI water. The DN precursor solutions with varying zwitterionic comonomer content consisted of NIPAAm (2.0 M), MEDSAH (5-15 wt%), BIS (0.1 mol%), 2-oxoglutaric acid photo-initiator (0.1 mol%), and DI water.

4.3.3 Compressive Modulus and Strength

The compressive mechanical properties were evaluated with an Instron 3340 at RT. Hydrogels were punched into 3 discs (6 mm diameter) with a die. Each disc was blotted to remove surface water and then placed between the parallel plates with an initial pre-load force of 0.5 N. The hydrogel was compressed at a constant strain rate of 1 mm min^{-1} until fracture. The elastic compressive modulus (E) was obtained from the slope of the linear portion of the stress-strain curve from 0 to 10% strain. The ultimate compressive strength (σ_f) and the % strain at break (ε_f) were defined respectfully as the stress and strain values at the point of fracture.

4.4 Results and Discussion

Towards achieving a thermoresponsive DN hydrogel with combined strength and stiffness, we systematically evaluated the concentration of AMPS in the 1st network and the concentration of MEDSAH in the 2nd network. First, a series of PAMPS/PNIPAAm DN hydrogels were prepared with variable AMPS monomer concentrations to form the 1st network and with a PNIPAAm-only 2nd network (2.0 M NIPAAm; no MEDSAH) (**Table**

4-1, **Figure A-13**). To assess their mechanical properties, a constant compressive strain was applied until fracture. As the concentration of AMPS was increased from 0.5-2.0 M, the compressive modulus increased from <0.5 to ~2.5 MPa (**Figure 4-3a**, **Table A-3**). This is attributed to an increase in electrostatic repulsive forces, which lead to chain expansion and increase in effective crosslink density, as well as the slight decrease in hydration stemming from an increased hydrogel concentration. Although modulus continuously increased with increasing AMPS concentration, strength reached a maximum with 1.5 M AMPS in the 1st network (~14 MPa) (**Figure 4-3b**, **Table A-3**). Thus, despite the presence of a loosely crosslinked 2nd network, a higher concentration of AMPS reduced the DN's ability to dissipate stress, thereby decreasing strength. Additionally, the mechanical behavior of this "1.5-AMPS-0%" DN hydrogel was demonstrated to be unique versus that of its independent, 1st and 2nd network components: a single network (SN) of 1.5 M AMPS ("1.5-AMPS SN"'; i.e. the 1st network) and a SN of 2.0 M NIPAAm ("2-NIPAAm-SN"; i.e. the 2nd network) (**Figure 4-3c**). Specifically, the "1.5-AMPS-0%" DN hydrogel displayed higher modulus and much higher strength versus the constituent hydrogels while still also able to undergo appreciable strain (~79%) prior to fracture. Moreover, all PAMPS/PNIPAAm DN hydrogels, irrespective of the concentration of AMPS in the 1st network, maintained a VPTT characteristic of PNIPAAm hydrogels (~35 °C, **Table 4-1**).

Table 4-1. Hydrogel compositions listing values for equilibrium water content and VPTT.

	1st Network[a)]		2nd Network[b)]	Equilibrium Water Content (%)	VPTT[c)]	
Nomenclature (X-AMPS-Y)	AMPS (X)	NIPAAm	MEDSAH (Y) (wt% of NIPAAm)	DN	T_o [°C]	T_{max} [°C]
PAMPS/PNIPAAm DNs:						
0.5-AMPS-0%	0.5 M	2.0 M	0 wt%	95.4 ± 0.28	33.0	34.2
1.0-AMPS-0%	1.0 M	2.0 M	0 wt%	89.2 ± 0.16	32.5	34.7
1.5-AMPS-0%	1.5 M	2.0 M	0 wt%	85.0 ± 0.06	31.8	34.8
2.0-AMPS-0%	2.0 M	2.0 M	0 wt%	81.9 ± 0.34	31.0	34.5
PAMPS/(PNIPAAm-*co*-MEDSAH) DNs:						
1.5-AMPS-5%	1.5 M	2.0 M	5 wt%	84.1 ± 0.12	31.5	35.3
1.5-AMPS-10%	1.5 M	2.0 M	10 wt%	84.2 ± 0.10	31.0	35.0
1.5-AMPS-15%	1.5 M	2.0 M	15 wt%	83.3 ± 0.08	31.5	35.1

[a)]4 mol% BIS crosslinker, 0.1 mol% 2-oxoglutaric acid initiator;
[b)]0.1 mol% BIS crosslinker, 0.1 mol% 2-oxoglutaric acid initiator;
[c)]VPTT: T_o (onset) and T_m (maximum) temperature.

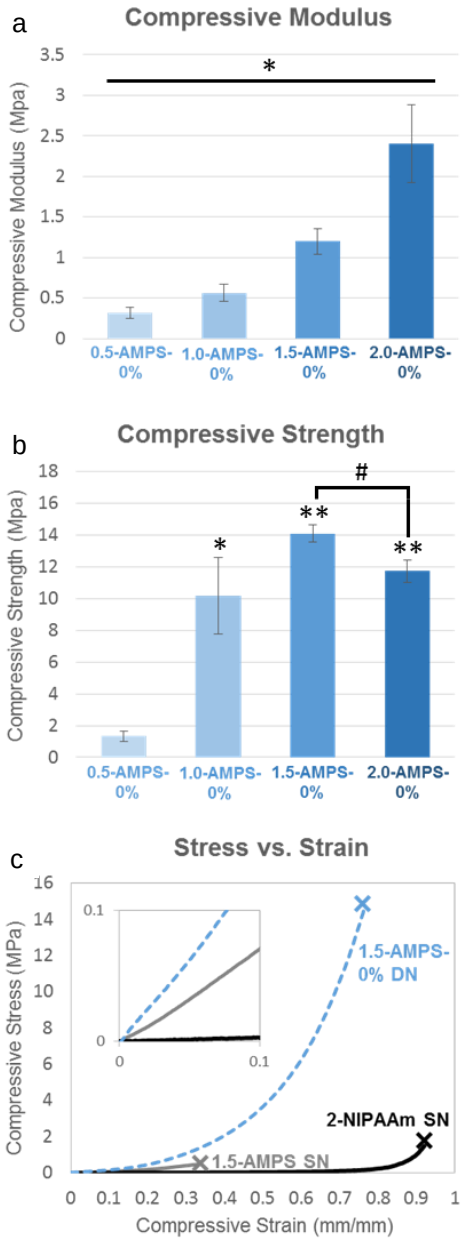

Figure 4-3. Mechanical properties of the PAMPS/PNIPAAm DN hydrogel series (i.e. no MEDSAH). Graphs include: (a) Compressive modulus [significant difference between all indicated by * ($p < 0.05$)], (b) compressive strength [significant difference from 0.5-AMPS-0% indicated by * ($p < 0.05$) and ** ($p < 0.01$); significant difference between 1.5-AMPS-0% and 2.0-AMPS-0% indicated by # ($p < 0.05$)] and (c) representative stress vs. strain curves "1.5-AMPS-0%" DN hydrogel versus independent, 1st and 2nd network components: a single network (SN) of 1.5 M AMPS ("1.5-AMPS SN"'; i.e. the 1st network) and a SN of 2.0 M NIPAAm ("2-NIPAAm-SN"; i.e. the 2nd network).

Next, a series of PAMPS/P(NIPAAm-*co*-MEDSAH) DN hydrogels were formed in which the 1st network maintained a 1.5 M AMPS concentration (based on the above results) and the 2nd network was formed with varying levels of MEDSAH copolymerized with NIPAAm (5-15 wt% based on NIPAAm) (**Table 4-1**, **Figure 4-2**). For these DN hydrogels, only "1.5-AMPS-15%" (i.e. 15 wt% MEDSAH) exhibited a somewhat higher compressive modulus (~1.53 MPa) versus "1.5-AMPS-0%" (i.e. no MEDSAH; ~1.20 MPa) (**Figure 4-4a**, **Table A-3**). Additionally, "1.5-AMPS-15%" exhibited substantially higher compressive strength (~23 MPa) versus "1.5-AMPS-0%" (~14 MPa) (**Figure 4-4b**, **Table A-3**). This DN hydrogel also withstood ~85% strain prior to fracture, increased from that of "1.5-AMPS-0%" (~79% strain) (**Figure 4-3c**, **Table A-3**). As previously noted, this DN hydrogel's combination of modulus and strength is quite notable.[31, 76, 100, 210] Moreover, increasing the MEDSAH from 15 wt% to 20, 25 and 30 wt% (based on NIPAAm) resulted in DN hydrogels with relatively diminished compressive modulus and strength (**Table A-3**, **Figure A-14**). Finally, despite its hydrophilicity, introduction of 5 – 15 wt% MEDSAH into the 2nd network did not cause the VPTT to shift above ~35 °C and both the rate of deswelling (T > VPTT) and reswelling (T < VPTT) remained similar to "1.5-AMPS-0%" (**Figure A-15 & A-16**).

To investigate if the zwitterionic component (MEDSAH) was uniquely able to produce this combination of high modulus and ultra-high strength observed for "1.5-AMPS-15%", two analogous DN hydrogels were prepared in which the 15 wt% MEDSAH (based on NIPAAm) of the 2nd network was replaced with either a cationic monomer [(3-acrylamidopropyl)trimethylammonium chloride (AAPTAC)] or an anionic

monomer [AMPS] (**Table A-3**, **Figure A-14**). In this way, these DNs were similarly comprised of a highly crosslinked and negatively charged PAMPS 1st network. When combined with a positively charged P(NIPAAm-*co*-AAPTAC) 2nd network, electrostatic attractive forces with the 1st network were expected to form. In contrast, when combined with a negatively charged P(NIPAAm-*co*-AMPS) 2nd network, electrostatic repulsive forces with the 1st network should have developed. Despite these ionic interactions between the networks, the resulting DNs did not achieve the simultaneous increase in strength and modulus observed for the "1.5-AMPS-15%" DN hydrogel. For the AAPTAC-based DN, while compressive strength was similar to "1.5-AMPS-15%", modulus was substantially diminished (~0.4 MPa). Conversely, for the AMPS-based DN, the compressive modulus was similar but strength was substantially reduced (~7.8 MPa). For "1.5-AMPS-15%", the zwitterionic nature of its 2nd network, versus an analogous cationic or anionic 2nd network, is unique in its ability to achieve ultra-high strength and an excellent modulus. In this way, the mechanical properties of "1.5-AMPS-15%" is believed to stem from the specific types of intra- and inter-network charge-charge interactions of the two networks (**Figure 4-2: inset**).

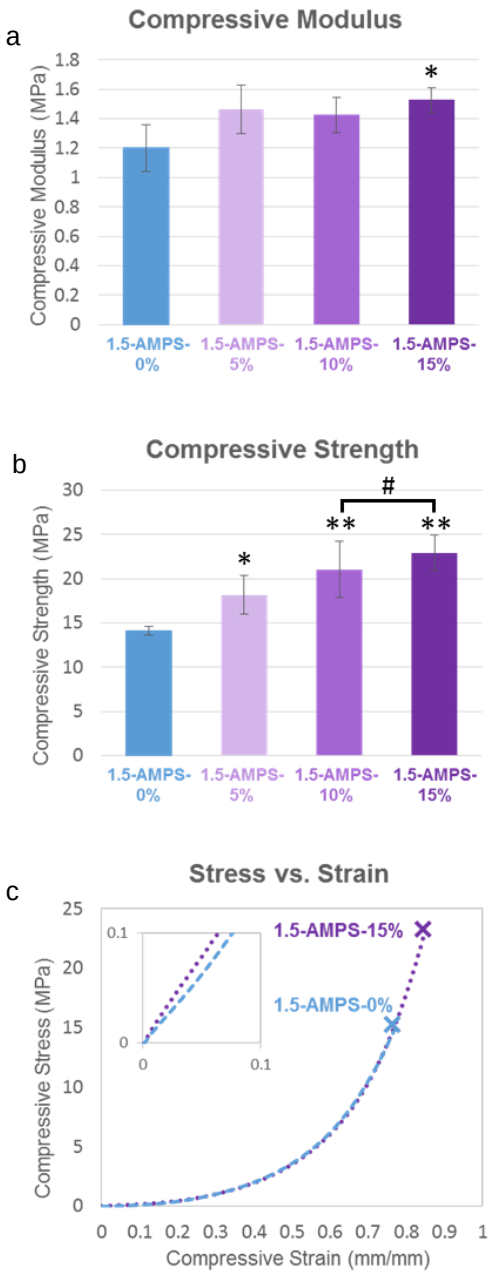

Figure 4-4. Mechanical properties of the PAMPS/P(NIPAAm-*co*-MEDSAH) hydrogel series. Graphs include: (a) Compressive modulus [significant difference from 1.5-AMPS-0% indicated by * ($p = 0.05$)], (b) compressive strength [significant difference from 1.5-AMPS-0% indicated by * ($p < 0.05$) and ** ($p < 0.01$); similarity of 1.5-AMPS-10% to 1.5-AMPS-15% indicated by # ($p > 0.05$)] and (c) representative stress vs. strain curves demonstrating the enhanced strength and modulus gained from the addition of MEDSAH into the 1.5-AMPS-0% DN hydrogel from the 1st series.

4.5 Conclusions

In summary, this work led to a thermoresponsive DN hydrogel ("1.5-AMPS-15%") with the unusual combination of ultra-high compressive strength (~23 MPa) and a compressive modulus nearly triple that of other ultra-strong hydrogels (~1.5 MPa). This was achieved through a PAMPS/P(NIPAAm-*co*-MEDSAH) DN design comprised of a tightly crosslinked, highly negatively charged PAMPS 1st network and a loosely crosslinked, zwitterionic P(NIPAAm-*co*-MEDSAH) 2nd network. Towards achieving these mechanical properties, these studies demonstrated the necessity to optimize both the molar concentration of AMPS in the 1st network (1.5 M) as well as the MEDSAH content in the 2nd network (15 wt% based on NIPAAm). Its unique mechanical behavior is believed to stem from the zwitterionic nature of the 2nd network which provides additional electrostatic attractive forces between the anionic sulfonate groups of the PAMPS 1st network and the cationic ammonium groups of the P(NIPAAm-*co*-MEDSAH) 2nd network. These intra- and inter-network electrostatic interactions effectively provided reversible crosslinks such that this DN hydrogel was not brittle and underwent appreciable strain (~85%) before fracture. Additionally, because relatively low levels of MEDSAH were copolymerized with NIPAAm in the 2nd network, the VPTT remained "PNIPAAm-like" at ~35 °C which is useful for biomedical applications. Thus, this PAMPS/P(NIPAAm-*co*-MEDSAH) DN design provides an opportunity to expand the utility and efficacy of thermoresponsive hydrogels in a variety of smart material applications.

CHAPTER V

DOUBLE NETWORK HYDROGELS THAT MIMIC THE MODULUS, STRENGTH AND LUBRICITY OF CARTILAGE

5.1 Overview

The development of a hydrogel-based synthetic cartilage has the potential to overcome many limitations of current chondral defect treatments. Many efforts have attempted to replicate the unique characteristics of cartilage in hydrogels, but none simultaneously achieved high modulus, strength and toughness while maintaining the necessary hydration required for lubricity. Herein, double network (DN) hydrogels, composed of a poly(2-acrylamido-2-methylpropane sulfonic acid) (PAMPS) 1st network and a poly(*N*-isopropyl-acrylamide-*co*-acrylamide) [P(NIPAAm-*co*-AAm)] 2nd network, are evaluated as a potential off-the-shelf material for cartilage replacement. While predominantly used for its thermosensitivity, PNIPAAm is employed to achieve superior mechanical properties and its thermal transition temperature tuned above the physiological range. These PNIPAAm-based DNs demonstrate a 50-fold increase in compressive strength (~25 MPa, similar to cartilage) compared to traditional single network hydrogels while also achieving a cartilage-like modulus (~1 MPa) and hydration (~80%). By directly comparing to healthy cartilage (porcine), these hydrogels are confirmed not only to parallel the strength, modulus and hydration of native articular cartilage but also exhibit a 50% lower coefficient of friction (COF) (**Figure 5-1**). The exceptional cartilage-like properties of the PAMPS/P(NIPAAm-*co*-AAm) DN hydrogels makes them candidates for

synthetic cartilage grafts for chondral defect repair, even in load-bearing regions of the body.

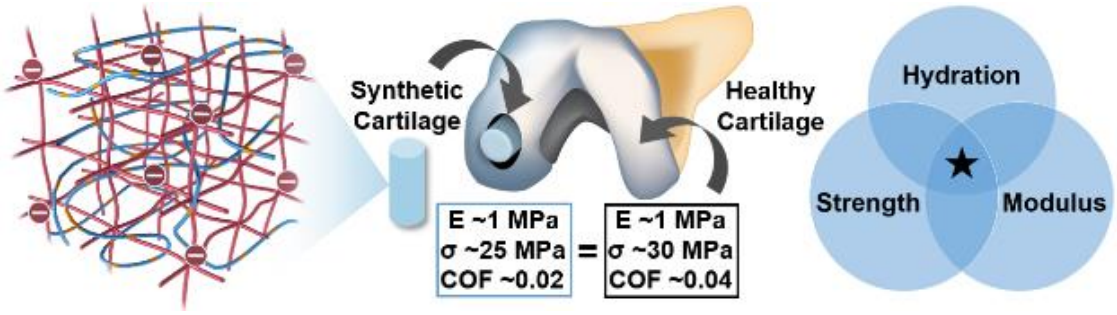

Figure 5-1. Summary of cartilage-mimetic properties, including modulus (E), strength (σ) and coefficient of friction (COF), of the synthetic hydrogel versus healthy cartilage.

5.2 Introduction

Articular cartilage provides a robust interface that minimizes friction between bones in load-bearing joints.[220] When this tissue is damaged, it can induce pain, reduced joint movement and potentially lead to degenerative joint disease or osteoarthritis (OA).[221] Although progress has been made towards the treatment of chondral and osteochondral defects, significant challenges remain due to its poor healing capacity.[222] Current treatments for articular cartilage defects include microfracturing, autologous chondrocyte implantation (ACI) and osteochondral autograft transplantation (OATS) (i.e. mosaicplasty).[223-226] Microfracturing has shown success in restoring joint function; although, the newly formed fibrocartilage has limited mechanical properties compared to native hyaline cartilage making it susceptible to re-injury. ACI has emerged as a viable method to regenerate hyaline-like cartilage, however it requires an expensive, 2-stage

procedure.[226] When a more regenerative approach (e.g. microfracturing and ACI) is not applicable, due to damage or disease of the underlying bone, a replacement strategy such as OATS must be taken.[227] Although autografting has a notably high success rate, it suffers from many limitations such as donor site morbidity, defect size (~1-4 cm^2), patient age (< ~50 years) and tissue availability.[226-228] If these treatments fail, a total knee replacement (TKR) is required which entails a costly, intensive surgery. Currently, the number of TKRs is projected to grow to > 3 million procedures by 2030 in the United States alone.[229, 230] More recently, techniques such as focal resurfacing have developed as a synthetic cartilage replacement of the localized defect area. These BioPoly® implants utilize a titanium anchoring pin capped with an UHMWPE-based surface which avoids the biological limitations of autografts and provides a treatment that does not rely on the regeneration of hyaline cartilage.[231] Although studies on focal resurfacing have shown promise so far, the inherent mechanical mismatch between the metallic/hard plastic device and the surrounding osteochondral tissue are associated with complications (e.g. stress-shielding).

Towards improving the treatment of cartilage defects, we propose to bridge the gap between focal resurfacing and OATS by developing a cartilage-mimetic, synthetic hydrogel. Conventional hydrogels are not suitable for load-bearing applications due to their relatively poor mechanical properties.[7, 232] For example, Cartiva® is a commercially available hydrogel-based synthetic cartilage implant composed of poly(vinyl alcohol) (PVA), but it is thus far only FDA-approved for use in the toe joints (i.e. low weight-bearing joints).[233] Remarkable progress was seen with the introduction

of double network (DN) hydrogels, originally reported by Gong *et al.*,[31] which have achieved notable strengths in the MPa range. Although great strides have been made in strengthening hydrogels, most do not exhibit the high moduli and/or water content equal to that of articular cartilage tissue.[39, 46, 59, 65, 68-72, 104, 234, 235] This inability of hydrogels to simultaneously mimic the strength, modulus and hydration of cartilage is shown in **Figure 5-2**, in which the properties of native porcine articular cartilage tested herein are plotted alongside previously reported ultra-strong hydrogels.[31, 46, 59, 68-72, 104]

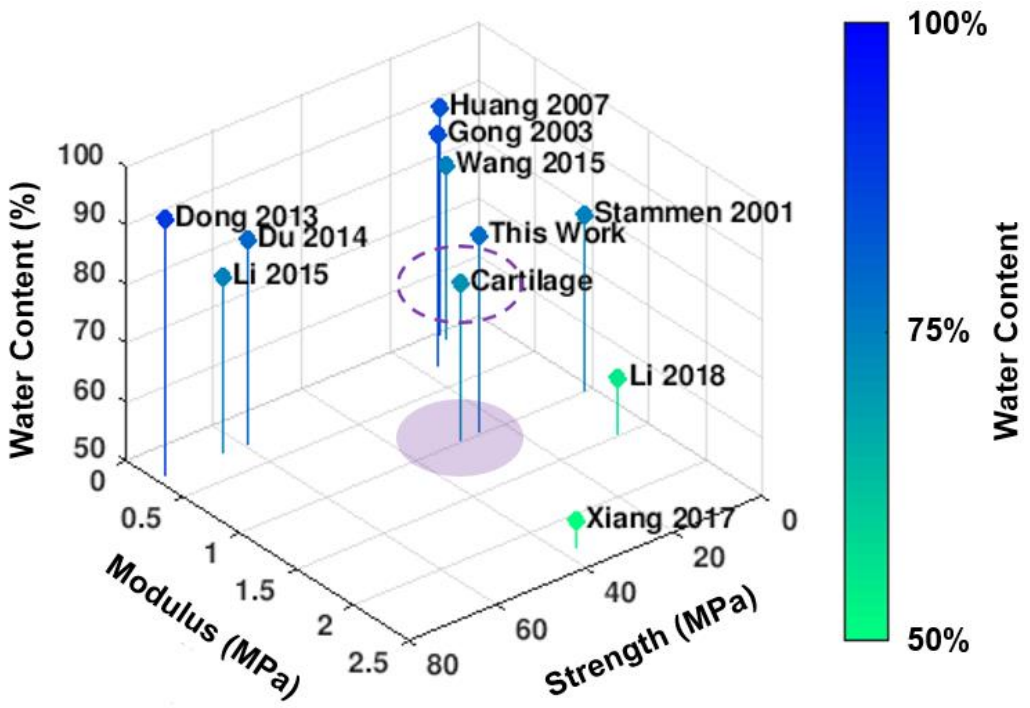

Figure 5-2. A summary of previously reported ultra-strong hydrogels alongside porcine cartilage demonstrating the unique ability of the PAMPS/P(NIPAAm-*co*-AAm) DN hydrogels ("This Work") to exhibit high modulus, strength and hydration similar to that of articular cartilage (circled in purple).[31, 46, 59, 68-72, 104]

Mimicking the native cartilage deformation/recovery response is also important to avoid any imbalance in contact stress surrounding the synthetic implant.[236] Thus, beyond the general mechanical properties such as modulus and strength, similar viscoelastic behavior and lubricity is essential for a synthetic cartilage material. Typical ultra-strong hydrogels, due to their low moduli (**Figure 5-2**), exhibit much greater deformation than cartilage at a similarly applied stress.[31, 39, 46, 65, 68-71] This mechanical mismatch can lead to stress concentration at the defect edges and potentially failure of the implant-tissue interface. Additionally, the primary function of cartilage tissue is to provide a lubricious surface to minimize friction during reticulation of joints.[220] Although hydrogels are known as a class of materials with high lubricity, current methods to enhance their compressive modulus typically result in a decrease in water content and a subsequent reduction in lubricity.[36, 72, 90, 101, 237, 238] To overcome this, one approach utilized a bilayer hydrogel design with a robust, low water content region and a lubricious, high water content region with reduced mechanical properties as the low friction surface.[239] However, the cartilage-mimetic DN hydrogel reported herein is intended to achieve all requisite properties, including strength, modulus, hydration and lubricity, without the need for a bilayer system that could suffer from delamination or damage to the soft, lubricious layer.

In our previous work, we demonstrated DN hydrogels that simultaneously achieved both high strength (~23 MPa) and stiffness (~1.5 MPa) without compromising water content (> 80%).[74] These membranes consisted of a tightly crosslinked, anionic

poly(2-acrylamido-2-methylpropane sulfonic acid) (PAMPS) network interpenetrated by a loosely crosslinked, zwitterionic poly(*N*-isopropylacrylamide-*co*-[2-(methacryloyloxy) ethyl] dimethyl-(3-sulfopropyl) ammonium hydroxide) [P(NIPAAm-*co*-MEDSAH)] network that utilized intra- and inter-chain electrostatic interactions to enhance the compressive mechanical properties. Due to PNIPAAm's thermosensitivity, such DN hydrogels with volume phase transition temperatures (VPTT) ~35 °C would experience shrinkage upon implantation as a synthetic cartilage graft and would not statically remain in a fully swollen state due to local temperature fluctuations. This dimensional instability could potentially cause implant loosening with variations in local body temperature.

Herein, we have developed cartilage-mimetic DN hydrogels comprised of asymmetrically crosslinked networks of PAMPS and NIPAAm copolymerized with acrylamide (AAm) [P(NIPAAm-*co*-AAm)]. The VPTTs of the DNs were progressively tuned above normal physiologic temperatures, establishing dimensional stability in a physiological environment (i.e. a lack of deswelling/reswelling). Notably, NIPAAm was utilized for its ability to enhance the stiffness of the DN hydrogels rather than its prominent use as a thermosensitive polymer. This stiffening phenomenon has been demonstrated previously in AAm-based semi-interpenetrating network (semi-IPN) hydrogels, in which physical interactions between the PNIPAAm chains were shown to increase the apparent crosslink density and thus, stiffness at all temperature ranges (i.e. above and below the VPTT).[105] In this work, key properties of the PAMPS/P(NIPAAm-*co*-AAm) DNs, including water content, modulus, strength and toughness, were evaluated to determine their potential as synthetic cartilage candidates. Additionally, the viscoelastic behavior of

the DN hydrogels was analyzed through observing the creep response to an applied load. Finally, the coefficient of friction (COF) was measured to determine the lubricity of the hydrogels. To enable a direct comparison, all mechanical testing was likewise performed on harvested articular cartilage (porcine). Through the material design and subsequent testing, the goal of this work was to develop a material that closely mimics native cartilage to act as a synthetic replacement strategy to avoid the disadvantages of current autografting treatments as well as the large mechanical mismatch of recent focal resurfacing techniques.

5.3 Experimental Section

5.3.1 Materials

N-Isopropylacrylamide (NIPAAm, 97%), 2-acrylamido-2-methylpropane sulfonic acid (AMPS, 97%), acrylamide (AAm, >99%), 3-(acrylamidopropyl)trimethylammonium chloride solution (AAPTAC, 75 wt% in H_2O), *N*,*N*'-methylenebisacrylamide crosslinker (BIS, 99%) and 2-oxoglutaric acid photo-initiator, sodium azide (≥99.5%) and ethylene-diaminetetraacetic acid (EDTA) disodium salt dihydrate were obtained from Sigma-Aldrich. For hydrogel fabrication, deionized water (DI) with a resistance of 18 MΩ·cm (Cascada LS MK2, Pall) was used. Phosphate-buffered saline (PBS, 1X, pH 7.4, without calcium and magnesium), lactate dehydrogenase (LDH) cytotoxicity assay kit (Pierce™) and fetal bovine serum (FBS, Hyclone) were obtained from Fisher Scientific. Antibiotic solution (100X) (stabilized bioreagent sterile filtered with 10,000 units of penicillin and 10 mg of streptomycin per mL), sodium bicarbonate ($NaHCO_3$) and Dulbecco's Modified Eagle's Medium (DMEM) (1000 mg dL^{-1} glucose and L-glutamine without Na_2CO_3 and

phenol red) were purchased from Sigma-Aldrich. Mesenchymal progenitor cells C3H/10T1/2, Clone 8 (CCL226™) were obtained from the American Type Culture Collection (ATCC®).

5.3.2 DN Hydrogel Fabrication

DN hydrogels were fabricated through a two-step, UV-cure process in which single network (SN) hydrogels are soaked in a 2nd network precursor solution and subsequently cured to form an interpenetrating network hydrogel. The SN precursor solutions consisted of AMPS (1.5 M), BIS crosslinker (4 mol%) and 2-oxoglutaric acid (0.1 mol%) in DI water. The precursor solution was injected between two glass slides separated by 1 mm thick spacers and exposed to UV light (UV-transilluminator, 6 mW cm^{-2}, 365 nm) for 5 hr. The SN hydrogel was removed from the mold and immediately immersed in the DN precursor solution for 48 h at 4 °C. The DN precursor solution consisted of NIPAAm (2.0 M), BIS (0.1 mol%) and 2-oxoglutaric acid (0.1 mol%) in DI water with varying amounts of a hydrophilic comonomer (AAm, 0-15 wt% w.r.t. NIPAAm). After soaking, the hydrogel was enclosed with two glass slides separated by spacers (~1.25 mm) and then exposed to UV light for 5 hr while submerged in an ice bath (~7 °C). The resulting DN hydrogels were then removed from the molds and soaked in DI water for 1 week before testing. As supplementary controls, anionic AMPS, cationic AAPTAC or additional NIPAAm were incorporated at 10 wt% w.r.t. NIPAAm as comonomers in the 2nd network instead of AAm and prepared similarly. Finally, an AAm-only control was also prepared similar to the "*DN-AAm-0%*" with a 1.5 M AMPS 1st network and a 2.0 M AAm 2nd network (i.e. no NIPAAm).

5.3.3 Equilibrium Water Content

The values for equilibrium water content were calculated as $[(W_s - W_d)/ W_s] \times 100$, where W_s was the swollen weight of the hydrogel or cartilage disc and W_d was the dry weight of the hydrogel or cartilage disc after exposure to high vacuum at 60 °C overnight.

5.3.4 VPTT

Differential scanning calorimetry (DSC, TA Instruments Q100) was used to determine the VPTT of swollen DN hydrogels. A small square hydrogel specimen (~10 mg, cut with a razor blade) was blotted dry with a Kim Wipe and sealed in a hermetic pan. The sample was first cooled to 0 °C then the temperature was ramped up to 65 °C and back down to 0 °C at a rate of 3 °C min^{-1} for two continuous cycles. The VPTT was characterized by the peak temperature of the endotherm (T_{max}) and the initial temperature at which the endothermic phase transition peak starts (T_o). Reported data are from the second heating cycle to ensure any thermal history has been erased and to simulate an arbitrary n^{th} heating cycle.

5.3.5 Tension

The tensile mechanical properties were evaluated with an Instron 3340 at RT. Hydrogels were punched into 3 dog-bone specimens (3 mm width, ~30 mm gauge length) with a die. Each sample was blotted with a Kim Wipe to remove surface water and then placed in the tensile clamps with an initial pre-load force of 0.2 N. The hydrogels were tested at a constant strain rate of 10 mm min^{-1} until fracture. The elastic tensile modulus (E) was obtained from the slope of the linear portion of the stress-strain curve (0-10%

strain). The ultimate tensile strength (σ_f) and the % strain at break (ε_f) was defined respectfully as the stress and strain values at the point of fracture.

5.3.6 Static Compression

The compressive mechanical properties, including elastic modulus and strength, were evaluated with an Instron 3340 at RT. Hydrogels were punched into 3 discs (6 mm x ~2 mm, diameter x thickness) with a 6 mm biopsy punch. Healthy porcine articular cartilage was harvested from humeral condyles obtained within 24 hr after slaughter from the Rosenthal Meat Science and Technology Center at Texas A&M University. Using a 6 mm biopsy punch, cartilage discs (~6 mm x ~1-2 mm, diameter x thickness) were removed from the bone and tested immediately. All cartilage samples were never frozen before testing to avoid damage and/or dehydration that could lead to reduced mechanical performance. Each hydrogel and cartilage disc was blotted to remove surface water and then placed between the parallel plates with an initial pre-load force of 0.5 N. The samples were compressed at a constant strain rate of 1 mm min^{-1} until fracture. The elastic compressive modulus (E) was obtained from the slope of the linear portion of the stress-strain curve (0-5% strain). The ultimate compressive strength (σ_f) and the % strain at break (ε_f) were defined respectfully as the stress and strain values at the point of fracture. Finally, the toughness (U_t) was obtained from the integration of the stress-strain curve.

5.3.7 Creep

A dynamic mechanical analyzer (DMA) was utilized to examine the creep response of the DN hydrogels and porcine cartilage to compare their viscoelastic behavior. Discs of each specimen type were prepared as in static compression testing (6 mm x ~2

mm, diameter x thickness). Creep strain was recorded over time to evaluate the instantaneous strain and final creep strain reached after 1 hr of loading under a constant load of 0.35 MPa. Recovery % from maximum strain value after 1 hr of creep compression was reported immediately after removal of the load as well as 30 min after removal of load to observe differences in recovery rates.

5.3.8 Lubricity

The coefficient of friction (COF) was examined through tribology using a simulative synovial fluid lubricant comprised of fetal bovine serum (FBS) diluted with DI (60% v/v) to a protein content of ~20 g/L with 0.2 w/v% sodium azide (antibacterial) and 20 mM ethylene-diaminetetraacetic acid (EDTA) disodium salt dehydrate (chelating agent), adopted from ASTM F732 'Standard Test Method for Wear Testing of Polymeric Materials Used in Total Joint Prostheses'.[240] Hydrogel and cartilage specimens were soaked in the FBS solution then clamped into the base of the tribometer chamber and fully covered with FBS. The indenting pin, alumina ball (ø ~6 mm), was articulated at 20 mm/s in a straight line reciprocating motion of ~10 mm in length. The COF was determined at 300 reciprocating cycles or after reaching equilibrium.[241, 242] The mean Hertzian contact pressure was calculated as ~0.6 MPa with an applied load of 5 N. Average joint peak stresses range from ~0.1 to 5.0 MPa, thus the contact pressure used was within the physiologic range.[243, 244]

5.3.9 Cytocompatibility

DN hydrogel cytocompatibility was assessed by measuring LDH concentrations released by mouse mesenchymal progenitor 10T1/2 cells 24 hr after cell seeding onto the

hydrogel specimens versus tissue culture plastic (i.e. polystyrene, PS). Four hydrogel discs of each composition were punched (8 mm x ~2 mm, diameter x thickness) and sterilized by two changes of ethanol/water (70/30; 45 min). The discs were then transferred to a sterile 48-well plate and washed with sterile PBS (3 x 30 min) then immersed in sterile PBS for 48 hr (PBS exchanged at 24 hr). Next, 10T1/2 cells suspended in DMEM (without phenol red) supplemented with 10% FBS and 1% PS were seeded onto each hydrogel disc and also into four empty tissue culture plastic wells at a concentration of ~6000 cells cm^{-2}. Cells were incubated for 24 hr at ~37 °C with 5% CO_2. Finally, media was collected from each well and assessed for LDH level per the manufacture's protocol (Pierce™). The relative LDH activity was calculated by normalizing to the absorption of PS.

5.3.10 Statistics

For all testing, statistical analysis values were compared using either one-way ANOVA with Dunnett's correction or 2-way ANOVA with Tukey's correction to determine *p*-values.

5.4 Results and Discussion

Briefly, the PAMPS/P(NIPAAm-*co*-AAm) DN hydrogels were fabricated in a two-step UV-cure method (**Figure 5-3**) with compositions denoted as "*DN-AAm-X%*" where *X* represents the wt% of AAm copolymerized into the 2nd network (5, 10 or 15 wt% based on NIPAAm) (**Table A-4**). A single network (SN) control, composed only of the 1st network, as well as a DN control, containing no AAm in the 2nd network, were also prepared. For all DN hydrogels, a 1.5 M AMPS 1st network and a 2.0 M NIPAAm 2nd network were maintained as this was previously optimized for the best combination of

high modulus and high strength.[74] However, with no further modification, dimensional instability (i.e. thermally driven cyclical deswelling/reswelling) would occur with body temperature fluctuations, making it an unsuitable candidate as a synthetic cartilage replacement. Therefore, by the addition of a hydrophilic comonomer (i.e. AAm) to the PNIPAAm 2nd network, the VPTT of the resulting DN was shown to be successfully tuned above the physiologic range (>40 °C) with as little as 10 wt% AAm (**Table A-4**, **Figure 5-4**). This is attributed to the increased hydrophilicity of the P(NIPAAm-*co*-AAm) network requiring greater thermal energy to disrupt hydrogen bonding and to subsequently permit hydrophobic interactions to dominate between the isopropyl groups of NIPAAm. Such tunability of the VPTT via copolymerization with a hydrophilic comonomer has been demonstrated previously in conventional and DN hydrogels.[27, 245] Having established dimensional stability at physiologically relevant temperatures, these PNIPAAm-based DN hydrogels could potentially be utilized as a synthetic cartilage replacement and were further evaluated versus healthy cartilage (porcine) as a direct comparison.

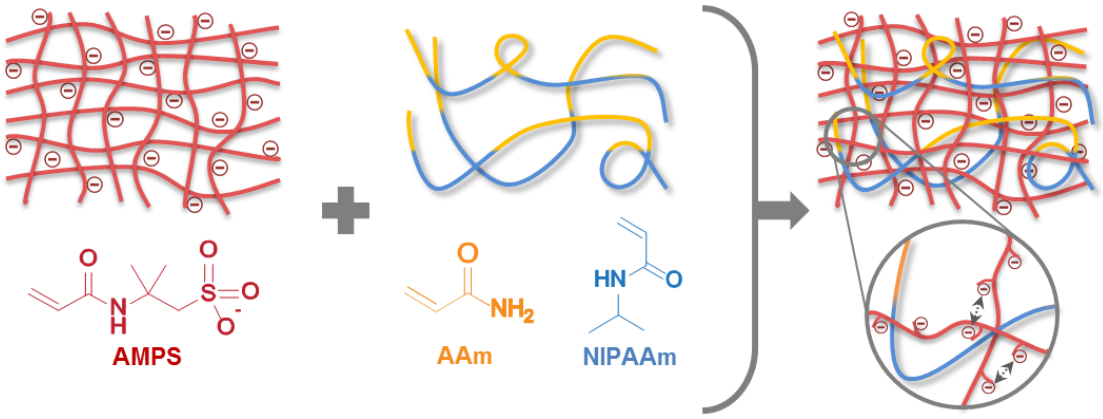

Figure 5-3. Non-thermoresponsive PAMPS/P(NIPAAm-*co*-AAm) DN hydrogels formed with an anionic PAMPS 1st network and a tunable, thermoresponsive 2nd network comprised of NIPAAm copolymerized with AAm. Inset: Ionic interactions within 1st network.

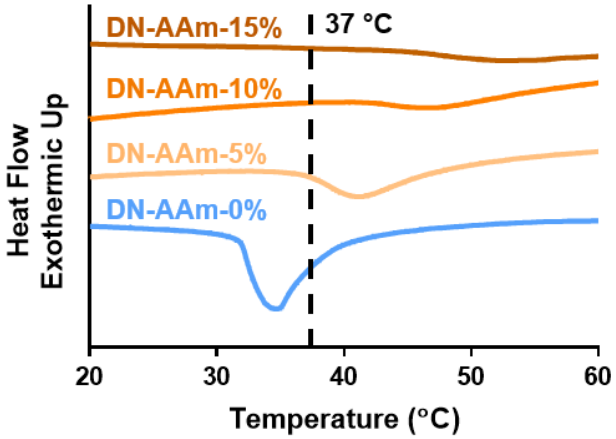

Figure 5-4. DSC thermograms of the PAMPS/P(NIPAAm-*co*-AAm) DN hydrogel series showing the shift of the VPTT with increasing AAm in the 2nd network. With 10 wt% AAm, the onset of the thermal transition can be tuned well above the physiologic range (T_{onset} > 37 °C).

A major challenge of achieving cartilage-like properties is maintaining high water content while attaining the requisite mechanical properties (e.g. modulus, strength and

toughness). Since, the extent of hydration greatly impacts the lubricity of a surface,[238] it was crucial that the equilibrium water content (EWC) of the DN hydrogels was similar to that of the cartilage. Notably, the water content of all the DN compositions (~80-85%, **Table A-4**) was slightly higher than the cartilage (~75%, **Table A-4**), in contrast to current resurfacing strategies utilizing UHMWPE-based coatings which have minimal water content. We expect this ability to mimic the hydration of native cartilage to not only enhance the lubricity, but also the durability and biocompatibility of the device long-term. Currently, previously reported hydrogels exhibiting high water contents (>~70%) have not been able to achieve both cartilage-like stiffness and strength simultaneously (**Figure 5-2**).[31, 46, 59, 68-71, 76, 100, 210] The reported values for compressive properties of articular cartilage widely vary (e.g. compressive modulus (E) ranges from ~0.5 to 60 MPa)[246, 247] due to large variations in biological tissue and experimental methods. Thus, in this work, porcine articular cartilage was harvested from fresh (i.e. non-frozen) humeral condyles (**Figure A-17**) and tested alongside the DN hydrogels to permit direct comparison. In previous studies of DN hydrogels,[31, 76, 79] the introduction of a 2nd, interpenetrating network dramatically increased the compressive strength and toughness versus conventional SN hydrogels; however, their moduli typically remain in the sub-MPa range. In contrast, the unique combination of a PAMPS 1st network and PNIPAAm 2nd network demonstrated not only an increase in strength and toughness but also in modulus when compared to the PAMPS SN control (i.e. "SN-AAm-0%", **Figure 5-5**, **Table A-5**). Furthermore, the incorporation of just 5-15 wt% AAm into these DN hydrogels significantly enhanced the compressive strength compared to "DN-AAm-0%" (i.e. no

AAm; **Figure 5-5b**) while maintaining comparably high compressive moduli (>1 MPa, **Figure 5-5a**), similar to that of the harvested cartilage (~1 MPa, **Figure 5-5a**). Notably, the "DN-AAm-10%" displayed a compressive strength >25 MPa, a substantial increase versus "DN-AAm-0%" (~14 MPa, **Figure 5-5b**). Although the cartilage exhibited a slightly higher average compressive strength (~30 MPa), all AAm-containing DN hydrogels were not statistically lower due to the variability exhibited by the cartilage. In addition, these DNs exhibited a compressive fracture toughness (>4 MJ m^{-3}) approaching that of the cartilage (~7 MJ m^{-3}, **Figure 5-5c**). Finally, it should be noted that the DN hydrogels sustained greater percent strains before fracture than the cartilage, as demonstrated by the representative stress vs. strain curves (**Figure 5-5d**). The ability of these double networks to reach such high strains (>80%) before failure could improve durability at common contact stresses and strains experienced during normal activity (~0.1-2.0 MPa, ~10-30% strain) as well as at less frequent peak contact stresses (~2-10 MPa).[243, 248]

Interestingly, the addition of increasing amounts of AAm (5, 10 or 15 wt% based on NIPAAm) did not result in significant differences in tensile or compressive modulus, strength and toughness between the AAm-containing DNs (**Figure 5-5**, **Table A-5**). However, the VPTT values (**Table A-4**, **Figure 5-4**) systematically increased with increasing levels of AAm, indicating a gradual increase in hydrophilicity and successful incorporation of AAm into the PNIPAAm network. We hypothesize that the addition of the less-bulky AAm segments increases the overall mobility of the 2^{nd} network allowing for greater energy dissipation while not hindering the chain stiffening induced by the

electrostatic repulsion of the anionic PAMPS 1st network and the physical interactions between the PNIPAAm chains of the 2nd network. To further confirm this enhancement of strength and modulus was unique to the combination of NIPAAm and AAm, we evaluated several additional controls, including the addition of anionic (AMPS, "DN-AMPS-10%") and cationic 3-(acrylamidopropyl)trimethylammonium chloride (AAPTAC, DN-AAPTAC-10%") comonomers at 10 wt% to the PNIPAAm 2nd network as well as an AAm only (2.0 M, no NIPAAm, "DN-AAm-100%") 2nd network. Additionally, to eliminate concentration as a variable, an extra 10 wt% NIPAAm was added to the original 2.0 M NIPAAm 2nd network denoted as "DN-NIPAAm-10%" which displayed similar properties to the DN-AAm-0% control. Notably, none of these controls exhibited the same combination of cartilage-like mechanical properties as the DN-AAm-10% (**Figure A-18**), demonstrating the importance of using AAm, a small, non-ionic, hydrophilic comonomer, as the additive.

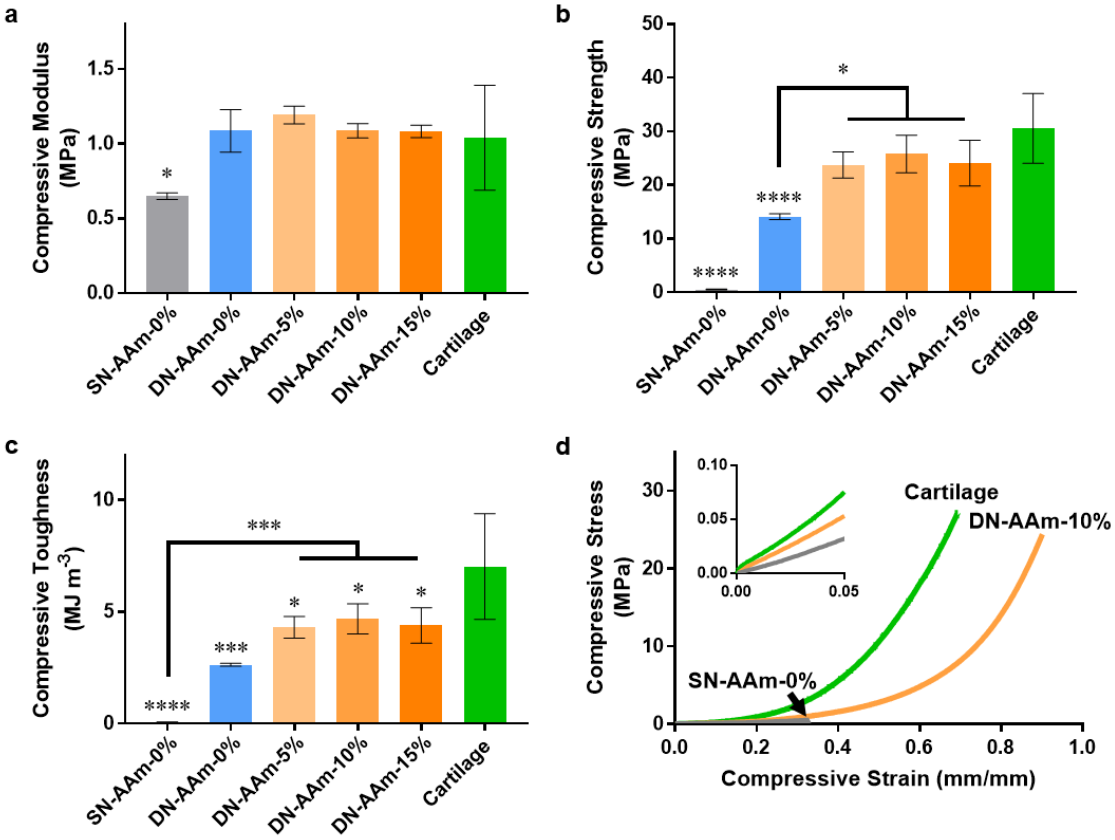

Figure 5-5. Compressive mechanical properties of the PAMPS/P(NIPAAm-*co*-AAm) DN hydrogel series alongside porcine articular cartilage demonstrating the high (a) modulus, (b) strength and (c) toughness with incorporation of AAm in the 2nd network. (d) Representative stress vs. strain curves showing the compressive behavior at both small and large strains. All *'s indicate statistical significance from cartilage unless otherwise denoted, in which "*" represents $p < 0.05$, "***" represents $p < 0.001$ and "****" represents $p < 0.0001$.

After confirming the general swelling and mechanical properties of the DN hydrogels were desirable for synthetic cartilage (**Table A-5**), additional cartilage-specific characteristics were assessed including viscoelasticity and lubricity. To evaluate the viscoelastic properties of the DN hydrogels versus that of the cartilage, the creep response as well as subsequent recovery was observed after applying a constant stress of 0.35 MPa,

representative of the normal averaged joint stress[243], for one hour. As seen in **Figure 5-6a**, the initial creep strain immediately reached after step compression was slightly higher for the DN hydrogels (~35% strain) than for the cartilage (~25% strain). However, due to the larger creep deformation of the cartilage over time, both the DN hydrogels and the cartilage reached a similar final creep strain (~50%, **Figure 5-6a**). We hypothesize that the creep deformation of the DN hydrogels is reduced by strong electrostatic repulsive forces as well as covalent crosslinking that reduces molecular deformation and relaxation of the polymer network. While cartilage similarly consists of electrostatic proteoglycans as well as collagen, these form duplexes based on physical rather than covalent bonds, allowing for molecular movement through the breaking and reforming of these reversible interactions. Thus, cartilage will exhibit a larger amount of creep flow when exposed to the same step stress as the DN hydrogels. This ability of chemical crosslinking to enhance the long-term stability of hydrogels has been demonstrated previously.[249] Therefore, the inherent difference in structure of covalently crosslinked hydrogels compared to biological tissue explains the more elastic response exhibited by the DN hydrogels compared to the slower, more viscous nature of cartilage. Likewise, this trend in response was also seen during recovery, in which the DN hydrogels recovered much more rapidly than cartilage. Notably, the AAm-containing DNs initially recovered to a greater extent than the "1.5-AMPS-0%" control without AAm (**Figure 5-6b**). This could indicate that less plastic deformation occurred within the AAm DNs, potentially enhancing the lifetime of the material.

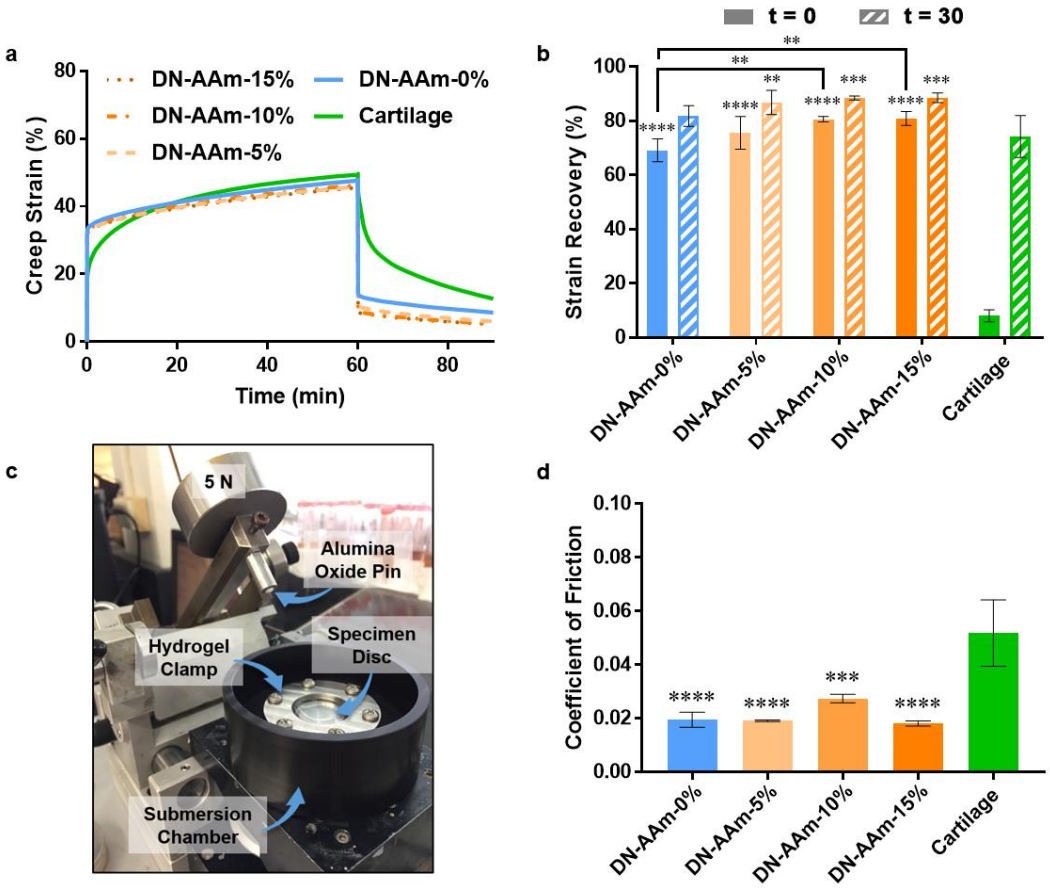

Figure 5-6. (a) Creep response of the PAMPS/P(NIPAAm-*co*-AAm) DN hydrogel series comparing the viscoelastic behavior of the DNs to porcine cartilage and (b) the percent recovery immediately after removal of load (t = 0, solid) and 30 min after removal of load (t = 30, striped). (c) Tribological testing design and (d) COF of the PAMPS/P(NIPAAm-*co*-AAm) DN hydrogel series comparing the lubricity of the DNs to porcine cartilage. All *'s indicate statistical significance from cartilage at respective time points unless otherwise denoted, in which "**" represents $p < 0.01$, "***" represents $p < 0.001$ and "****" represents $p < 0.0001$.

One of the most important purposes of cartilage is to provide an articulating surface with high lubricity. Thus, the COF of the DN hydrogels was assessed through standard pin-on-disc tribological methods. A ceramic ball bearing was chosen as the pin to represent a common biomaterial used in total knee replacements (TKRs). To simulate

synovial fluid present in joints, a dilute fetal bovine serum (FBS) solution (adopted from ASTM F732)[240] was utilized as the lubricant with a protein concentration similar to that of healthy synovial fluid. To hold the hydrogel specimens in place in a hydrated environment, a custom clamp and submersion chamber were built (**Figure 5-6c** and **Scheme A-1, A-2**). A constant load of 5 N was applied to achieve contact pressures of ~0.6 MPa, well-within the range of normal averaged joint stresses[243]. As a direct comparison to native tissue, a strip of harvested porcine cartilage was evaluated similarly (**Figure A-19**). Notably, all DN hydrogel compositions exhibited significantly lower COF values versus the cartilage. Thus, these hydrogels have great potential to perform as well as healthy cartilage as a synthetic articulating surface with high lubricity.

Lastly, to confirm cytocompatibility, mesenchymal progenitor 10T1/2 cells were seeded onto all DN hydrogel compositions and an LDH assay was performed on the surrounding media after 24 hrs of incubation. Tissue culture polystyrene (PS) represented a cytocompatible control and thus, all LDH absorption was normalized to PS. LDH levels of all hydrogel specimens were determined similar to the PS control (**Figure 5-7a**), confirming cytocompatibility of the DN hydrogels. Notably, the addition of AAm into the PNIPAAm 2nd network produced a reduction in cell adhesion as observed through brightfield microscopy (**Figure 5-7b**). This trend showed a direct correlation between increased hydrophilicity and decreased cellular attachment. Although the observed results were expected due to the known higher affinity of proteins and thus cells to more hydrophobic surfaces, the prominent differences seen in cellular response with only small additions of AAm (~5-10%) demonstrated the facile tunability of these DN hydrogels.

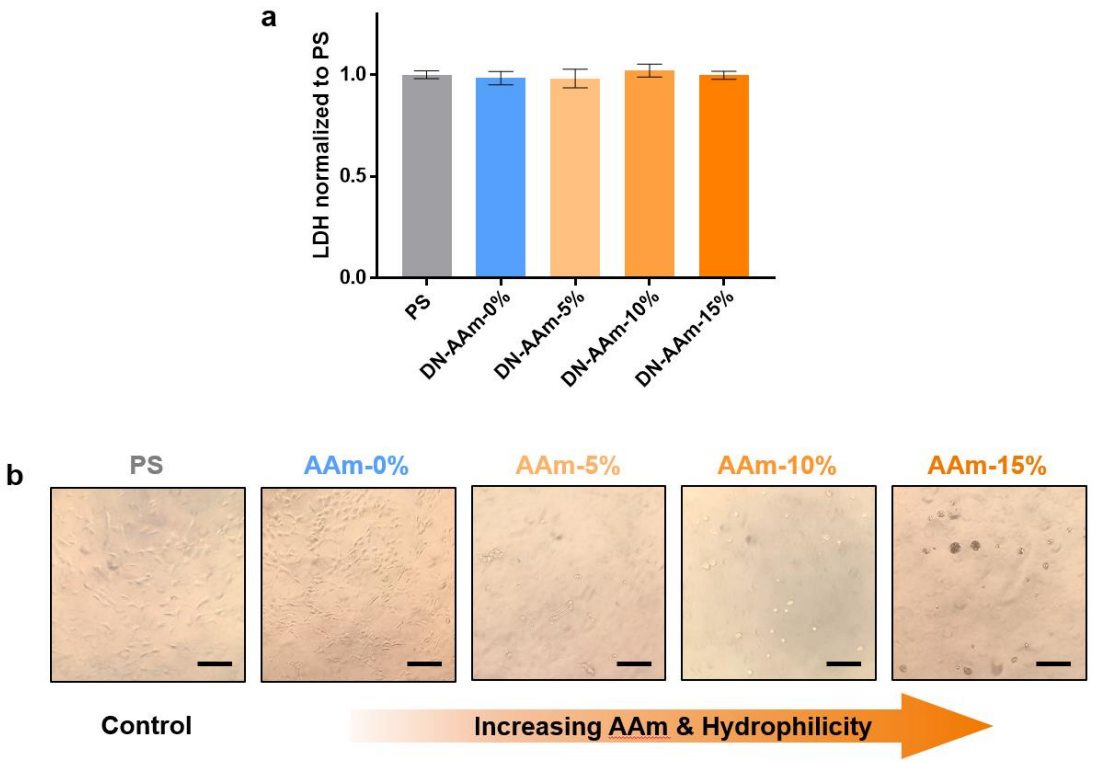

Figure 5-7. (a) Normalized LDH absorption confirming cytocompatibility of the PAMPS/P(NIPAAm-*co*-AAm) DN hydrogel series. (b) Representative images demonstrating reduced cell adhesion with increasing AAm comonomer after 24 hr incubation of 10T1/2 cells on the surface of the PAMPS/P(NIPAAm-*co*-AAm) DN hydrogel series and polystyrene (PS) as an adhesive control. All scale bars = 200 µm.

5.5 Conclusions

In summary, this work sought to develop a cartilage-mimetic hydrogel that could serve as a synthetic cartilage substitute for current cartilage defect treatment methods such as focal resurfacing and autograft transplantation. Through the use of a PNIPAAm-based DN hydrogel design, the modulus, strength and toughness were enhanced simultaneously without reducing the water content, something not previously achieved in other hydrogels to our knowledge. Interestingly, the addition of AAm not only achieved the intended

dimensional stability by tuning of the VPTT out of the physiologic range, but also significantly enhanced the compressive strength (~25 MPa) of the membranes while maintaining a cartilage-like modulus (~1 MPa) and hydration (~80%). Although the PAMPS/P(NIPAAm-*co*-AAm) DN hydrogels exhibited a more elastic response compared to cartilage, the final creep strain of the each were nearly equal after 1 hr indicating they may reach a similar equilibrium strain under the same constant stress. Additionally, the recovery of the DN-AAm hydrogels was more rapid than the porcine cartilage, showing potential for long-term durability. Most notably, all DN hydrogels reported herein achieved significantly lower COF values versus native cartilage. This ability to mimic the hydration, stiffness, strength and lubricity of cartilage as well as demonstrate resistance to creep make these PNIPAAm-based DN hydrogels promising candidates as synthetic cartilage grafts.

CHAPTER VI

CONCLUSIONS

6.1 Conclusions

By enhancing and tailoring the mechanical properties of hydrogels, their utility may be extended to a variety of next-generation biomedical devices. In this work, PNIPAAm-based DN hydrogels were designed to achieve mechanically robust subcutaneous glucose biosensor membranes and synthetic cartilage. The polymer composition of each network was used to customize hydrogel modulus, strength, hydration, permeability, lubricity and thermosensitivity, depending on the intended use. The first two DN hydrogels described in Chapters II and III were designed as actively antifouling membranes whose thermally-driven, cyclical deswelling/reswelling could extend the lifetime of subcutaneous glucose biosensors by minimizing the foreign body reaction. The latter two DN hydrogels reported in Chapters IV and V, by achieving cartilage-like mechanical properties, were intended as synthetic cartilage for use in load-bearing joints. Through studies that systematically probed structure-property relationships, a variety of advanced PNIPAAm-based DN hydrogels with tuned and notable mechanical properties were developed.

Briefly, in Chapter II, the biocompatibility of the first generation self-cleaning hydrogel was assessed. This thermoresponsive, DN nanocomposite (DNNC) membrane was composed of two PNIPAAm networks and embedded polysiloxane nanoparticles. Previous work demonstrated its sufficient glucose diffusivity, optical clarity and

cytocompatibility. Thus, the DNNC hydrogel membrane was formed as small, biosensor-sized cylinders (~1.5 mm x ~5 mm, diameter x length) and implanted subcutaneously into the dorsal tissue of rats. After 30 days, the DNNC hydrogels exhibited very thin fibrous capsules (~30 μm) and higher microvascular densities near the implant surface in comparison to a benchmark biocompatible PEG-DA control. Although these membranes showed great promise in controlling the foreign body reaction, their mechanical strength was not appreciably high, potentially limiting their durability during implantation, peak impact forces and explantation.

Based on the results of the prior chapter, the focus of Chapter III was the development of a second generation self-cleaning hydrogel membrane with improved mechanical strength but similar modulus, key to minimizing the foreign body reaction. This membrane design incorporated anionic AMPS into the first network, forming thermoresponsive, electrostatic P(NIPAAm-*co*-AMPS)/PNIPAAm membranes able to remove adhered cells from their surfaces *in vitro* via thermal cycling. The membrane whose first network contained a ratio of 75:25 wt% NIPAAm:AMPS (DN-25%) showed the best combination of properties in previous studies. Thus, the DN-25% membranes were prepared as cylinders (~2.5 mm x ~5 mm, diameter x length) and implanted subcutaneously in rats for up to 90 days. The particular PEG-DA control used exhibited a lower modulus and higher water content versus the PEG-DA implant in Chapter II in order to provide a benchmark control with greater minimization of the foreign body reaction. The DN-25% membranes were not only 25x stronger and 30x tougher than the PEG-DA implants, but also demonstrated rapid healing and minimal fibrous capsule formation

(~20-25 μm). Thus, this second generation self-cleaning membrane has the potential to extend the lifetimes of implantable glucose biosensors through their unique ability to minimize the foreign body reaction and their robust mechanical properties.

In Chapter IV, thermoresponsive PNIPAAm-based DN hydrogels based on a zwitterionic design were prepared to further enhance mechanical properties towards the development of synthetic cartilage. By adjusting the molar concentrations of the anionic PAMPS first network and the PNIPAAm second network, both stiffness and strength were mutually maximized without altering the VPTT. Additionally, a zwitterionic comonomer (MEDSAH) was incorporated into the second network (5-15 wt% based on NIPAAm) to produce electrostatic interactions between the two networks as well as within the second network. These reversible bonds were able to increase the apparent crosslinking density, and thus modulus, without imparting brittleness typically associated with permanent, covalent bonds. As a result, these PAMPS/P(NIPAAm-*co*-MEDSAH) DN hydrogels were able to achieve cartilage-like mechanical properties in terms of high stiffness (~1.5 MPa) and high strength (~23 MPa) as well as high water content (~83%). Furthermore, the addition of MEDSAH also did not significantly alter the VPTT. Thus, this DN hydrogel may be useful as a "self-fitting" synthetic cartilage implant wherein insertion/implantation is done in the deswollen state and subsequent reswelling serves to lock the implant in place.

Because the Chapter IV zwitterionic DN hydrogels exhibited a VPTT ~35 °C, they may exhibit slight deswelling/reswelling induced by body temperature fluctuations following implantation, leading to poor integration and loosening. Therefore, in Chapter

V, this thermal transition was tuned out of the physiologic range (>40 °C) through the addition of a neutral, hydrophilic comonomer, AAm (>10 wt%), to the second network instead of MEDSAH. The PAMPS/P(NIPAAm-*co*-AAm) DN hydrogels were subjected to testing alongside freshly harvested porcine articular cartilage. These hydrogels exhibited a unique combination of high strength (~26 MPa), high modulus (~1.1 MPa) and hydration (~84%), similar to that of tested cartilage, as well as showed a 50% lower coefficient of friction. It was considered that the hydrophilic comonomer increased the molecular mobility of the second network, enhancing its ability to dissipate stress and resulting in a significant increase in strength versus control DN hydrogels. This DN hydrogel, with cartilage-mimetic mechanical properties, may be a candidate for an off-the-shelf, synthetic cartilage biomaterial.

In summary, this work has led to the development of multiple PNIPAAm-based DN hydrogels targeted for two distinct biomedical applications – self-cleaning glucose biosensor membranes and synthetic cartilage. *In vivo* studies of two distinct self-cleaning hydrogels showed remarkable biocompatibility for up to 90 days in a rat model, demonstrating the feasibility of a an active approach to minimize the foreign body reaction. This success, particularly of the more mechanically robust membrane, warrants further studies to utilize it to house a glucose biosensor. By developing cartilage-mimetic DN hydrogels, a synthetic replacement for a tissue with an inherently poor healing capacity may be realized. The exceptional properties of these DN membranes make them uniquely suited for load-bearing joints that require high strength, stiffness, hydration and lubricity simultaneously for proper function. Additional characterization under

physiologically simulative conditions could provide more insight on their similarity to cartilage and their potential as a synthetic replacement. Overall, the development of PNIPAAm-based hydrogels, by leveraging the DN design and polymer network composition, has produced candidates for next generation biomaterial applications.

6.2 Future Directions

6.2.1 Subcutaneous Glucose Biosensor

The *in vitro* and *in vivo* characterization of the self-cleaning DN-25% hydrogels has demonstrated their potential for housing and extending the lifetime of subcutaneous glucose biosensors. Moving forward with this work, these membranes will be utilized to encapsulate a liquid based glucose sensing assay and evaluated as a complete biosensor. Previously, Coté *et al.* reported a competitive binding assay based on Förster Resonance Energy Transfer (FRET) with high glucose sensitivity.[250] A fluorescent assay that can be detected through the skin would eliminate the need for bulky electronics within the implantable biosensor, thus minimizing the size and reducing costs. Additionally, the use of FRET would avoid effects of long-term bleaching by utilizing the intensity ratio instead of absolute intensity values. Through our collaboration with Coté and coworkers, we have begun preliminary testing of the complete biosensor (**Figure 6-1**).

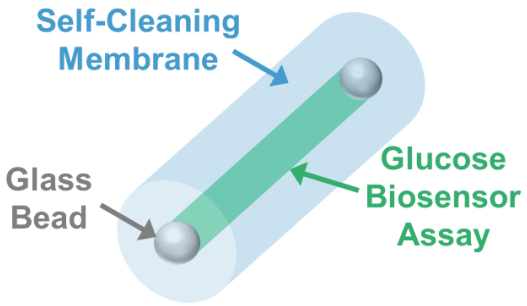

Figure 6-1. Current encapsulation strategy utilizing inserted glass beads as end caps.

Thus far, the greatest challenge has been in the encapsulation of the sensing assay as a free solution within our hollow cylindrical membrane. This is due to the similarity of hydrodynamic diameter (D_h) of one of the assay components (amino-pyrene trisulfonate mannotetraose, APTS-MT; D_h ~3 nm) and glucose (D_h ~1 nm), creating a tremendous challenge to limit the permeability of the assay while maintaining adequate glucose diffusion. Multiple strategies are currently being evaluated in the Grunlan and Coté labs to mitigate this issue: (1) adjusting the DN-25% hydrogel mesh size to <3 nm but >1 nm using a DN comb architecture, (2) applying layer-by-layer (LBL) to the inner wall of the DN-25% hydrogel,[188] (3) bulking up of APTS-MT (e.g. conjugation with a polymer), (4) chemical anchoring of the APTS-MT to the inner wall of the hydrogel and (5) encapsulation of the assay inside of hydrogel microspheres prior to direct embedding a solid DN-25% membrane cylinder. In a separate collaboration with the McShane lab, an alternative sensing assay based on phosphorescence lifetime has been encapsulated in alginate microspheres[251] and embedded within DN-25% membranes for preliminary testing. Each of these encapsulation strategies will be thoroughly evaluated for their

efficacy in preventing assay leaching while maintaining glucose diffusion rates similar to that of the surrounding tissue (D_{dermis} ~2.6 x 10^{-6} cm^2s^{-1}).[166]

Although this work was focused on applying the self-cleaning membranes to fully implantable subcutaneous glucose biosensors, the DN-25% hydrogel could also be utilized on transcutaneous CGM probes. Current electroenzymatic transcutaneous probes require frequent replacement, every 7-14 days, due to biofouling on the electrode surface.[252, 253] Thus, the self-cleaning membrane could likewise serve as a protective membrane to reduce the foreign body reaction on these probes, reducing costs and improving broad adoption by diabetic populations. To accomplish this, the fabrication method will need to be modified to promote adhesion to the metallic, needle-like electrodes[254] as a thin hydrogel film (**Figure 6-2**). Conventional SN PNIPAAm-based hydrogels have been commonly applied as thin films to substrates; however, forming a DN hydrogel on the surface may present a greater challenge.[255-257]

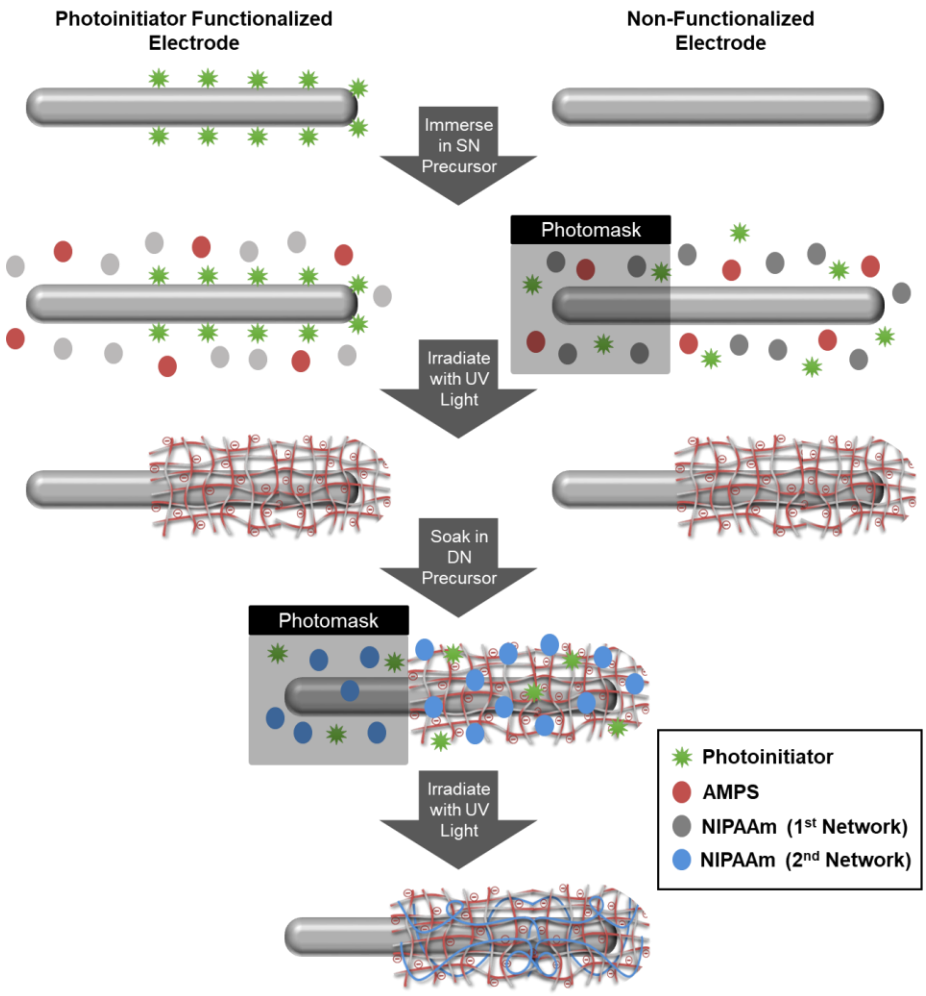

Figure 6-2. Two potential strategies to apply the DN-25% self-cleaning hydrogel membranes to the surface of transcutaneous electrodes as thin films through UV photopolymerization. (Note: The uncoated end of the electrode would be affixed to the CGM transmitter.)

The reported DN-25% hydrogel fabrication used free radical UV-polymerization with a photo-initiator (Irgacure 2959) and crosslinker (BIS). The most direct way to adapt this to enclose a transcutaneous electrode is through photopolymerization that is spatially controlled by either pre-functionalization of the surface or a projection photomask (**Figure 6-2**). A first approach may involve incorporating a surface-bound photoinitiator to the

outer layer of the probe to the desired region.[256] In this way, the surface functionalized electrode could be immersed in first network precursor solution (without Irgacure 2959) and irradiated with a UV lamp to initiate polymerization directly from the functionalized surface. Using this method, hydrogel film thickness has been shown to be highly controllable through regulating the UV exposure time.[256] Alternatively, the standard first network precursor solution could be coated on the electrode surface and a photomask applied to limit the region of polymerization.[258] Photomasks have been used extensively to produce patterns in polymer films. Additionally, this method would more similarly replicate the previously established bulk fabrication of the DN-25% membrane. Thus, these or other methods previously used to produce PNIPAAm thin films (e.g. electrochemically-induced polymerization[257]) are predicted to be easily adapted to prepare a SN hydrogel on an electrode. However, the sequential formation of a DN has not yet been reported. Theoretically, the SN-coated electrode could be soaked in the second network precursor solution, as with the bulk hydrogels, and subsequently cured (**Figure 6-2**). Alternatively, one-pot preparation of DNs could be achieved if non-interfering reactions (e.g. physical, ionic or condensation crosslinking) are used for the independent but simultaneous formation of first and second networks alongside the free radical polymerization.[78] However, this would dramatically change the network structure and thus affect the already well-established physical and thermoresponsive properties of the self-cleaning hydrogels.

Ultimately, the facile fabrication of the DN-25% membranes through photopolymerization allows for their use in a wide range of biomedical applications. In

addition to subcutaneous and transcutaneous glucose biosensors, we envision these self-cleaning membranes as biocompatible coatings for a variety of indwelling electrodes (e.g. deep brain stimulation, intraneural interfaces) that currently exhibit short lifetimes predominantly due to surface biofouling.

6.2.2 Synthetic Cartilage

The DN hydrogels developed in Chapters IV and V were shown to parallel the strength, stiffness, hydration and lubricity of healthy articular cartilage. To determine their suitability as a synthetic cartilage replacement, more testing under physiological conditions is warranted, including: (1) confined creep compression, (2) fatigue and (3) COF/wear while submerged in simulated synovial fluid at 37 °C. In order to facilitate these complex analyses, customized testing equipment would be designed and fabricated (**Figure 6-3**).

The DN hydrogel synthetic cartilage is anticipated to be implanted as a cylindrical disc or plug into a pre-drilled hole within a defect. Thus, confined creep compression would better demonstrate the ability of the DN to resist stress-induced strain over time following loading by taking into account the interstitial fluid load support. To evaluate confined creep compression, cylindrical specimens would be placed in a solid cylindrical chamber having an ID equal to that of the hydrogel OD and fitted with a porous platen to permit fluid exudation during compression (**Figure 6-3a**). A compressive creep test would be performed by applying a constant load until reaching equilibrium with subsequent steps-up of physiological stresses to 5 MPa.[243] The aggregate modulus would be calculated from the equilibrium stress-strain data of the final cycle. With the same testing

configuration, fatigue performance of the specimen would be assessed by subjecting to 100k cycles reaching a peak stress of 5 MPa at 1 Hz. Afterwards, the specimen would be inspected (visually and via brightfield microscopy) for signs of failure.[246, 259]

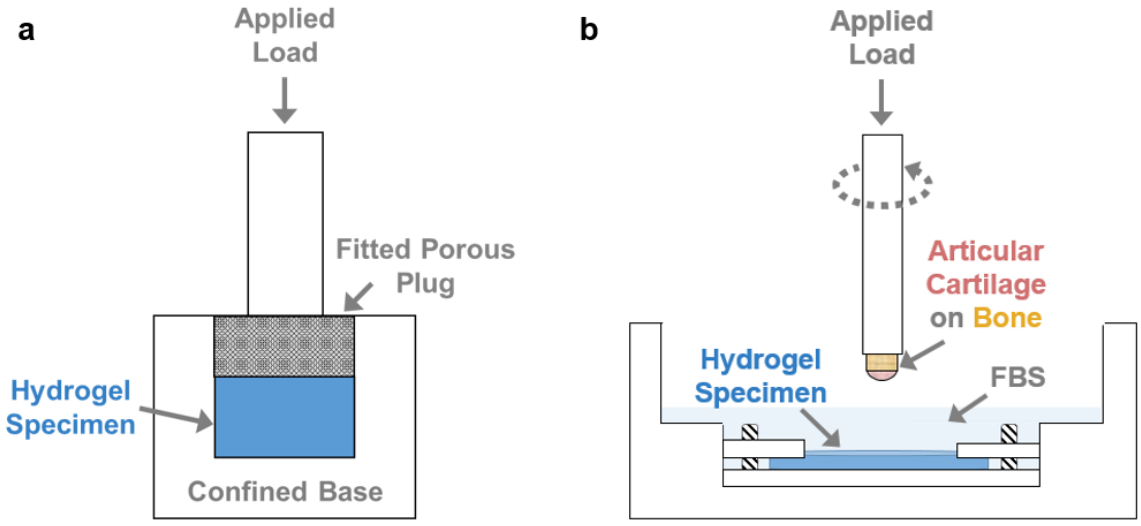

Figure 6-3. Potential testing designs for (a) confined creep compression and (b) friction/wear against harvested cartilage under physiologic environments.

Preliminary COF results were obtained with a pin-on-disc tribometer against an alumina pin submerged in dilute FBS. In future work, native cartilage could be used as the counter-surface in a disc on disc configuration to better mimic the *in vivo* environment of implanted synthetic cartilage. Briefly, hydrogel specimens would be fixed to a rotary stage, exposed to dilute FBS and a harvested cylindrical osteochondral plug will be secured to the pin shaft (**Figure 6-3b**) (0.5 – 10 N loads, 1 – 100 mm/s surface velocities) for 3k cycles.[260] COF data could then be used to form a Stribeck curve (i.e. COF plotted as a function of the Hersey number) which would reveal the mode of lubrication.[242,

261] Wear resistance may also be assessed with surface profilometry following a torsional disc-on-disc configuration (DN hydrogel-on-cartilage and cartilage-on-cartilage control) immersed in dilute FBS (1 N load, 360 °/s rotational speed, 10k rotations).

To create a suitable cartilage replacement, the DN hydrogel must be anchored into the defect site. As noted, this is anticipated to be a drilled, cylindrical defect extended into the cancellous bone as is the case for autograft plugs. In this way, tissue integration with both adjacent cartilage and osseous tissue is key for implant success. Ongoing work in our lab seeks to develop a bilayered "cartilage-capped, regenerative osteochondral plugs (cc-ROPs)" comprised of a synthetic cartilage layer (for resurfacing) and macroporous, osseous hydrogel scaffold layer[189] (for bone regeneration). Thus, this implant would provide immediate cartilage-like properties at the articulating surface while the osseous region would, based on its osteoinductivity, osteoconductivity and bioactivity, undergo regeneration over time. For this cc-ROP device to be realized, two major issues must be addressed in future work: (1) connection of the synthetic cartilage layer to the osseous scaffold and (2) integration of the synthetic cartilage layer with the adjacent tissue. Approaches to do so are described below.

The adhesion of the synthetic cartilage layer to the osseous scaffold may be accomplished through the addition of a "connecting network" that would effectively act as a third network in the cartilage cap and a second network in the bone scaffold. The cc-ROP would be fabricated by first soaking the pre-fabricated DN hydrogel disc in connecting network precursor solution then press-fitting the cartilage cap against the osseous scaffold in a confined mold, allowing for slight absorption of the precursor

solution into the porous scaffold from the saturated DN. The combined cc-ROP would then be UV-cured to covalently crosslink the connecting network within both hydrogel layers. The impact of the connecting network on the material properties of the cap and scaffold would be evaluated. It is anticipated that the connecting network may in fact impart improved properties to the cap, such as increased lubricity, strength or modulus. For example, studies have shown the addition of a anionic PAMPS third network to a PAMPS/PAAm DN can reduce COF due to increased osmotic repulsion.[42] Alternatively, a cationic network, such as PAAPTAC, may improve modulus through increasing the apparent crosslinking density via electrostatic interactions with PAMPS. Likewise, the incorporation of another slightly hydrophobic network (e.g. PNIPAAm) could also further enhance the mechanical properties by introducing inter-network hydrophobic interactions.[43]

Due to the non-porous nature of the DN hydrogels, no significant cartilage tissue ingrowth into the cap of the cc-ROP would be expected. Utilization of sutures or sealants to limit cap movement or delamination from the adjacent tissue is expected to produce uneven edges on the surface, hindering long-term durability through increased wear. Instead, incorporation of macropores into the DN hydrogel of the cc-ROP, at the perimeter, may achieve tissue integration. Previously in our lab, fused salt-templating has been utilized to create interconnected pores with tunable size.[189] However, this method is not possible with aqueous precursors due to the high solubility of sodium chloride in water. Additionally, the sequential formation of DN hydrogels will require the macropores to be formed post-fabrication or via insoluble porogens that can remain throughout the

multi-step fabrication process, eliminating the use of any foaming techniques. Therefore, two potential methods to achieve controllable pore size and connectivity within DN hydrogels are proposed, including (1) cryo-treatments and (2) inorganic or polymer porogens (**Figure 6-4**). To maintain the requisite mechanical properties, spatial control of porosity will be vital to attain a non-porous, tough cartilage layer at the surface while producing macropores ranging in size from ~100-200 µm for optimal chondral tissue ingrowth at the scaffold-tissue interface.[262]

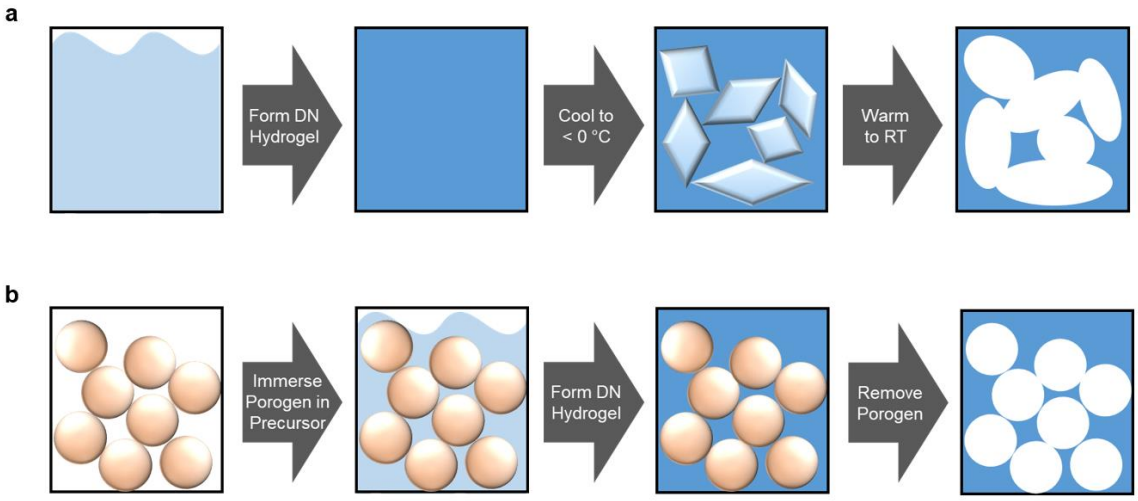

Figure 6-4. Potential fabrication methods to incorporate macropores into DN hydrogels to assist in cartilage tissue ingrowth after implantation.

Recently, cryo-treatment has been commonly used to form macropores in hydrogels through the crystallization of ice. Typically, cryogels are fabricated through the polymerization of frozen aqueous precursors at sub-zero temperatures to construct the hydrogel network around the ice crystals.[263] Although some reported DNs have used

this method during both the SN and DN cure sequentially,[264, 265] it would be preferable to induce pore formation post-fabrication of the ultra-strong DNs to better maintain the established cartilage-like properties (**Figure 6-4a**). In general, cryo-treatment has the potential to provide multiple advantages towards a synthetic cartilage replacement. First, a dense skin layer is produced due to the outermost surface of the hydrogel freezing more rapidly than crystallization can occur.[263] This non-porous layer could serve as the tough cartilage cap while all other edges could be trimmed, exposing the macropores and allowing for tissue infiltration. Moreover, cryogels inherently have high pore interconnectivity due to the fractal nature of ice crystallization, therefore allowing cells and nutrients to penetrate deep into the scaffold.[266] Additionally, it has been shown that aligned macropores can be obtained through directional freezing, providing further potential for spatial control.[267, 268] Overall, post-fabrication cryo-gelation would be the most facile method to achieve a porous DN hydrogel; although, the ability to obtain large scale macropores (~100s μm) without changing the molecular structure remains unclear.

Alternatively, porogens can be introduced during the formation of the first network that remain present throughout the DN fabrication process and are later solubilized under various conditions (e.g. acidic/alkaline, solvent extraction, heat, etc.) (**Figure 6-4b**). Previously, numerous different porogens have been utilized, including calcium carbonate ($CaCO_3$)[269], gelatin[270], alginate[271], PMMA[272] and paraffin[273] microspheres. The use of porogens provides precise control over pore size and has been shown to produce a wide range of pore geometries and diameters (~10's-100's μm).[269-273] Although pore

interconnectivity is typically limited, this can be avoided by gently fusing the porogens together before injection and polymerization of the precursor solution. Additionally, it has been shown in our group that spatial control can be achieved through the use of incrementally sized porogens to create a pore size gradient within hydrogels. Due to the high chemical stability of the ultra-strong DNs under most conditions (acidic/alkaline, solvent extraction, heat, etc.), any of the above porogens would be suitable to incorporate macropores. However, one of the primary concerns with porogens is their potential toxicity if not completely removed during fabrication. Thus, the porogen would be chosen based on the known toxicity of its components as well as the harshness of the required leaching process. In summary, numerous strategies are available to incorporate macropores within DN hydrogels, including the use of cryo-treatments or porogens. Thus, the major challenge will be spatially controlling pore formation within the ultra-strong hydrogels to maintain the cartilage-mimetic mechanical properties at the surface (non-porous region) while permitting cellular infiltration around the scaffold perimeter (macroporous region).

REFERENCES

1. Anseth, K.S., C.N. Bowman, and L. Brannon-Peppas, *Mechanical properties of hydrogels and their experimental determination.* Biomaterials, 1996. **17**(17): p. 1647-1657.

2. Bergel, D.H., *The static elastic properties of the arterial wall.* J Physiol, 1961. **156**(3): p. 445-457.

3. Stemper, B.D., N. Yoganandan, and F.A. Pintar, *Methodology to study intimal failure mechanics in human internal carotid arteries.* J Biomech, 2005. **38**(12): p. 2491-2496.

4. Li, C., et al., *Determining elastic properties of skin by measuring surface waves from an impulse mechanical stimulus using phase-sensitive optical coherence tomography.* J R Soc Interface, 2012. **9**(70): p. 831-841.

5. Ní Annaidh, A., et al., *Characterization of the anisotropic mechanical properties of excised human skin.* J Mech Behav Biomed Mater, 2012. **5**(1): p. 139-148.

6. Schleifenbaum, S., et al., *Load and failure behavior of human muscle samples in the context of proximal femur replacement.* BMC Musculoskel Disord, 2016. **17**(1): p. 149.

7. Hoffman, A.S., *Hydrogels for biomedical applications.* Adv Drug Deliv Rev, 2012. **64**: p. 18-23.

8. Qiu, Y. and K. Park, *Environment-sensitive hydrogels for drug delivery.* Adv Drug Deliv Rev, 2001. **53**(3): p. 321-339.

9. Hoare, T.R. and D.S. Kohane, *Hydrogels in drug delivery: Progress and challenges.* Polymer, 2008. **49**(8): p. 1993-2007.

10. Boateng, J.S., et al., *Wound healing dressings and drug delivery systems: A review.* J Pharm Sci, 2008. **97**(8): p. 2892-2923.

11. Kamoun, E.A., E.-R.S. Kenawy, and X. Chen, *A review on polymeric hydrogel membranes for wound dressing applications: PVA-based hydrogel dressings.* J Adv Res, 2017. **8**(3): p. 217-233.

12. Nicolson, P.C. and J. Vogt, *Soft contact lens polymers: an evolution.* Biomaterials, 2001. **22**(24): p. 3273-3283.

13. Lee, K.Y. and D.J. Mooney, *Hydrogels for tissue engineering.* Chem Rev, 2001. **101**(7): p. 1869-1880.

14. Nicodemus, G.D. and S.J. Bryant, *Cell encapsulation in biodegradable hydrogels for tissue engineering applications.* Tissue Eng Part B Rev, 2008. **14**(2): p. 149-165.

15. Boschetti, F., et al., *Biomechanical properties of human articular cartilage under compressive loads.* Biorheology, 2004. **41**: p. 159-66.

16. Kerin, A., M. Wisnom, and M. Adams, *The compressive strength of articular cartilage.* Proc Inst Mech Eng H J Eng Med, 1998. **212**(4): p. 273-280.

17. Maganaris, C.N. and J.P. Paul, *In vivo human tendon mechanical properties.* J Physiol, 1999. **521 Pt 1**(Pt 1): p. 307-313.

18. Smeets, K., et al., *Mechanical analysis of extra-articular knee ligaments. Part one: Native knee ligaments.* Knee, 2017. **24**(5): p. 949-956.

19. Skardal, A., J. Zhang, and G.D. Prestwich, *Bioprinting vessel-like constructs using hyaluronan hydrogels crosslinked with tetrahedral polyethylene glycol tetracrylates.* Biomaterials, 2010. **31**(24): p. 6173-6181.

20. Hahn, M.S., et al., *Physiologic pulsatile flow bioreactor conditioning of poly(ethylene glycol)-based tissue engineered vascular grafts.* Ann Biomed Eng, 2007. **35**(2): p. 190-200.

21. Liu, Z. and P. Calvert, *Multilayer hydrogels as muscle-like actuators.* Adv Mater, 2000. **12**(4): p. 288-291.

22. Takashima, Y., et al., *Expansion–contraction of photoresponsive artificial muscle regulated by host–guest interactions.* Nat Commun, 2012. **3**: p. 1270.

23. Xu, Y., et al., *Self-assembled graphene hydrogel via a one-step hydrothermal process.* ACS Nano, 2010. **4**(7): p. 4324-4330.

24. Lin, S., et al., *Stretchable hydrogel electronics and devices.* Adv Mater, 2016. **28**(22): p. 4497-4505.

25. Calvert, P., *Hydrogels for soft machines.* Adv Mater, 2009. **21**(7): p. 743-756.

26. Abraham, A.A., et al., *Foreign body reaction to a subcutaneously implanted self-cleaning, thermoresponsive hydrogel membrane for glucose biosensors.* ACS Biomater Sci Eng, 2018.

27. Fei, R., et al., *Self-cleaning, thermoresponsive P(NIPAAm-co-AMPS) double network membranes for implanted glucose biosensors.* Macromol Mater Eng, 2016. **301**(8): p. 935-943.

28. Woodard, H.Q.W., D.R., *The composition of body tissues.* Brit J Radiol, 1986. **59**(708): p. 1209-1218.

29. Gong, J.K., J.S. Arnold, and S.H. Cohn, *Composition of trabecular and cortical bone.* Anat Rec, 1964. **149**(3): p. 325-331.

30. Reilly, D.T. and A.H. Burstein, *The elastic and ultimate properties of compact bone tissue.* J Biomech, 1975. **8**(6): p. 393-405.

31. Gong, J.P., et al., *Double-network hydrogels with extremely high mechanical strength.* Adv Mater, 2003. **15**(14): p. 1155-1158.

32. Okay, O. and S. Durmaz, *Charge density dependence of elastic modulus of strong polyelectrolyte hydrogels.* Polymer, 2002. **43**(4): p. 1215-1221.

33. Henderson, K.J., et al., *Ionically cross-linked triblock copolymer hydrogels with high strength.* Macromolecules, 2010. **43**(14): p. 6193-6201.

34. Yıldız, B., B. Işık, and M. Kış, *Synthesis and characterization of thermoresponsive isopropylacrylamide–acrylamide hydrogels.* Eur Polym J, 2002. **38**(7): p. 1343-1347.

35. Ning, J., et al., *Characteristics of zwitterionic sulfobetaine acrylamide polymer and the hydrogels prepared by free-radical polymerization and effects of physical and chemical crosslinks on the UCST.* React Funct Polym, 2013. **73**(7): p. 969-978.

36. Yasuda, K., et al., *Biomechanical properties of high-toughness double network hydrogels.* Biomaterials, 2005. **26**(21): p. 4468-4475.

37. Haque, M.A., T. Kurokawa, and J.P. Gong, *Super tough double network hydrogels and their application as biomaterials.* Polymer, 2012. **53**(9): p. 1805-1822.

38. Milner, P.E., et al., *A low friction, biphasic and boundary lubricating hydrogel for cartilage replacement.* Acta Biomater, 2018. **65**: p. 102-111.

39. Chen, Q., et al., *Simultaneous enhancement of stiffness and toughness in hybrid double-network hydrogels via the first, physically linked network.* Macromolecules, 2015. **48**(21): p. 8003-8010.

40. Sun, J.-Y., et al., *Highly stretchable and tough hydrogels.* Nature, 2012. **489**: p. 133.

41. Chen, F., et al., *Conductive regenerated silk-fibroin-based hydrogels with integrated high mechanical performances.* J Mater Chem B, 2019.

42. Kaneko, D., et al., *Mechanically strong hydrogels with ultra-low frictional coefficients.* Adv Mater, 2005. **17**(5): p. 535-538.

43. Argun, A., et al., *Nonionic double and triple network hydrogels of high mechanical strength.* Macromolecules, 2014. **47**(18): p. 6430-6440.

44. Fu, J., *Strong and tough hydrogels crosslinked by multi-functional polymer colloids.* J Polym Sci B Polym Phys, 2018. **56**(19): p. 1336-1350.

45. Li, J., J. Yang, and W. Liu, *A mechanically robust, stiff, and tough hyperbranched supramolecular polymer hydrogel.* Macromol Rapid Commun, 2018. **0**(0): p. 1800819.

46. Huang, T., et al., *A novel hydrogel with high mechanical strength: A macromolecular microsphere composite hydrogel.* Adv Mater, 2007. **19**(12): p. 1622-1626.

47. Haraguchi, K. and H.-J. Li, *Mechanical properties and structure of polymer−clay nanocomposite gels with high clay content.* Macromolecules, 2006. **39**(5): p. 1898-1905.

48. Gaharwar, A.K., et al., *Highly extensible, tough, and elastomeric nanocomposite hydrogels from poly(ethylene glycol) and hydroxyapatite nanoparticles.* Biomacromolecules, 2011. **12**(5): p. 1641-1650.

49. Tanpichai, S. and K. Oksman, *Cross-linked nanocomposite hydrogels based on cellulose nanocrystals and PVA: Mechanical properties and creep recovery.* Compos Part A Appl Sci Manuf, 2016. **88**: p. 226-233.

50. King, D.R., et al., *Extremely tough composites from fabric reinforced polyampholyte hydrogels.* Mater Horiz, 2015. **2**(6): p. 584-591.

51. Kundanati, L., et al., *Fabrication and mechanical characterization of hydrogel infused network silk scaffolds.* Int J Mol Sci, 2016. **17**(10): p. 1631.

52. Huang, Y., et al., *Energy-dissipative matrices enable synergistic toughening in fiber reinforced soft composites.* Adv Funct Mater, 2017. **27**(9): p. 1605350.

53. Castilho, M., et al., *Mechanical behavior of a soft hydrogel reinforced with three-dimensional printed microfibre scaffolds.* Sci Rep, 2018. **8**(1): p. 1245-1245.

54. Feng, H., et al., *Poly(acrylamide)-MWNTs hybrid hydrogel with extremely high mechanical strength*, in *Open Chem*. 2016. p. 150.

55. Peppas, N.A. and S.R. Stauffer, *Reinforced uncrosslinked poly (vinyl alcohol) gels produced by cyclic freezing-thawing processes: a short review.* J Control Release, 1991. **16**(3): p. 305-310.

56. Li, A., et al., *Polyvinyl alcohol nanocrystal assisted hydrogels with high toughness and elastic modulus for 3D printing.* ACS Appl Nano Mater, 2019.

57. Liu, T., et al., *Super-strong and tough poly(vinyl alcohol)/poly(acrylic acid) hydrogels reinforced by hydrogen bonding.* J Mater Chem B, 2018. **6**(48): p. 8105-8114.

58. Mredha, M.T.I., et al., *Hydrogels with superior mechanical properties from the synergistic effect in hydrophobic–hydrophilic copolymers.* Chem Eng J, 2019. **362**: p. 325-338.

59. Stammen, J.A., et al., *Mechanical properties of a novel PVA hydrogel in shear and unconfined compression.* Biomaterials, 2001. **22**(8): p. 799-806.

60. Luo, F., et al., *Strong and tough polyion-complex hydrogels from oppositely charged polyelectrolytes: A comparative study with polyampholyte hydrogels.* Macromolecules, 2016. **49**(7): p. 2750-2760.

61. Luo, F., et al., *Oppositely charged polyelectrolytes form tough, self-healing, and rebuildable hydrogels.* Adv Mater, 2015. **27**(17): p. 2722-2727.

62. Sun, T.L., et al., *Physical hydrogels composed of polyampholytes demonstrate high toughness and viscoelasticity.* Nat Mater, 2013. **12**: p. 932.

63. Lin, P., et al., *Molecularly engineered dual-crosslinked hydrogel with ultrahigh mechanical strength, toughness, and good self-recovery.* Adv Mater, 2015. **27**(12): p. 2054-2059.

64. Lin, P., et al., *Freezing molecular orientation under stretch for high mechanical strength but anisotropic hydrogels.* Small, 2016. **12**(32): p. 4386-4392.

65. Zhang, J., et al., *Intermolecular hydrogen bonding strategy to fabricate mechanically strong hydrogels with high elasticity and fatigue resistance.* Soft Matter, 2013. **9**(27): p. 6331-6337.

66. Liang, Y., et al., *Ultrastiff, tough, and healable ionic–hydrogen bond cross-linked hydrogels and their uses as building blocks to construct complex hydrogel structures.* ACS Appl Mater Interfaces, 2019.

67. Wang, Z., et al., *3D-printable self-healing and mechanically reinforced hydrogels with host–guest non-covalent interactions integrated into covalently linked networks.* Mater Horiz, 2019.

68. Dong, W., et al., *Superior mechanical properties of double-network hydrogels reinforced by carbon nanotubes without organic modification.* Int J Mol Sci, 2013. **14**(11): p. 22380-22394.

69. Du, G., et al., *Tough and fatigue resistant biomimetic hydrogels of interlaced self-assembled conjugated polymer belts with a polyelectrolyte network.* Chem Mater, 2014. **26**(11): p. 3522-3529.

70. Li, Z., et al., *A novel biocompatible double network hydrogel consisting of konjac glucomannan with high mechanical strength and ability to be freely shaped.* J Mater Chem B, 2015. **3**(9): p. 1769-1778.

71. Wang, J., et al., *Ion-linked double-network hydrogel with high toughness and stiffness.* J Mater Sci, 2015. **50**(16): p. 5458-5465.

72. Xiang, S., et al., *Hierarchical structural double network hydrogel with high strength, toughness, and good recoverability.* New J Chem, 2017. **41**(23): p. 14397-14402.

73. Huang, S., et al., *Nanocellulose reinforced P(AAm-co-AAc) hydrogels with improved mechanical properties and biocompatibility.* Compos Part A Appl Sci Manuf, 2018. **112**: p. 395-404.

74. Means, A.K., et al., *Thermoresponsive double network hydrogels with exceptional compressive mechanical properties.* Macromol Rapid Commun, 2017. **38**(20): p. 1700351.

75. Means, A.K., et al., *Double network hydrogels that mimic the modulus, strength and lubricity of cartilage.* submitted, 2019.

76. Fei, R., et al., *Ultra-strong thermoresponsive double network hydrogels.* Soft Matter, 2013. **9**(10): p. 2912-2919.

77. Wang, L., G. Shan, and P. Pan, *A strong and tough interpenetrating network hydrogel with ultrahigh compression resistance.* Soft Matter, 2014. **10**(21): p. 3850-3856.

78. Chen, P., et al., *One-pot preparation of ultrastrong double network hydrogels.* J Polym Res, 2012. **19**(3): p. 1-4.

79. Gong, J.P., *Why are double network hydrogels so tough?* Soft Matter, 2010. **6**(12): p. 2583-2590.

80. Panteli, P.A. and C.S. Patrickios, *Complex hydrogels based on multiply interpenetrated polymer networks: Enhancement of mechanical properties via network multiplicity and monomer concentration.* Macromolecules, 2018. **51**(19): p. 7533-7545.

81. Groll, J., *Mechanically strong microstructured hydrogels based on reactive star-shaped prepolymers.* Macromol Symp, 2015. **358**(1): p. 148-156.

82. Sun, Y., et al., *Multi-responsive and tough hydrogels based on triblock copolymer micelles as multi-functional macro-crosslinkers.* Chem Commun, 2015. **51**(40): p. 8512-8515.

83. Wang, H., et al., *Synthesis and characterization of multi-sensitive microgel-based polyampholyte hydrogels with high mechanical strength.* Colloid Polym Sci, 2016. **294**(2): p. 367-380.

84. Haraguchi, K. and T. Takehisa, *Nanocomposite hydrogels: A unique organic–inorganic network structure with extraordinary mechanical, optical, and swelling/de-swelling properties.* Adv Mater, 2002. **14**(16): p. 1120-1124.

85. Gao, G., et al., *Tough nanocomposite double network hydrogels reinforced with clay nanorods through covalent bonding and reversible chain adsorption.* J Mater Chem B, 2014. **2**(11): p. 1539-1548.

86. Rose, S., et al., *Time dependence of dissipative and recovery processes in nanohybrid hydrogels.* Macromolecules, 2013. **46**(10): p. 4095-4104.

87. Lin, W.-C., et al., *Large strain and fracture properties of poly(dimethylacrylamide)/silica hybrid hydrogels.* Macromolecules, 2010. **43**(5): p. 2554-2563.

88. Wang, Q., et al., *Super-tough double-network hydrogels reinforced by covalently compositing with silica-nanoparticles.* Soft Matter, 2012. **8**(22): p. 6048-6056.

89. Bilici, C., et al., *Melt-processable shape-memory hydrogels with self-healing ability of high mechanical strength.* Macromolecules, 2016. **49**(19): p. 7442-7449.

90. Li, J., Z. Suo, and J.J. Vlassak, *Stiff, strong, and tough hydrogels with good chemical stability.* J Mater Chem B, 2014. **2**(39): p. 6708-6713.

91. Sun, Y., et al., *Preparation of high tough poly(vinyl alcohol) hydrogel by soaking in NaCl aqueous solution.* Mater Lett, 2017. **194**: p. 34-37.

92. Chen, L., et al., *Effects of polyelectrolyte complexation on the UCST of zwitterionic polymer.* Polymer, 2000. **41**(1): p. 141-147.

93. Haque, M.A., et al., *Lamellar bilayers as reversible sacrificial bonds to toughen hydrogel: Hysteresis, self-recovery, fatigue resistance, and crack blunting.* Macromolecules, 2011. **44**(22): p. 8916-8924.

94. Eslami, M., et al., *Fiber-reinforced hydrogel scaffolds for heart valve tissue engineering.* J Biomater Appl, 2014. **29**(3): p. 399-410.

95. Coburn, J., et al., *Biomimetics of the extracellular matrix: An integrated three-dimensional fiber-hydrogel composite for cartilage tissue engineering.* Smart Struct Syst, 2011. **7**(3): p. 213-222.

96. Agrawal, A., N. Rahbar, and P.D. Calvert, *Strong fiber-reinforced hydrogel.* Acta Biomater, 2013. **9**(2): p. 5313-5318.

97. Lin, S., et al., *Design of stiff, tough and stretchy hydrogel composites via nanoscale hybrid crosslinking and macroscale fiber reinforcement.* Soft Matter, 2014. **10**(38): p. 7519-7527.

98. Young, C.-D., J.-R. Wu, and T.-L. Tsou, *High-strength, ultra-thin and fiber-reinforced pHEMA artificial skin.* Biomaterials, 1998. **19**(19): p. 1745-1752.

99. Yang, X., et al., *Extremely stiff and strong nanocomposite hydrogels with stretchable cellulose nanofiber/poly(vinyl alcohol) networks.* Cellulose, 2018. **25**: p. 6571-6580.

100. Hagiwara, Y., et al., *Ligament-like tough double-network hydrogel based on bacterial cellulose.* Cellulose, 2010. **17**(1): p. 93-101.

101. Nakayama, A., et al., *High mechanical strength double-network hydrogel with bacterial cellulose.* Adv Funct Mater, 2004. **14**(11): p. 1124-1128.

102. Zhang, H.J., et al., *Tough physical double-network hydrogels based on amphiphilic triblock copolymers.* Adv Mater, 2016. **28**(24): p. 4884-4890.

103. Xu, Z., et al., *Tough and self-recoverable hydrogels crosslinked by triblock copolymer micelles and Fe3+ coordination.* J Polym Sci B Polym Phys, 2018. **56**(11): p. 865-876.

104. Li, H., et al., *A highly tough and stiff supramolecular polymer double network hydrogel.* Polymer, 2018. **153**: p. 193-200.

105. Muniz, E.C. and G. Geuskens, *Compressive elastic modulus of polyacrylamide hydrogels and semi-IPNs with poly(N-isopropylacrylamide).* Macromolecules, 2001. **34**(13): p. 4480-4484.

106. Moschou, E.A., et al., *Voltage-switchable artificial muscles actuating at near neutral pH.* Sens Actuators B Chem, 2006. **115**(1): p. 379-383.

107. Jiao, C., et al., *Rigid and strong thermoresponsive shape memory hydrogels transformed from poly(vinylpyrrolidone-co-acryloxy acetophenone) organogels.* ACS Appl Mater Interfaces, 2018. **10**(38): p. 32707-32716.

108. Liu, S., et al., *Tough and responsive oppositely charged nanocomposite hydrogels for use as bilayer actuators assembled through interfacial electrostatic attraction.* J Mater Chem B, 2016. **4**(19): p. 3239-3246.

109. Chen, Y., et al., *Tough robust dual responsive nanocomposite hydrogel as controlled drug delivery carrier of asprin.* J Mech Behav Biomed Mater, 2019. **92**: p. 179-187.

110. Tang, J., et al., *Magnetic double-network hydrogels for tissue hyperthermia and drug release.* J Mater Chem B, 2019.

111. Wang, N., et al., *High-strength photoresponsive hydrogels enable surface-mediated gene delivery and light-induced reversible cell adhesion/detachment.* Langmuir, 2014. **30**(39): p. 11823-11832.

112. Zhang, H., et al., *A thermo-responsive dual-crosslinked hydrogel with ultrahigh mechanical strength.* RSC Adv, 2016. **6**(68): p. 63848-63854.

113. Zhao, J., et al., *Mechanically strong and thermosensitive macromolecular microsphere composite poly(N-isopropylacrylamide) hydrogels.* Polymer, 2013. **54**(6): p. 1596-1602.

114. Sun, Y.-n., et al., *Super tough, ultrastretchable, and thermoresponsive hydrogels with functionalized triblock copolymer micelles as macro-cross-linkers.* ACS Macro Lett, 2014. **3**(5): p. 496-500.

115. Shin, M.K., et al., *Nanocomposite hydrogel with high toughness for bioactuators.* Adv Mater, 2009. **21**(17): p. 1712-1715.

116. Gao, H., et al., *Double hydrogen-bonding pH-sensitive hydrogels retaining high-strengths over a wide pH range.* Macromol Rapid Commun, 2013. **34**(1): p. 63-68.

117. Naficy, S., et al., *A pH-sensitive, strong double-network hydrogel: Poly(ethylene glycol) methyl ether methacrylates–poly(acrylic acid).* J Polym Sci B Polym Phys, 2012. **50**(6): p. 423-430.

118. Giammanco, G.E., et al., *Photoresponsive polysaccharide-based hydrogels with tunable mechanical properties for cartilage tissue engineering.* ACS Appl Mater Interfaces, 2016. **8**(23): p. 14423-14429.

119. Li, Z., et al., *Preparation and characterization of pH- and temperature-responsive nanocomposite double network hydrogels.* Mater Sci Eng C, 2013. **33**(4): p. 1951-1957.

120. Fei, R., et al., *Thermoresponsive nanocomposite double network hydrogels.* Soft Matter, 2012. **8**(2): p. 481-487.

121. Xu, K., et al., *A novel multi-responsive polyampholyte composite hydrogel with excellent mechanical strength and rapid shrinking rate.* J Colloid Interface Sci, 2010. **345**(2): p. 360-368.

122. Gant, R.M., et al., *Development of a self-cleaning sensor membrane for implantable biosensors.* J Biomed Mater Res A, 2009. **90**(3): p. 695-701.

123. Hou, Y., et al., *Thermoresponsive nanocomposite hydrogels with cell-releasing behavior.* Biomaterials, 2008. **29**(22): p. 3175-84.

124. Kobayashi, J. and T. Okano, *Fabrication of a thermoresponsive cell culture dish: a key technology for cell sheet tissue engineering.* Sci Technol Adv Mater, 2010. **11**(1): p. 014111.

125. Okano, T., et al., *Mechanism of cell detachment from temperature-modulated, hydrophilic-hydrophobic polymer surfaces.* Biomaterials, 1995. **16**(4): p. 297-303.

126. Tang, Z., Y. Akiyama, and T. Okano, *Temperature-responsive polymer modified surface for cell sheet engineering.* Polymers, 2012. **4**(3): p. 1478-1498.

127. Yang, J., et al., *Cell delivery in regenerative medicine: the cell sheet engineering approach.* J Control Release, 2006. **116**(2): p. 193-203.

128. Dong, L.-C. and A.S. Hoffman, *Synthesis and application of thermally reversible heterogels for drug delivery.* J Control Release, 1990. **13**(1): p. 21-31.

129. Yamato, M., et al., *Temperature-responsive cell culture surfaces for regenerative medicine with cell sheet engineering.* Prog Polym Sci, 2007. **32**(8): p. 1123-1133.

130. Cummins, B.M., et al., *Overcoming the aggregation problem: A new type of fluorescent ligand for ConA-based glucose sensing.* Biosens Bioelectron, 2015. **63**: p. 53-60.

131. Abraham, A.A., et al., *Self-cleaning membrane to extend the lifetime of an implanted glucose biosensor.* ACS Appl Mater Interfaces, 2013. **5**(24): p. 12832-8.

132. Pailler-Mattei, C., S. Bec, and H. Zahouani, *In vivo measurements of the elastic mechanical properties of human skin by indentation tests.* Med Eng Phys, 2008. **30**(5): p. 599-606.

133. Liang, X. and S.A. Boppart, *Biomechanical properties of in vivo human skin from dynamic optical coherence elastography.* IEEE Trans Biomed Eng, 2010. **57**(4): p. 953-959.

134. Helton, K.L., B.D. Ratner, and N.A. Wisniewski, *Biomechanics of the sensor-tissue interface—effects of motion, pressure, and design on sensor performance and foreign body response—part II: Examples and application.* J Diabetes Sci Technol, 2011. **5**(3): p. 647-656.

135. Voskerician, G. and J.M. Anderson, *Foreign body reaction*, in *Wiley Encyclopedia of Biomedical Engineering*. 2006, John Wiley & Sons, Inc.

136. Bota, P.C., et al., *Biomaterial topography alters healing in vivo and monocyte/macrophage activation in vitro.* J Biomed Mater Res A, 2010. **95**(2): p. 649-57.

137. Morais, J.M., F. Papadimitrakopoulos, and D.J. Burgess, *Biomaterials/tissue interactions: possible solutions to overcome foreign body response.* AAPS J, 2010. **12**(2): p. 188-96.

138. Ratner, B.D. and S.J. Bryant, *Biomaterials: Where we have been and where we are going.* Annu Rev Biomed Eng, 2004. **6**(1): p. 41-75.

139. Novak, M.T., F. Yuan, and W.M. Reichert, *Modeling the relative impact of capsular tissue effects on implanted glucose sensor time lag and signal attenuation.* Anal Bioanal Chem, 2010. **398**(4): p. 1695-1705.

140. Anderson, J.M., A. Rodriguez, and D.T. Chang, *Foreign body reaction to biomaterials.* Semin immunol, 2008. **20**(2): p. 86-100.

141. Brauker, J.H., et al., *Neovascularization of synthetic membranes directed by membrane microarchitecture.* J Biomed Mater Res, 1995. **29**(12): p. 1517-24.

142. Sharkawy, A.A., et al., *Engineering the tissue which encapsulates subcutaneous implants. II. Plasma–tissue exchange properties.* J Biomed Mater Res, 1998. **40**(4): p. 586-597.

143. Ward, W.K., et al., *The effect of microgeometry, implant thickness and polyurethane chemistry on the foreign body response to subcutaneous implants.* Biomaterials, 2002. **23**(21): p. 4185-92.

144. Lynn, A.D., T.R. Kyriakides, and S.J. Bryant, *Characterization of the in vitro macrophage response and in vivo host response to poly(ethylene glycol)-based hydrogels.* J Biomed Mater Res A, 2010. **93**(3): p. 941-53.

145. Quinn, C.A., R.E. Connor, and A. Heller, *Biocompatible, glucose-permeable hydrogel for in situ coating of implantable biosensors.* Biomaterials, 1997. **18**(24): p. 1665-70.

146. Swartzlander, M.D., et al., *Understanding the host response to cell-laden poly(ethylene glycol)-based hydrogels.* Biomaterials, 2013. **34**(4): p. 952-64.

147. Vashist, S.K., et al., *Technology behind commercial devices for blood glucose monitoring in diabetes management: A review.* Anal Chim Acta, 2011. **703**(2): p. 124-136.

148. Nichols, S.P., et al., *Biocompatible materials for continuous glucose monitoring devices.* Chem Rev, 2013. **113**(4): p. 2528-2549.

149. Turner, R.F.B., D.J. Harrison, and R.V. Rojotte, *Preliminary in vivo biocompatibility studies on perfluorosulphonic acid polymer membranes for biosensor applications.* Biomaterials, 1991. **12**(4): p. 361-368.

150. Galeska, I., et al., *Calcification-resistant nafion/Fe3+ assemblies for implantable biosensors.* Biomacromolecules, 2000. **1**(2): p. 202-207.

151. Moussy, F., et al., *Performance of subcutaneously implanted needle-type glucose sensors employing a novel trilayer coating.* Anal Chem, 1993. **65**(15): p. 2072-2077.

152. Hu, Y., Y. Zhang, and G.S. Wilson, *A needle-type enzyme-based lactate sensor for in vivo monitoring.* Anal Chim Acta, 1993. **281**(3): p. 503-511.

153. Yu, B., et al., *A long-term flexible minimally-invasive implantable glucose biosensor based on an epoxy-enhanced polyurethane membrane.* Biosens Bioelectron, 2006. **21**(12): p. 2275-2282.

154. Liao, K.-C., et al. *Design and fabrication of disposable percutaneous chemical sensors*. in *SPIE*. 2005.

155. Sung, W.J., K. Na, and Y.H. Bae, *Biocompatibility and interference eliminating property of pullulan acetate/polyethylene glycol/heparin membrane for the outer layer of an amperometric glucose sensor.* Sens Actuators B Chem, 2004. **99**(2): p. 393-398.

156. Chen, C., et al., *Current and emerging technology for continuous glucose monitoring.* Sensors (Basel, Switzerland), 2017. **17**(1): p. 182.

157. Klonoff, D.C., D. Ahn, and A. Drincic, *Continuous glucose monitoring: A review of the technology and clinical use.* Diabetes Res Clin Pract, 2017. **133**: p. 178-192.

158. Bode, B.W. and T. Battelino, *Continuous glucose monitoring.* Int J Clin Pract, 2010. **64**(s166): p. 11-15.

159. Bolles, R.C. and P.M. Duncan, *Daily course of activity and subcutaneous body temperature in hungry and thirsty rats.* Physiol Behav, 1969. **4**(1): p. 87-89.

160. Shido, O., et al., *Day—Night changes of body temperature and feeding activity in heat-acclimated rats.* Physiol Behav, 1994. **55**(5): p. 935-939.

161. Canal, T. and N.A. Peppas, *Correlation between mesh size and equilibrium degree of swelling of polymeric networks.* J Biomed Mater Res, 1989. **23**(10): p. 1183-1193.

162. Fänger, C., H. Wack, and M. Ulbricht, *Macroporous poly(N-isopropylacrylamide) hydrogels with adjustable size "cut-off" for the efficient and reversible immobilization of biomacromolecules.* Macromol Biosci, 2006. **6**(6): p. 393-402.

163. Liao, H., et al., *Influence of hydrogel mechanical properties and mesh size on vocal fold fibroblast extracellular matrix production and phenotype.* Acta Biomater, 2008. **4**(5): p. 1161-1171.

164. Horn, J., et al., *Comparison of shape memory polymer foam versus bare metal coil treatments in an in vivo porcine sidewall aneurysm model.* J Biomed Mater Res B, 2017. **105**(7): p. 1892-1905.

165. Armstrong, J.K., et al., *The hydrodynamic radii of macromolecules and their effect on red blood cell aggregation.* Biophys J, 2004. **87**(6): p. 4259-4270.

166. Khalil, E., K. Kretsos, and G.B. Kasting, *Glucose partition coefficient and diffusivity in the lower skin layers.* Pharm Res, 2006. **23**(6): p. 1227-1234.

167. Kort, W.J., et al., *A microchip implant system as a method to determine body temperature of terminally ill rats and mice.* Lab Anim, 1998. **32**(3): p. 260-269.

168. Braverman, I.M., *The cutaneous microcirculation.* J Investig Dermatol Symp Proc, 2000. **5**(1): p. 3-9.

169. Frost, M. and M.E. Meyerhoff, *In vivo chemical sensors: tackling biocompatibility.* Anal Chem, 2006. **78**(21): p. 7370-7377.

170. Bryers, J.D., C.M. Giachelli, and B.D. Ratner, *Engineering biomaterials to integrate and heal: The biocompatibility paradigm shifts.* Biotechnol Bioeng, 2012. **109**(8): p. 1898-1911.

171. Anderson, J.M., *Biological responses to materials.* Annu Rev Mater Res, 2001. **31**(1): p. 81-110.

172. Wisniewski, N., F. Moussy, and W.M. Reichert, *Characterization of implantable biosensor membrane biofouling.* Fresenius' J Anal Chem, 2000. **366**(6): p. 611-621.

173. Rebrin, K., et al., *Subcutaneous glucose monitoring by means of electrochemical sensors: fiction or reality?* J Biomed Eng, 1992. **14**(1): p. 33-40.

174. Caccomo, S., *FDA approves first continuous glucose monitoring system with a fully implantable glucose sensor and compatible mobile app for adults with diabetes*. 2018, U.S. Food & Drug Administration.

175. Wang, C., et al., *Synthesis and performance of novel hydrogels coatings for implantable glucose sensors.* Biomacromolecules, 2008. **9**(2): p. 561-567.

176. Gerritsen, M., J.A. Jansen, and J.A. Lutterman, *Performance of subcutaneously implanted glucose sensors for continuous monitoring.* Neth J Med, 1999. **54**(4): p. 167-179.

177. Onuki, Y., et al., *A review of the biocompatibility of implantable devices: Current challenges to overcome foreign body response.* J Diabetes Sci Technol, 2008. **2**(6): p. 1003-1015.

178. Daley, J.M., et al., *Glucose metabolism in injured tissue: a longitudinal study.* Surgery, 1990. **107**(2): p. 187-192.

179. Quinn, C.A.P., R.E. Connor, and A. Heller, *Biocompatible, glucose-permeable hydrogel for in situ coating of implantable biosensors.* Biomaterials, 1997. **18**(24): p. 1665-1670.

180. Espadas-Torre, C. and M.E. Meyerhoff, *Thrombogenic properties of untreated and poly(ethylene oxide)-modified polymeric matrixes useful for preparing intraarterial ion-selective electrodes.* Anal Chem, 1995. **67**(18): p. 3108-3114.

181. Quinn, C.P., et al., *Photo-crosslinked copolymers of 2-hydroxyethyl methacrylate, poly(ethylene glycol) tetra-acrylate and ethylene dimethacrylate for improving biocompatibility of biosensors.* Biomaterials, 1995. **16**(5): p. 389-396.

182. Yu, B., et al., *Use of hydrogel coating to improve the performance of implanted glucose sensors.* Biosens Bioelectron, 2008. **23**(8): p. 1278-1284.

183. Ratner, B.D., *Surface modification of polymers: chemical, biological and surface analytical challenges.* Biosens Bioelectron, 1995. **10**(9): p. 797-804.

184. Nishida, K., et al., *Development of a ferrocene-mediated needle-type glucose sensor covered with newly designed biocompatible membrane, 2-methacryloyloxyethyl phosphorylcholine-co-n-butyl methacrylate.* Med Prog Technol, 1995. **21**(2): p. 91-103.

185. Lewis, A.L., *Phosphorylcholine-based polymers and their use in the prevention of biofouling.* Colloids Surf B Biointerfaces, 2000. **18**(3–4): p. 261-275.

186. Adam, S.A., et al., *Engineering the tissue which encapsulates subcutaneous implants. III. Effective tissue response times.* J Biomed Mater Res, 1998. **40**(4): p. 598-605.

187. H., B.J., et al., *Neovascularization of synthetic membranes directed by membrane microarchitecture.* J Biomed Mater Res, 1995. **29**(12): p. 1517-1524.

188. Locke, A.K., et al., *A layer-by-layer approach to retain a fluorescent glucose sensing assay within the cavity of a hydrogel membrane.* ACS Appl Bio Mater, 2018.

189. Gacasan, E.G., et al., *Templated, macroporous PEG-DA hydrogels and their potential utility as tissue engineering scaffolds.* Macromol Mater Eng, 2017. **302**(5): p. 1600512.

190. Hou, Y., et al., *Photo-cross-linked PDMSstar-PEG hydrogels: Synthesis, characterization, and potential application for tissue engineering scaffolds.* Biomacromolecules, 2010. **11**(3): p. 648-656.

191. Choi, W.J. and S.N. Robinovitch, *Pressure distribution over the palm region during forward falls on the outstretched hands.* J Biomech, 2011. **44**(3): p. 532-539.

192. Blakney, A.K., M.D. Swartzlander, and S.J. Bryant, *The effects of substrate stiffness on the in vitro activation of macrophages and in vivo host response to poly(ethylene glycol)-based hydrogels.* J Biomed Mater Res A, 2012. **100**(6): p. 1375-1386.

193. Witte, M.B. and A. Barbul, *General principles of wound healing.* Surg Clin North Am, 1997. **77**(3): p. 509-528.

194. Metz, C.N., *Fibrocytes: a unique cell population implicated in wound healing.* Cell Mol Life Sci, 2003. **60**(7): p. 1342-1350.

195. Bucala, R., et al., *Circulating fibrocytes define a new leukocyte subpopulation that mediates tissue repair.* Mol Med, 1994. **1**(1): p. 71-81.

196. Adam, S.A., et al., *Engineering the tissue which encapsulates subcutaneous implants. I. Diffusion properties.* J Biomed Mater Res, 1997. **37**(3): p. 401-412.

197. Harmon, M.E., M. Tang, and C.W. Frank, *A microfluidic actuator based on thermoresponsive hydrogels.* Polymer, 2003. **44**(16): p. 4547-4556.

198. van der Linden, H.J., et al., *Stimulus-sensitive hydrogels and their applications in chemical (micro) analysis.* Analyst, 2003. **128**(4): p. 325-331.

199. Zhu, D., et al., *Tunable-focus microlens arrays on curved surfaces.* Appl Phys Lett, 2010. **96**(8): p. 081111.

200. De Rossi, D., et al., *Pseudomuscular gel actuators for advanced robotics.* J Intell Mater Syst Struct, 1992. **3**(1): p. 75-95.

201. Zheng, W.J., et al., *Tough Al-alginate/poly(N-isopropylacrylamide) hydrogel with tunable LCST for soft robotics.* ACS Appl Mater Interfaces, 2015. **7**(3): p. 1758-1764.

202. Gant, R.M., et al., *Design of a self-cleaning thermoresponsive nanocomposite hydrogel membrane for implantable biosensors.* Acta Biomater, 2010. **6**(8): p. 2903-2910.

203. Oktar, O., P. Caglar, and W.R. Seitz, *Chemical modulation of thermosensitive poly(N-isopropylacrylamide) microsphere swelling: a new strategy for chemical sensing.* Sens Actuators B Chem, 2005. **104**(2): p. 179-185.

204. Hoffman, A.S., *Applications of thermally reversible polymers and hydrogels in therapeutics and diagnostics.* J Control Release, 1987. **6**(1): p. 297-305.

205. da Silva, R.M.P., J.F. Mano, and R.L. Reis, *Smart thermoresponsive coatings and surfaces for tissue engineering: switching cell-material boundaries.* Trends Biotechnol, 2007. **25**(12): p. 577-583.

206. Tan, H., et al., *Thermosensitive injectable hyaluronic acid hydrogel for adipose tissue engineering.* Biomaterials, 2009. **30**(36): p. 6844-6853.

207. Hoffman, A.S., A. Afrassiabi, and L.C. Dong, *Thermally reversible hydrogels: II. Delivery and selective removal of substances from aqueous solutions.* J Control Release, 1986. **4**(3): p. 213-222.

208. Chen, Y., et al., *Double network hydrogel with high mechanical strength: Performance, progress and future perspective.* Sci China Technol Sc, 2012. **55**(8): p. 2241-2254.

209. Weng, L., et al., *Mechanically strong double network photocrosslinked hydrogels from N,N-dimethylacrylamide and glycidyl methacrylated hyaluronan.* Biomaterials, 2008. **29**(14): p. 2153-2163.

210. Tanaka, Y., J.P. Gong, and Y. Osada, *Novel hydrogels with excellent mechanical performance.* Prog Polym Sci, 2005. **30**(1): p. 1-9.

211. Sin, M.-C., S.-H. Chen, and Y. Chang, *Hemocompatibility of zwitterionic interfaces and membranes.* Polym J, 2014. **46**(8): p. 436-443.

212. Zhang, Z., et al., *Superlow fouling sulfobetaine and carboxybetaine polymers on glass slides.* Langmuir, 2006. **22**(24): p. 10072-10077.

213. Chang, Y., et al., *Highly protein-resistant coatings from well-defined diblock copolymers containing sulfobetaines.* Langmuir, 2006. **22**(5): p. 2222-2226.

214. Zhang, Z., et al., *Zwitterionic hydrogels: An in vivo implantation study.* J Biomater Sci Polym Ed, 2009. **20**(13): p. 1845-1859.

215. Wu, T., et al., *Influence of zwitterions on thermomechanical properties and morphology of acrylic copolymers: Implications for electroactive applications.* Macromolecules, 2011. **44**(20): p. 8056-8063.

216. Yang, B., et al., *A thermoresponsive poly(N-vinylcaprolactam-co-sulfobetaine methacrylate) zwitterionic hydrogel exhibiting switchable anti-biofouling and cytocompatibility.* Polym Chem, 2015. **6**(18): p. 3431-3442.

217. Chang, Y., et al., *Dual-thermoresponsive phase behavior of blood compatible zwitterionic copolymers containing nonionic poly(N-isopropyl acrylamide).* Biomacromolecules, 2009. **10**(8): p. 2092-2100.

218. Chang, Y., et al., *Tunable bioadhesive copolymer hydrogels of thermoresponsive poly(N-isopropyl acrylamide) containing zwitterionic polysulfobetaine.* Biomacromolecules, 2010. **11**(4): p. 1101-1110.

219. Schulz, D.N., et al., *Phase behaviour and solution properties of sulphobetaine polymers.* Polymer, 1986. **27**(11): p. 1734-1742.

220. Sophia Fox, A.J., A. Bedi, and S.A. Rodeo, *The basic science of articular cartilage: Structure, composition, and function.* Sports Health, 2009. **1**(6): p. 461-468.

221. Hjelle, K., et al., *Articular cartilage defects in 1,000 knee arthroscopies.* Arthroscopy, 2002. **18**(7): p. 730-734.

222. Camarero-Espinosa, S., et al., *Articular cartilage: from formation to tissue engineering.* Biomater Sci, 2016. **4**(5): p. 734-767.

223. Hunziker, E.B., *Articular cartilage repair: basic science and clinical progress. A review of the current status and prospects.* Osteoarthr Cartil, 2002. **10**(6): p. 432-463.

224. Horas, U., et al., *Autologous chondrocyte implantation and osteochondral cylinder transplantation in cartilage repair of the knee joint : A prospective, comparative trial.* J Bone Joint Surg, 2003. **85**(2): p. 185-192.

225. Gudas, R., et al., *A prospective randomized clinical study of mosaic osteochondral autologous transplantation versus microfracture for the treatment of osteochondral defects in the knee joint in young athletes.* Arthroscopy, 2005. **21**(9): p. 1066-1075.

226. Camp, C.L., M.J. Stuart, and A.J. Krych, *Current concepts of articular cartilage restoration techniques in the knee.* Sports Health, 2014. **6**(3): p. 265-273.

227. Gomoll, A.H., et al., *Surgical management of articular cartilage defects of the knee.* J Bone Joint Surg, 2010. **92**(14): p. 2470-2490.

228. Hangody, L. and P. Füles, *Autologous osteochondral mosaicplasty for the treatment of full-thickness defects of weight-bearing joints : Ten years of experimental and clinical experience.* J Bone Joint Surg, 2003. **85**(suppl_2): p. 25-32.

229. Maradit Kremers, H., et al., *Prevalence of total hip and knee replacement in the united states.* J Bone Joint Surg, 2015. **97**(17): p. 1386-1397.

230. Kurtz, S.M., et al., *Future young patient demand for primary and revision joint replacement: National projections from 2010 to 2030.* Clin Orthop Relat Res, 2009. **467**(10): p. 2606-2612.

231. Nathwani, D., et al., *Partial resurfacing of the knee with the biopoly implant: Interim report at 2 years.* J Bone Joint Surg, 2017. **2**(2): p. e0011.

232. Drury, J.L. and D.J. Mooney, *Hydrogels for tissue engineering: scaffold design variables and applications.* Biomaterials, 2003. **24**(24): p. 4337-4351.

233. Baumhauer, J.F., et al., *Prospective, randomized, multi-centered clinical trial assessing safety and efficacy of a synthetic cartilage implant versus first metatarsophalangeal arthrodesis in advanced hallux rigidus.* Foot Ankle Int., 2016. **37**(5): p. 457-469.

234. Li, J., et al., *Hybrid hydrogels with extremely high stiffness and toughness.* ACS Macro Lett, 2014. **3**(6): p. 520-523.

235. Beddoes, C.M., et al., *Hydrogels as a replacement material for damaged articular hyaline cartilage.* Materials, 2016. **9**(6): p. 443.

236. Brown, T.D., et al., *Effects of osteochondral defect size on cartilage contact stress.* J Orthop Res, 1991. **9**(4): p. 559-567.

237. Dunn, A.C., et al., *Lubricity of surface hydrogel layers.* Tribol Lett, 2013. **49**(2): p. 371-378.

238. Pitenis, A.A. and W.G. Sawyer, *Lubricity of high water content aqueous gels.* Tribol Lett, 2018. **66**(3): p. 113.

239. Lin, P., et al., *Articular cartilage inspired bilayer tough hydrogel prepared by interfacial modulated polymerization showing excellent combination of high load-bearing and low friction performance.* ACS Macro Lett, 2016. **5**(11): p. 1191-1195.

240. *ASTM F732-17 standard test method for wear testing of polymeric materials used in total joint prostheses*. 2017, ASTM International: West Conshohocken, PA.

241. Katta, J.K., et al., *Friction and wear behavior of poly(vinyl alcohol)/poly(vinyl pyrrolidone) hydrogels for articular cartilage replacement.* J Biomed Mater Res A, 2007. **83A**(2): p. 471-479.

242. Baykal, D., et al., *Evaluation of friction properties of hydrogels based on a biphasic cartilage model.* J Mech Behav Biomed Mater, 2013. **28**: p. 263-273.

243. Brand, R.A., *Joint contact stress: A reasonable surrogate for biological processes?* Iowa Orthop J, 2005. **25**: p. 82-94.

244. Li, F., A. Wang, and C. Wang, *Analysis of friction between articular cartilage and polyvinyl alcohol hydrogel artificial cartilage.* J Mater Sci Mater Med, 2016. **27**(5): p. 87.

245. Debord, J.D. and L.A. Lyon, *Synthesis and characterization of pH-responsive copolymer microgels with tunable volume phase transition temperatures.* Langmuir, 2003. **19**(18): p. 7662-7664.

246. Mow, V.C., et al., *Biphasic creep and stress relaxation of articular cartilage in compression: Theory and experiments.* J Biomech Eng, 1980. **102**(1): p. 73-84.

247. Park, S., C.T. Hung, and G.A. Ateshian, *Mechanical response of bovine articular cartilage under dynamic unconfined compression loading at physiological stress levels.* Osteoarthr. Cartil., 2004. **12**(1): p. 65-73.

248. Sanchez-Adams, J., et al., *The mechanobiology of articular cartilage: Bearing the burden of osteoarthritis.* Curr Rheumatol Rep, 2014. **16**(10): p. 451-451.

249. Karobi, S.N., et al., *Creep behavior and delayed fracture of tough polyampholyte hydrogels by tensile test.* Macromolecules, 2016. **49**(15): p. 5630-5636.

250. Locke, A.K., B.M. Cummins, and G.L. Coté, *High affinity mannotetraose as an alternative to dextran in conA based fluorescent affinity glucose assay due to improved FRET efficiency.* ACS Sensors, 2016. **1**(5): p. 584-590.

251. Bornhoeft, L.R., A. Biswas, and M.J. McShane, *Composite hydrogels with engineered microdomains for optical glucose sensing at low oxygen conditions.* Biosensors, 2017. **7**(1): p. 8.

252. Pickup, J.C., D.J. Claremont, and G.W. Shaw, *Responses and calibration of amperometric glucose sensors implanted in the subcutaneous tissue of man.* Acta Diabetol, 1993. **30**(3): p. 143-148.

253. Joubert, M. and Y. Reznik, *Personal continuous glucose monitoring (CGM) in diabetes management: Review of the literature and implementation for practical use.* Diabetes Research and Clinical Practice, 2012. **96**(3): p. 294-305.

254. Pickup, J., et al., *In vivo glucose sensing for diabetes management: progress towards non-invasive monitoring.* BMJ, 1999. **319**(7220): p. 1289.

255. Matsukuma, D., K. Yamamoto, and T. Aoyagi, *Stimuli-responsive properties of N-isopropylacrylamide-based ultrathin hydrogel films prepared by photo-cross-linking.* Langmuir, 2006. **22**(13): p. 5911-5915.

256. Harmon, M.E., et al., *A surface plasmon resonance study of volume phase transitions in N-isopropylacrylamide gel films.* Macromolecules, 2002. **35**(15): p. 5999-6004.

257. Reuber, J., H. Reinhardt, and D. Johannsmann, *Formation of surface-attached responsive gel layers via electrochemically induced free-radical polymerization.* Langmuir, 2006. **22**(7): p. 3362-3367.

258. Bashir, R., et al., *Micromechanical cantilever as an ultrasensitive pH microsensor.* Appl Phys Lett, 2002. **81**(16): p. 3091-3093.

259. Mansour, J.M., *Biomechanics of Cartilage*, in *Kinesiology: the mechanics and pathomechanics of human movement*, C.A. Oatis, Editor. 2003, Lippincott Williams & Wilkins: Baltimore, MD. p. 1992-1996.

260. Shi, L., V.I. Sikavitsas, and A. Striolo, *Experimental friction coefficients for bovine cartilage measured with a pin-on-disk tribometer: Testing configuration and lubricant effects.* Ann Biomed Eng, 2011. **39**(1): p. 132-146.

261. Gleghorn, J.P. and L.J. Bonassar, *Lubrication mode analysis of articular cartilage using Stribeck surfaces.* J Biomech, 2008. **41**(9): p. 1910-1918.

262. Duan, P., et al., *The effects of pore size in bilayered poly(lactide-co-glycolide) scaffolds on restoring osteochondral defects in rabbits.* J Biomed Mater Res A, 2014. **102**(1): p. 180-192.

263. Oxley, H.R., et al., *Macroporous hydrogels for biomedical applications: methodology and morphology.* Biomaterials, 1993. **14**(14): p. 1064-1072.

264. Zhao, Q., et al., *Macroporous double-network cryogels: formation mechanism, enhanced mechanical strength and temperature/pH dual sensitivity.* Soft Matter, 2011. **7**(9): p. 4284-4293.

265. Dragan, E.S. and A.I. Cocarta, *Smart macroporous IPN hydrogels responsive to pH, temperature, and ionic strength: Synthesis, characterization, and evaluation of controlled release of drugs.* ACS Appl Mater Interfaces, 2016. **8**(19): p. 12018-12030.

266. Henderson, T.M.A., et al., *Cryogels for biomedical applications.* J Mater Chem B, 2013. **1**(21): p. 2682-2695.

267. Li, Y., et al., *Toughening hydrogels by immersing with oppositely charged polymers.* J Polym Sci B Polym Phys, 2016. **54**(23): p. 2432-2441.

268. Zhang, L., et al., *Anisotropic tough poly(vinyl alcohol) hydrogels.* Soft Matter, 2012. **8**(40): p. 10439-10447.

269. Mahdavinia, G., et al., *Synthesis of porous poly (acrylamide) hydrogels using calcium carbonate and its application for slow release of potassium nitrate.* Express Polym. Lett, 2009. **3**: p. 279-285.

270. Hwang, C.M., et al., *Fabrication of three-dimensional porous cell-laden hydrogel for tissue engineering.* Biofabrication, 2010. **2**(3): p. 035003-035003.

271. Delaney, J.T., et al., *Reactive inkjet printing of calcium alginate hydrogel porogens—a new strategy to open-pore structured matrices with controlled geometry.* Soft Matter, 2010. **6**(5): p. 866-869.

272. Stachowiak, A.N., et al., *Bioactive hydrogels with an ordered cellular structure combine interconnected macroporosity and robust mechanical properties.* Adv Mater, 2005. **17**(4): p. 399-403.

273. Draghi, L., et al., *Microspheres leaching for scaffold porosity control.* J Mater Sci Mater Med, 2005. **16**(12): p. 1093-1097.

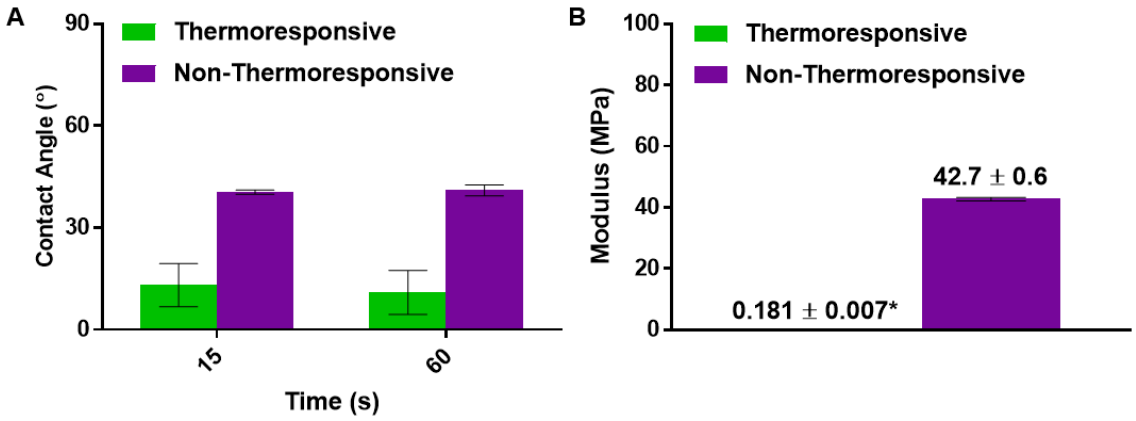

Figure A-1. (A) Contact angle of hydrogel implants confirming hydrophilicity of DNNC and PEG-DA hydrogel implants at 15 and 60 seconds. (B) Compressive modulus of both implanted materials showing the apparent difference in stiffness. *Mechanical data for the thermoresponsive DNNC membrane was previously reported by Grunlan *et al*.[120]

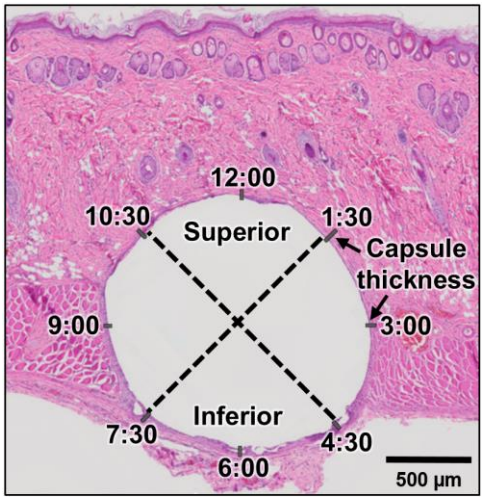

Figure A-2. Quantitative analysis of cellular presence was evaluated over four quadrants (depicted by the dotted lines) and capsule thickness was measured at 8 locations denoted on the representative histological image.

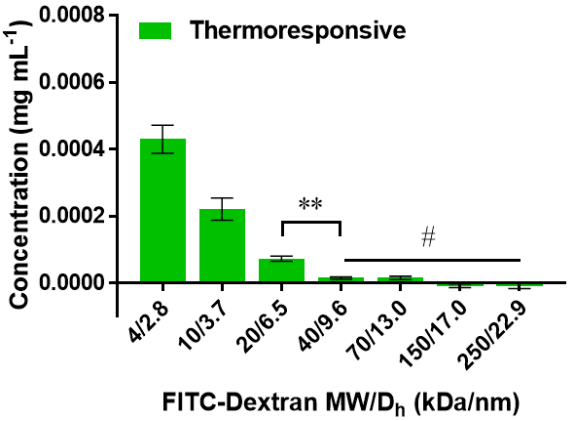

Figure A-3. Diffusion of a range of FITC-dextran MWs demonstrates the mesh size of the thermoresponsive membrane (between 6.5 to 9.6 nm), where ** indicates a significant difference of $p < 0.005$ and # indicates similarity $p > 0.05$.

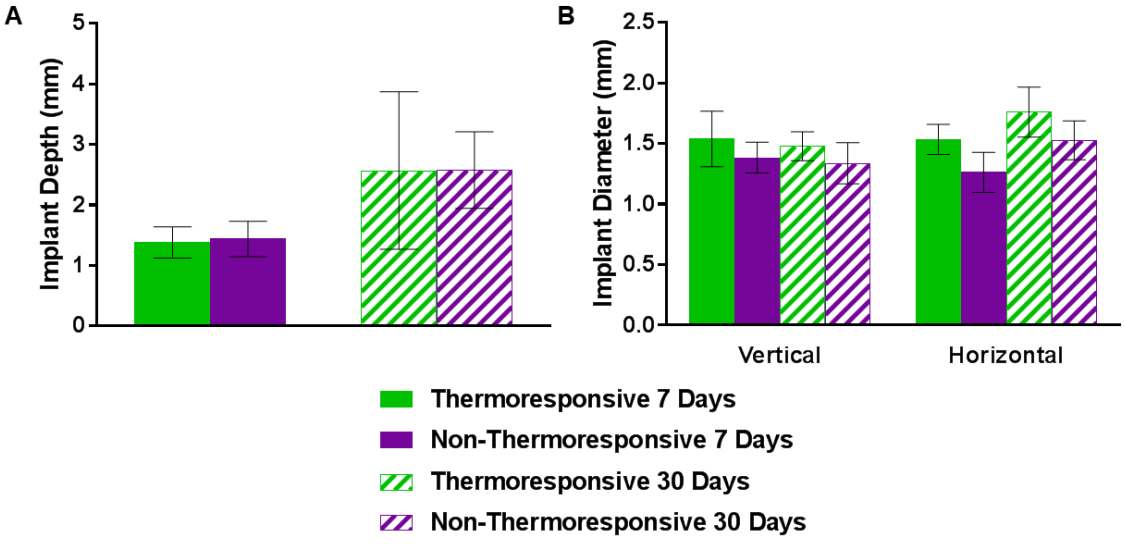

Figure A-4. Implant (A) depth measured from the surface of the skin to the top edge of the implant and (B) diameter measured perpendicular (vertical) and parallel (horizontal) to the skin after explantation.

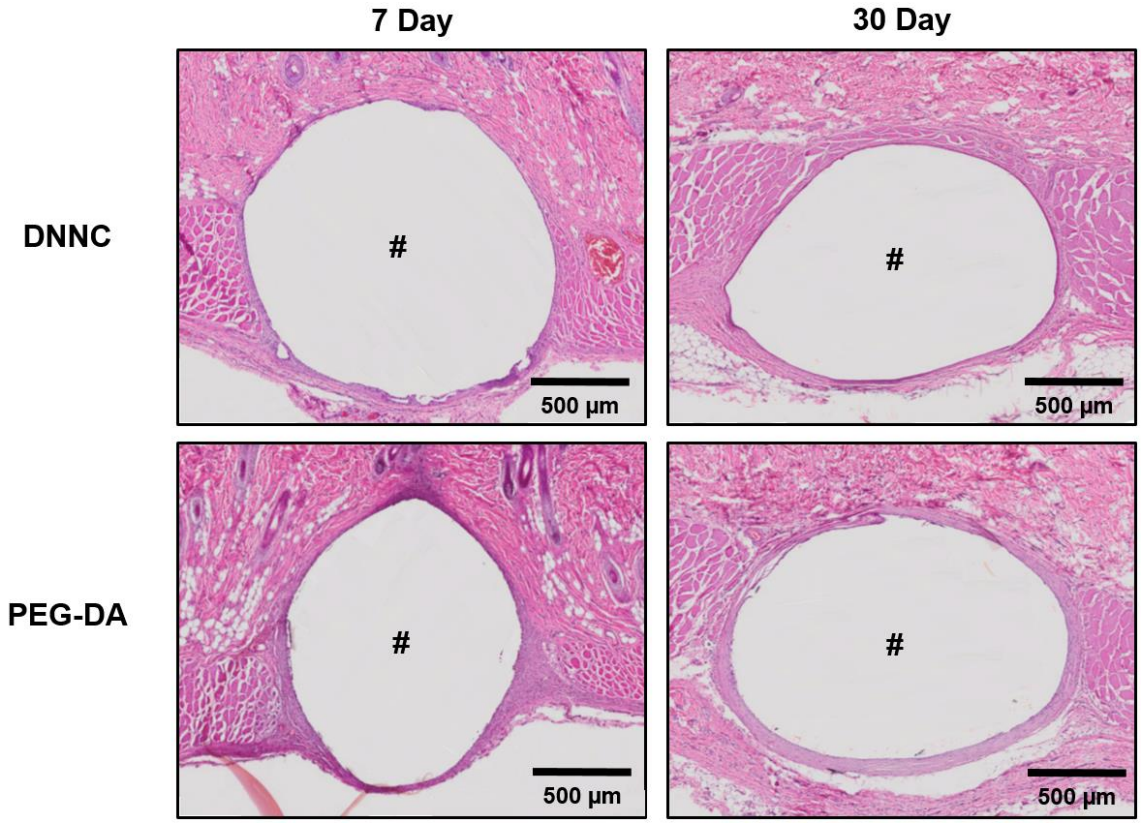

Figure A-5. Representative histological images of cross-sections of each implant marked by (#) at both 7 and 30 days broadly showing cellular response and capsule formation around circumference of each membrane, DNNC and PEG-DA.

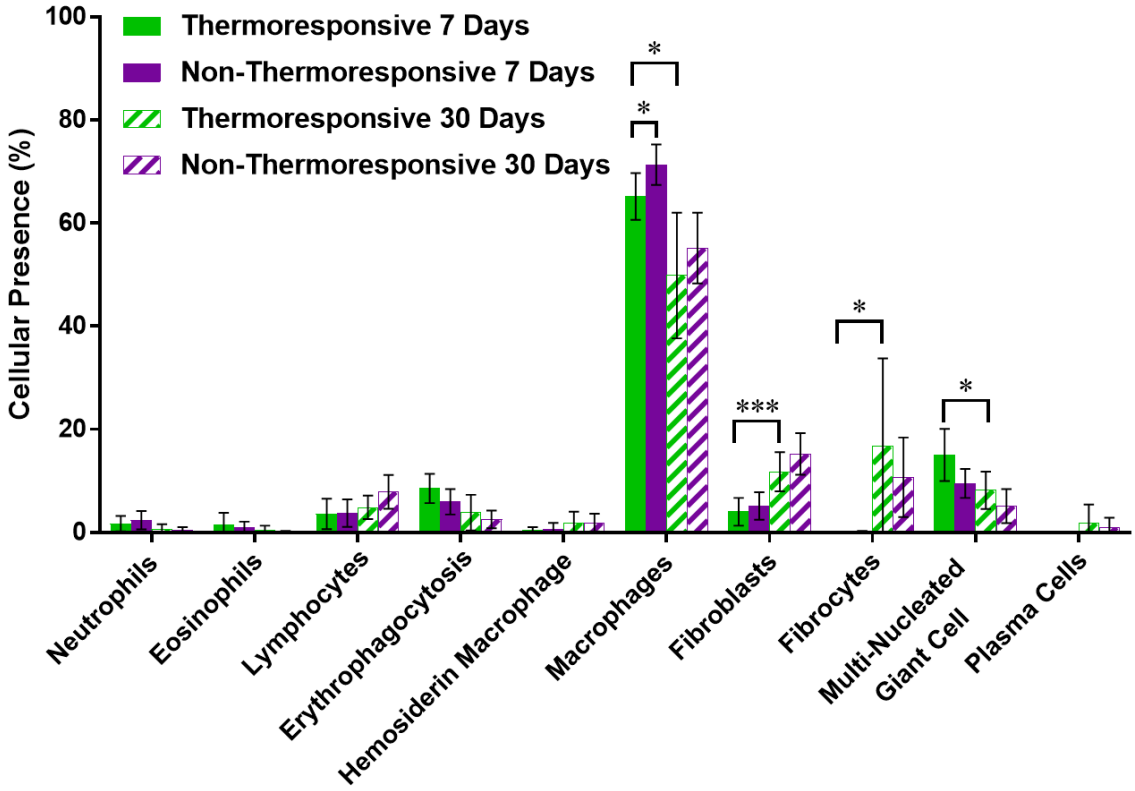

Figure A-6. Complete cellular response surrounding thermoresponsive and non-thremoresponsive implants, including other minor cell types. Graphical analysis displaying the various cell types and their approximate percentage adjacent to DNNC and PEG-DA implants after 7 and 30 days, where * indicates a significant difference of $p < 0.05$ and *** indicates a significant difference of $p < 0.005$.

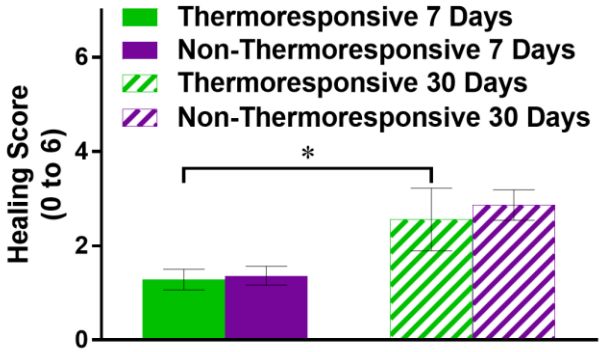

Figure A-7. The average healing score given to both implant types after 7 (solid) and 30 days (striped), with a score = 6 indicating fully healed (scores defined in Table S1). For statistics, * indicates a significant difference of $p < 0.05$.

Table A-1. Rubric for healing score combining both substrate and cellular components.

Score	Description	Substrate Components	Dominant Cellular Components
0	**Residual blood (day 0-3)**	Fibrin/proteins	Neutrophils, erythrocytes
1	**Residual blood to early-stage healing (day 3-10)**	Fibrin	Neutrophils, macrophages, lymphocytes
2	**Early-stage healing (day 10-21)**	Fibrin and loose collagen	Macrophages (erythrophagocytosis), fibroblasts, < neutrophils, lymphocytes, plasma cells
3	**Early- to mid- stage healing (day 21-30)**	Loose collagen	Macrophages, lymphocytes
4	**Mid-stage healing (day 30-60)**	Loose collagen with some dense collagen	Macrophages (hemosiderin laden), fibroblasts, fibrocytes, lymphocytes
5	**Mid-stage healing to healed (day 60-90)**	Dense collagen with some loose collagen	Lymphocytes, macrophages, decreased fibroblasts, increased fibrocytes
6	**Healed (day 90+)**	Dense collagen	Fibrocytes

Table A-2. Overall presence of vasculature (including capillaries and neovascular buds) and fibrotic tissue (including fibrin, loose collagen and dense collagen) around thermoresponsive and non-thermoresponsive implants with (-) indicating little to no presence, (+/-) indicating slight presence and (+) indicating high presence. (inner: within ~20 μm of the implant surface, outer: from ~20 μm to the outer edge of tissue capsule)

Presence of:	Implant	7 Days		30 Days	
		Inner	Outer	Inner	Outer
Capillaries	DNNC	-	+	+/-	+
	PEG-DA	-	+/-	+/-	+
Neovascular Buds	DNNC	-	+	+/-	+
	PEG-DA	-	+/-	+/-	+
Fibrin	DNNC	+		+/-	
	PEG-DA	+		+/-	
Collagen (Loose)	DNNC	+/-		+	
	PEG-DA	+/-		+	
Collagen (Dense)	DNNC	-		-	
	PEG-DA	-		-	

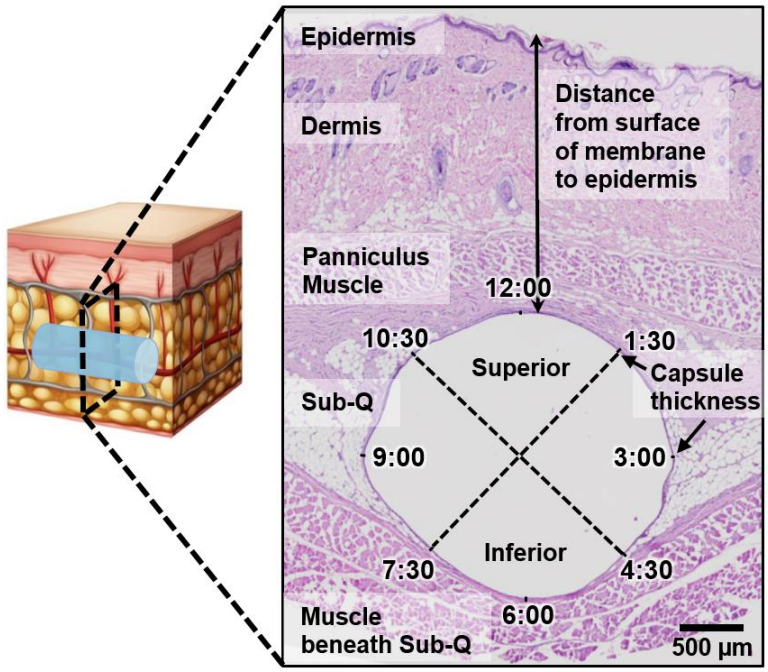

Figure A-8. Depiction of implant location, demonstrating method of measuring capsule thickness and implant depth as well as the division of four "sectors" for cell counting.

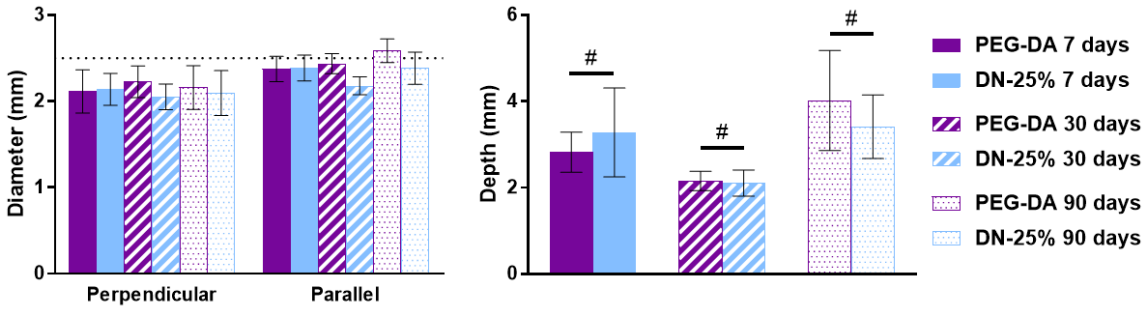

Figure A-9. Measured implant diameter (initial diameter of ~2.5 mm marked with dotted line) and depth at 7, 30 and 90 days after implantation.

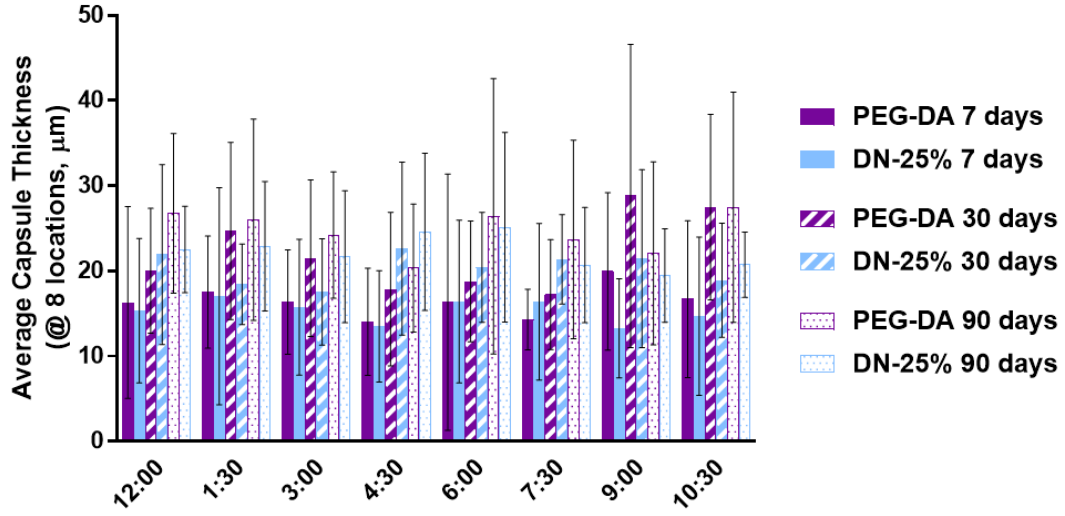

Figure A-10. Capsule thickness measurements averaged at each of the 8 locations around the implant cross-section showing little variability between different areas of the capsule.

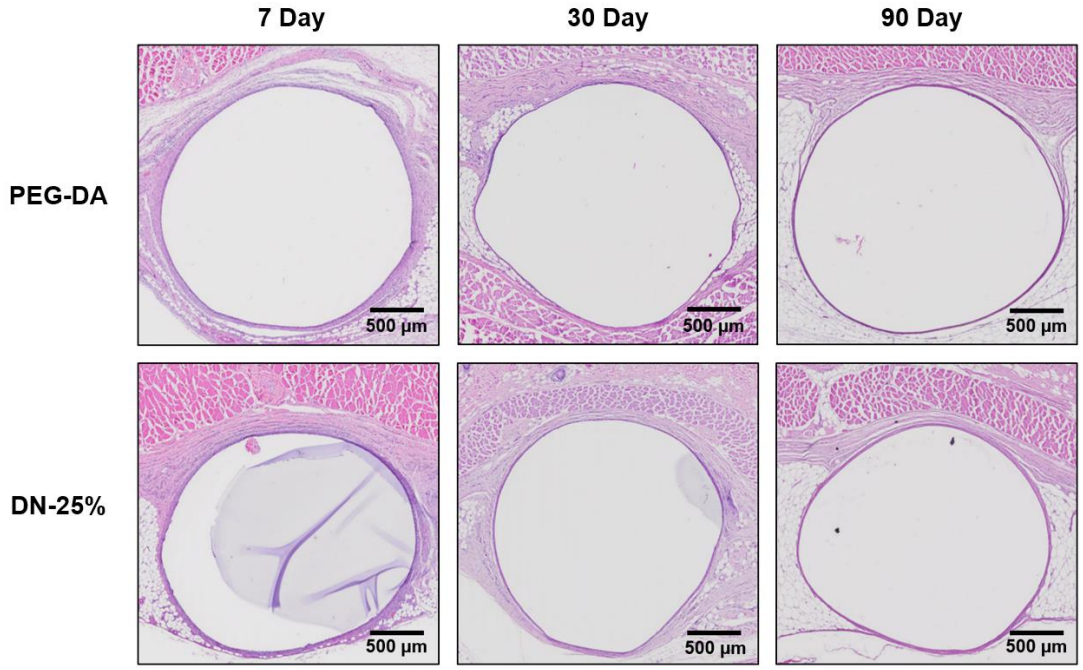

Figure A-11. H & E stained images representing tissue capsules (full cross-sections) formed around *PEG-DA* (top) and *DN-25%* (bottom) implants at 7, 30 and 90 days showing the progression towards resolution into a thin, organized tissue capsule at 90 days.

A

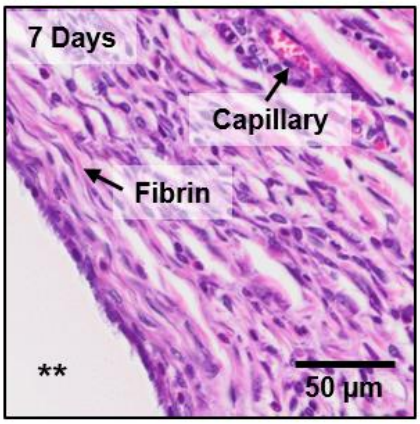

B

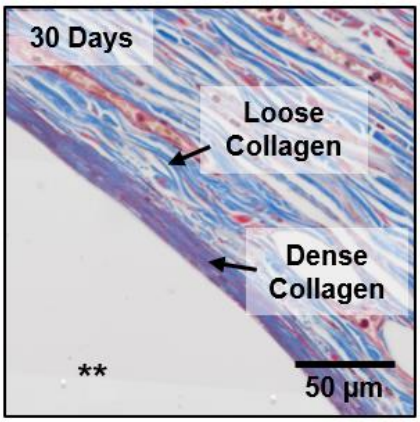

C

Presence of:	Implant	7 Days		30 Days		90 Days	
		Inner	Outer	Inner	Outer	Inner	Outer
Capillaries	DN-25%	+	+	+/-	+	-	+
	PEG-DA	+	+	+/-	+	-	+
Neovascular Buds	DN-25%	+	+	-	-	-	+
	PEG-DA	+	+	-	-	-	+
Fibrin	DN-25%	+/-		-		-	
	PEG-DA	+/-		-		-	
Collagen (Loose)	DN-25%	+		+		+/-	
	PEG-DA	+		+		+/-	
Collagen (Dense)	DN-25%	-		+		+	
	PEG-DA	-		+		+	

Figure A-12. Presence of microvasculature, fibrin and collagen within the fibrous capsule surrounding *DN-25%* implants (denoted by **). (A) Representative image showing fibrin and microvasculature at 7 days with H&E staining. (B) Representative image depicting loose and dense collagen formation at 30 days stained blue with Mason's trichrome. (C) Qualitative analysis of microvasculature and fibrous ECM components at 7, 30 and 90 days with (-) indicating little to no presence, (-/+) indicating low presence and (+) indicating a high presence within the capsule.

Table A-3. Hydrogel compositions listing values for modulus (E), strain at fracture (ε_f), and stress at fracture (σ_f).

	1st Network[a)]		2nd Network[b)]	Mechanical Properties		
Nomenclature (X-AMPS-Y)	AMPS (X)	NIPAAm	MEDSAH (Y) (wt% of NIPAAm)	E (MPa)	ε_f (mm/mm)	σ_f (MPa)
PAMPS/PNIPAAm DNs:						
0.5-AMPS-0%	0.5 M	2.0 M	0 wt%	0.32	0.49	1.33
1.0-AMPS-0%	1.0 M	2.0 M	0 wt%	0.56	0.80	10.17
1.5-AMPS-0%	1.5 M	2.0 M	0 wt%	1.20	0.79	14.10
2.0-AMPS-0%	2.0 M	2.0 M	0 wt%	2.40	0.68	11.74
PAMPS/P(NIPAAm-*co*-MEDSAH) DNs:						
1.5-AMPS-5%	1.5 M	2.0 M	5 wt%	1.46	0.81	18.18
1.5-AMPS-10%	1.5 M	2.0 M	10 wt%	1.42	0.84	21.06
1.5-AMPS-15%	1.5 M	2.0 M	15 wt%	1.53	0.85	22.94
1.5-AMPS-20%	1.5 M	2.0 M	20 wt%	1.39	0.83	18.03
1.5-AMPS-25%	1.5 M	2.0 M	25 wt%	1.27	0.83	18.07
1.5-AMPS-30%	1.5 M	2.0 M	30 wt%	1.29	0.80	15.06
PAMPS/P(NIPAAm-*co*-AAPTAC) & PAMPS/P(NIPAAm-*co*-AMPS) DNs:						
1.5-AMPS-15% AAPTAC	1.5 M	2.0 M	15 wt% AAPTAC	0.43	0.86	24.01
1.5-AMPS-15% AMPS	1.5 M	2.0 M	15 wt% AMPS	1.40	0.67	7.77

[a)] 4 mol% BIS crosslinker, 0.1 mol% 2-oxoglutaric acid initiator;
[b)] 0.1 mol% BIS crosslinker, 0.1 mol% 2-oxoglutaric acid initiator

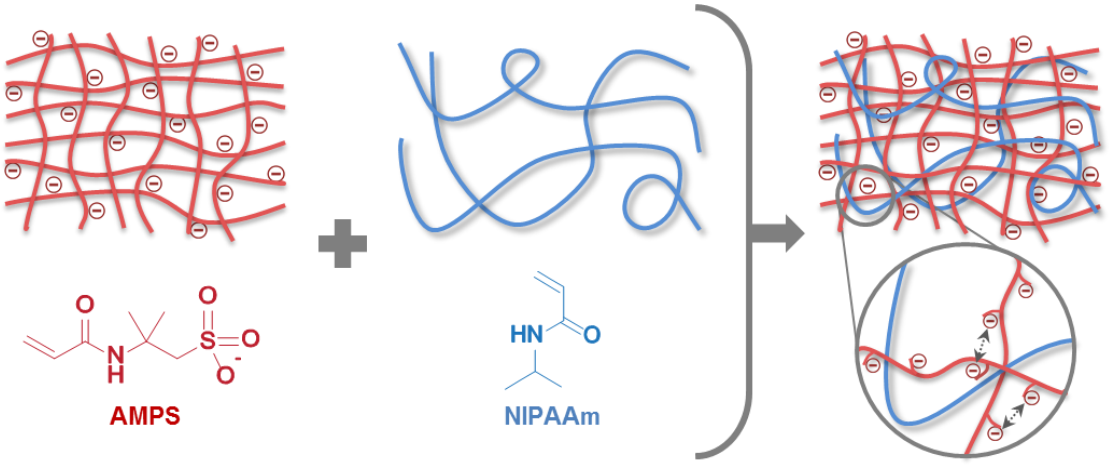

Figure A-13. PAMPS/PNIPAAm DN hydrogels formed with a tightly crosslinked, anionic PAMPS 1st network and a loosely crosslinked, neutral, thermoresponsive PNIPAAm 2nd network.

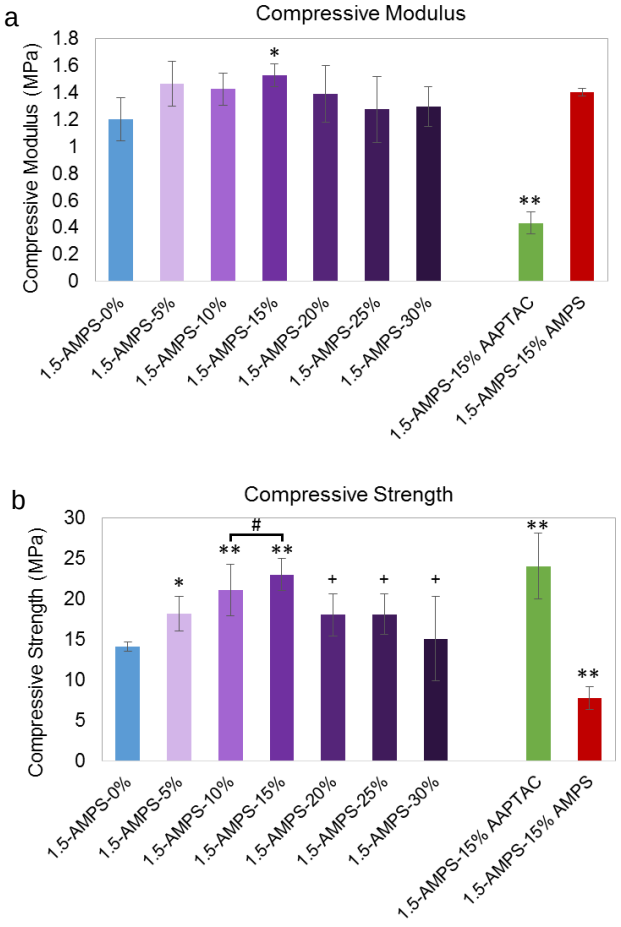

Figure A-14. Mechanical properties of the PAMPS/P(NIPAAm-*co*-MEDSAH) DN hydrogel series with additional 2nd network variations including high MEDSAH concentrations (20-30%), P(NIPAAm-co-AAPTAC) and P(NIPAAm-co-AMPS) compositions: (a) compressive modulus; [Significant difference from 1.5-AMPS-0% indicated by * ($p = 0.05$) and ** ($p < 0.01$)] and (b) compressive strength; [Significant difference from 1.5-AMPS-0% indicated by * ($p < 0.05$) and ** ($p < 0.01$), similarity of 1.5-AMPS-10% to 1.5-AMPS-15% indicated by # ($p > 0.05$), and significant difference from 1.5-AMPS-15% indicated by + ($p < 0.05$)].

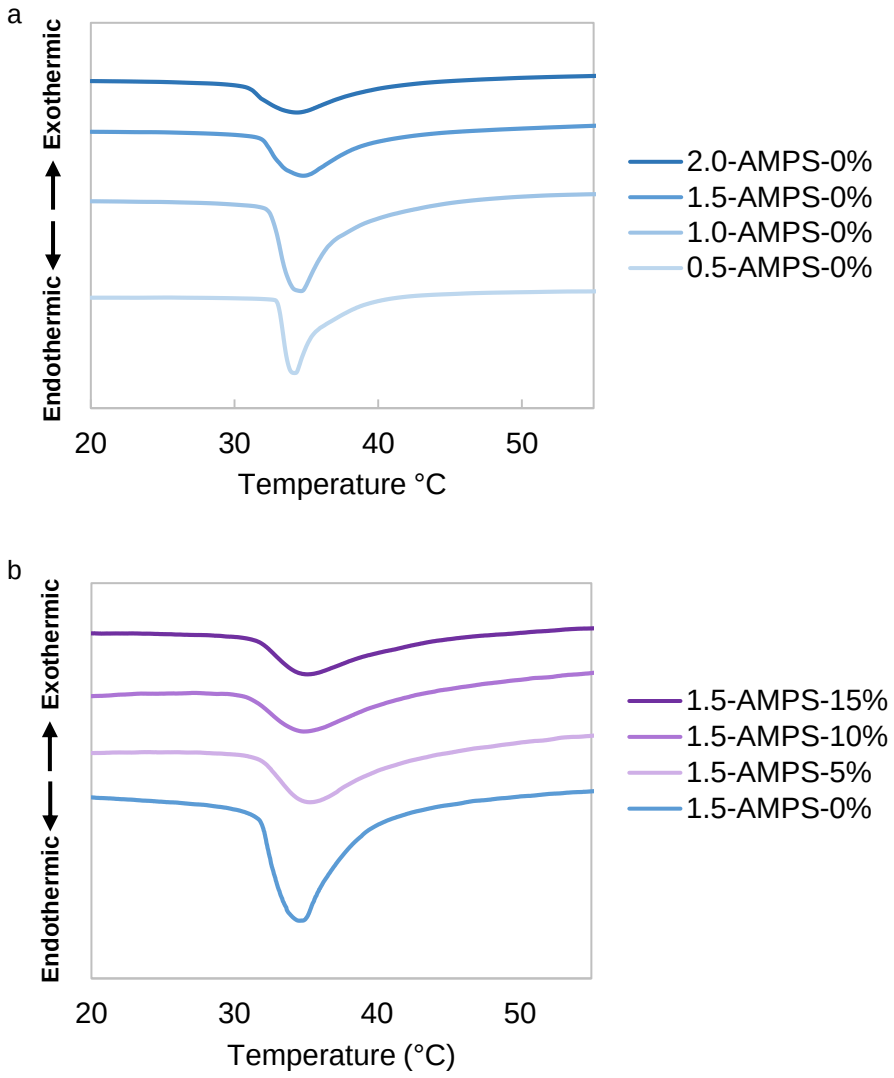

Figure A-15. DSC thermograms showing the similarity in VPTT between all DN hydrogel compositions: (a) PAMPS/PNIPAAm hydrogel series and (b) PAMPS/P(NIPAAm-*co*-MEDSAH) hydrogel series.

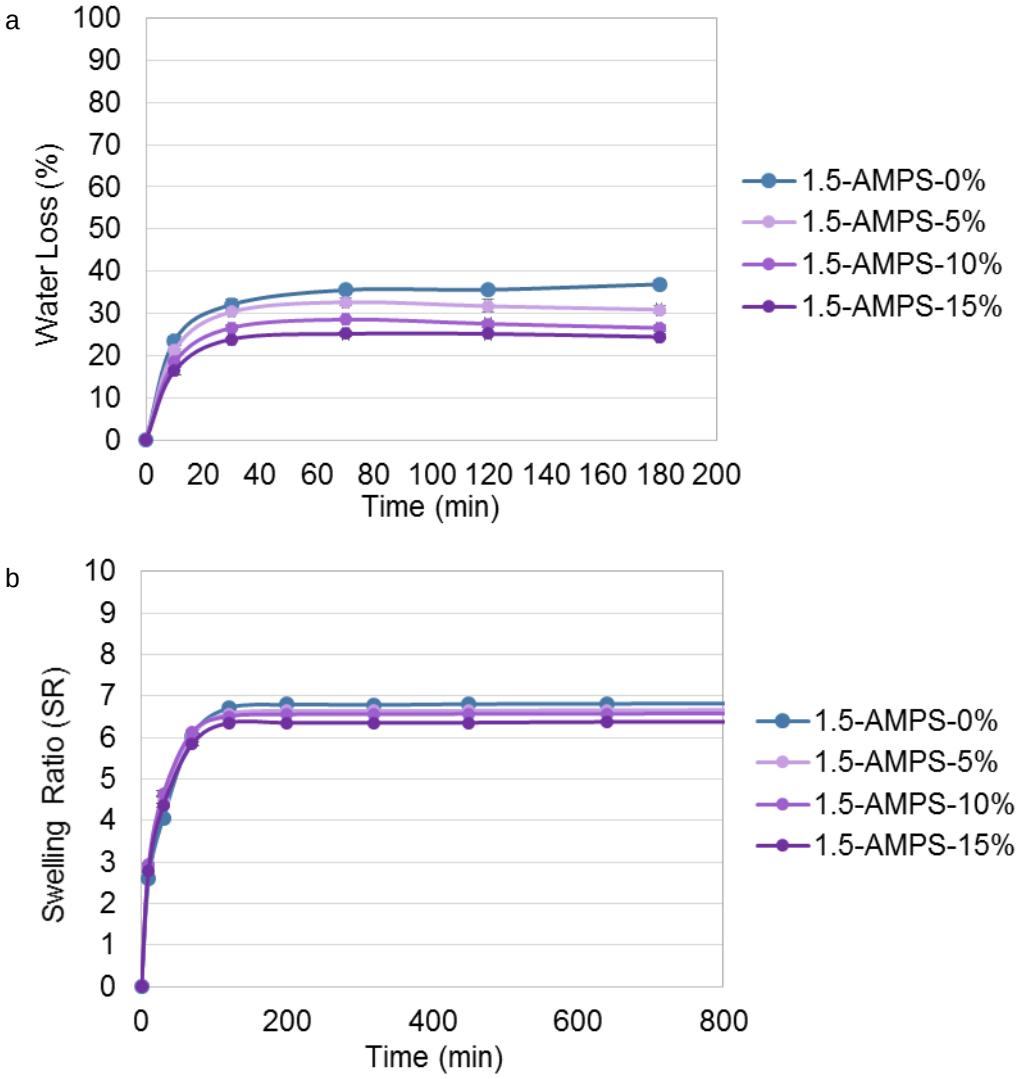

Figure A-16. Thermosensitivity of the PAMPS/P(NIPAAm-*co*-MEDSAH) hydrogel series including: (a) Deswelling rate shown by amount of water loss over time after exposure to 50 °C and (b) reswelling rate shown by increase in swelling ratio over time after dehydrated gels were immersed in 22 °C DI water.

Methods for Thermoresponsive Functionality (Chapter IV)

Equilibrium Water Content

The values for equilibrium water content reported in Table 1 were calculated as [(W_s - W_d)/ W_s] x 100, where W_s was the swollen weight of the hydrogel and W_d was the dry weight of the hydrogel after exposure to high vacuum at 50 °C overnight.

DSC for VPTT

Differential scanning calorimetry (DSC, TA Instruments Q100) was used to determine the VPTT of swollen DN hydrogels. A small square of hydrogel (~10 mg, cut with a razor blade) was blotted dry with a Kim Wipe and sealed in a hermetic pan. The sample was first cooled to 0 °C then the temperature was ramped up to 65 °C and back down to 0 °C at a rate of 3 °C min^{-1} for two continuous cycles. The VPTT was characterized by the peak temperature of the endotherm (T_{max}) and the initial temperature at which the endothermic phase transition peak starts (T_o). Reported data are from the second heating cycle to ensure any thermal history has been erased and to simulate an arbitrary n^{th} heating cycle.

Deswelling Kinetics

Hydrogels were punched into 3 discs (13 mm x 2 mm, diameter x thickness) and submerged in 20 mL of DI water in individual vials. The vials were sealed and placed in a water bath set to 22 °C overnight to equilibrate to their fully swollen state. The hydrogel discs were removed, blotted dry with a Kim Wipe and weighed (weight swollen, W_s). The hydrogels were immediately returned to the vials and quickly transferred to a water bath set to 50 °C to induce deswelling. The hydrogels were weighed similarly at 10, 30, 70, 120, and 180 min of heating (weight at time = t, W_t). After deswelling, the hydrogels were

blotted dry, placed in dry vials and exposed to high vacuum at 50 °C overnight to dehydrate. The dry weight of each sample was recorded (W_d). The water loss was calculated as W_L (%) = [(W_s –W_t)/(W_s –W_d)] x 100.

Reswelling Kinetics

Hydrogels were punched into 3 discs (13 mm x 2 mm, diameter x thickness), dried under high vacuum at 50 °C overnight and weighed (W_d). The dry hydrogel discs were transferred into individual vials with 20 mL of DI water at 22 °C. Over 24 hrs the swollen weights (W_t) of the hydrogels were measured at 10, 30, 70, 120, 200, 320, 450, 640, and 1440 min by removing the hydrogels from the vials, blotting them dry on a Kim Wipe and weighing them on a scale. The swelling ratio was calculated as SR = W_t/W_d.

Statistics

For compressive modulus and strength, values were compared using a Student's *t*-test to determine *p*-values.

Discussion for Equilibrium Water Content (Chapter IV)

The equilibrium water content of all DN hydrogel compositions prepared herein ranged from ~80 to 95% (**Table 4-1**). In the case of the "1.5-AMPS-15%", it displayed an appreciable hydration of ~83%. Thus, its exceptional mechanical properties are not attributed to a lack of hydration.

Discussion for Thermosensitivity (Chapter IV)

As noted, the volume phase transition temperature (VPTT) of both PAMPS/PNIPAAm (i.e. no MEDSAH in 2nd network) and PAMPS/P(NIPAAm-*co*-MEDSAH) (e.g. "1.5-AMPS-15%") DN hydrogels were determined to remain close to that of PNIPAAm hydrogels (~35 °C) (**Table 4-1**). Inspection of the endothermic VPTT peaks obtained via DSC revealed broadening with increased AMPS concentration in the 1st network (**Figure A-15a**) as well as increased MEDSAH in the 2nd network (**Figure A-15b**). Such peak broadening may indicate a reduction in thermosensitivity (i.e. a reduced rate and extent of deswelling and reswelling). Thus, for PAMPS/P(NIPAAm-*co*-MEDSAH) DN hydrogels, deswellling (T > VPTT) (**Figure A-16a**) and reswelling (T < VPTT) (**Figure A-16b**) was measured gravimetrically over time. Overall, only minor differences were observed, indicating that these DN hydrogels retained good thermosensitivity.

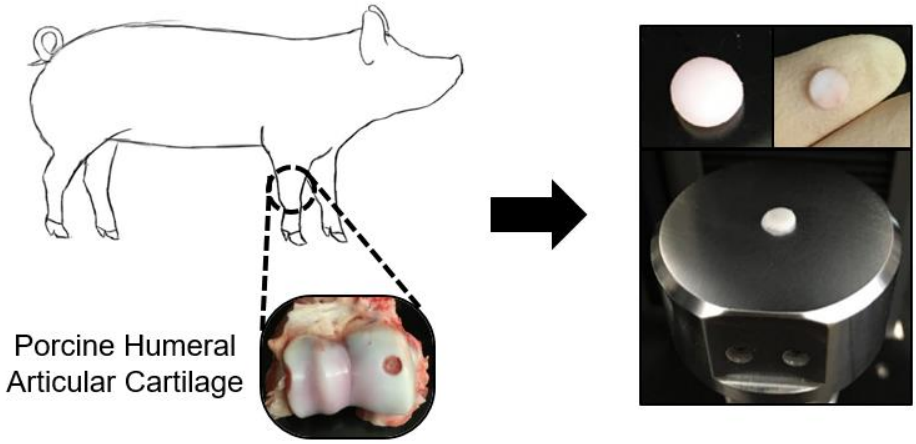

Figure A-17. Compression of harvested porcine articular cartilage specimen.

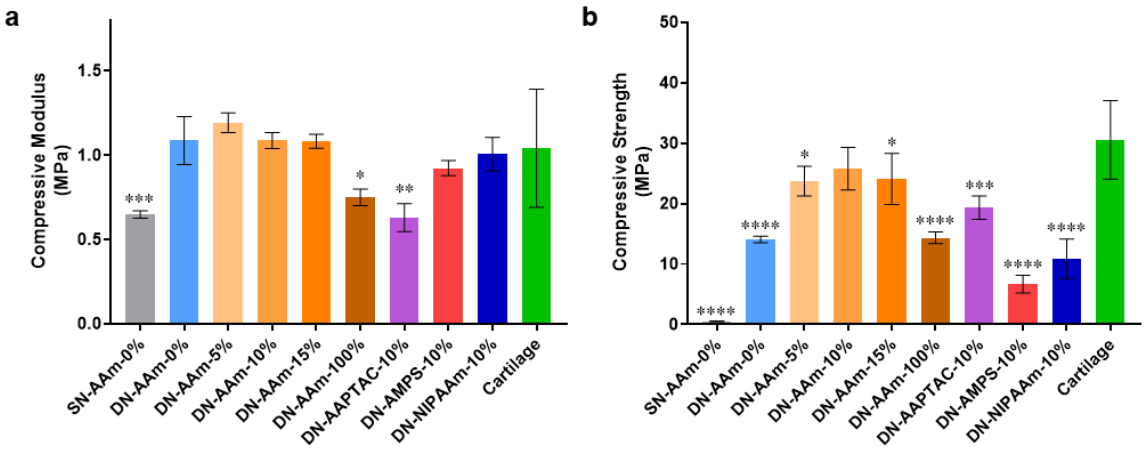

Figure A-18. Compressive (a) modulus and (b) strength of additional controls compared to porcine articular cartilage. All *'s indicate statistical significance from cartilage, in which "*" represents $p < 0.05$, "**" represents $p < 0.01$, "***" represents $p < 0.001$ and "****" represents $p < 0.0001$.

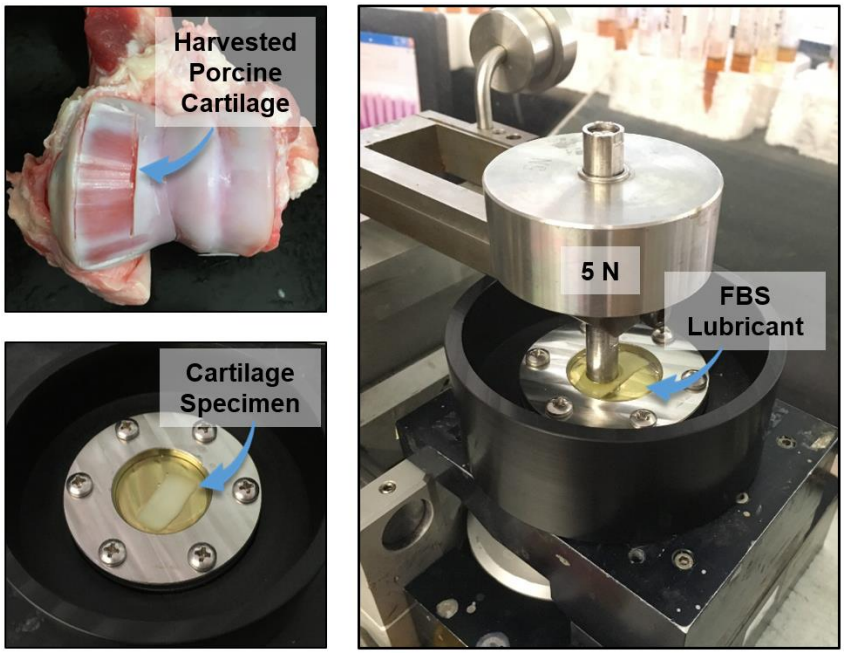

Figure A-19. Friction testing (tribology) of harvested porcine articular cartilage.

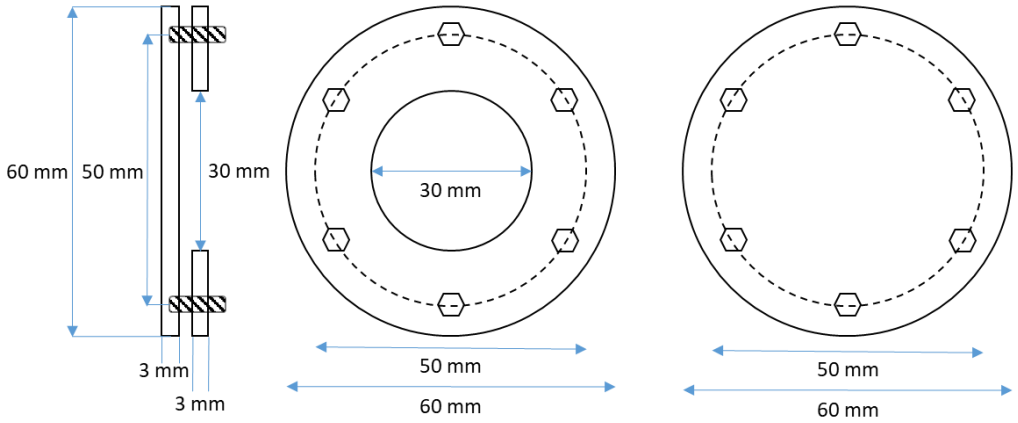

Scheme A-1. Friction testing (tribology) specimen clamp drawing.

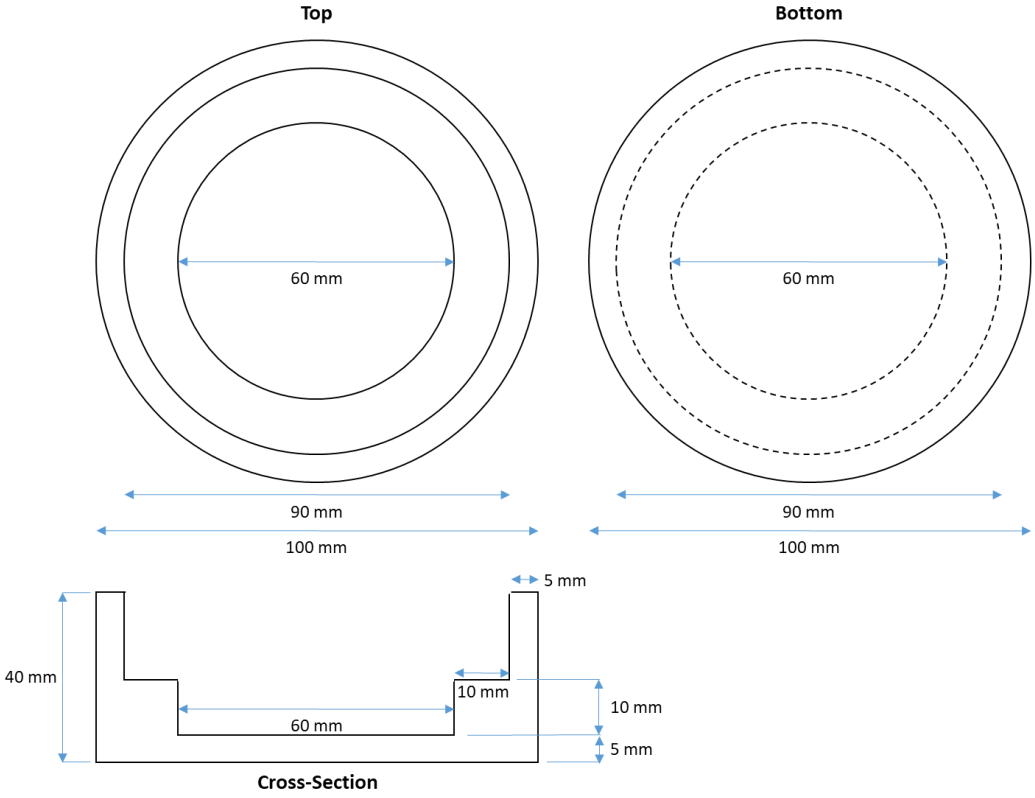

Scheme A-2. Friction testing (tribology) submersion chamber drawing.

Table A-4. DN hydrogels detailing 1st network and 2nd network compositions as well as their thermal transitions (VPTTs).

Hydrogel Type	Composition			VPTT	
	1st Network*	2nd Network+			
	AMPS (X)	NIPAAm	AAm (Y) (wt% of NIPAAm)	T_o(°C)	T_{max}(°C)
PAMPS SN:					
SN-AAm-0%	1.5M	-	-	-	-
PAMPS/PNIPAAm DN:					
DN-AAm-0%	1.5 M	2.0 M	0 wt%	32.8 ± 0.17	35.4 ± 0.22
PAMPS/(PNIPAAm-*co*-AAm) DNs:					
DN-AAm-5%	1.5 M	2.0 M	5 wt%	37.4 ± 0.33	41.6 ± 0.07
DN-AAm-10%	1.5 M	2.0 M	10 wt%	41.4 ± 0.68	48.0 ± 0.19
DN-AAm-15%	1.5 M	2.0 M	15 wt%	45.5 ± 0.25	52.6 ± 0.77

*4 mol% BIS crosslinker, 0.1 mol% 2-oxoglutaric acid initiator
+0.1 mol% BIS crosslinker, 0.1 mol% 2-oxoglutaric acid initiator

Table A-5. Overall mechanical properties of the PAMPS/PNIPAAm-*co*-AAm) hydrogel series, including equilibrium water content; tensile modulus, strength and fracture strain; and compressive modulus, strength, fracture strain and toughness.

	EWC (%)	Tensile Properties			Compressive Properties			
		E (MPa)	σ (MPa)	ε (%)	E (MPa)	σ (MPa)	ε (%)	U_t (MJ m^{-3})
PAMPS SN:								
SN-AAm-0%	96.55 ± 0.00	0.33 ± 0.046	0.04 ± 0.02	10.8 ± 4.1	0.65 ± 0.02	0.54 ± 0.1	34.4 ± 0.8	0.07 ± 0.01
PAMPS/PNIPAAm DN:								
DN-AAm-0%	86.3 ± 0.17	1.00 ± 0.04	1.61 ± 0.04	147.8 ± 9.2	1.09 ± 0.14	14.1 ± 0.5	78.8 ± 1.8	2.63 ± 0.07
PAMPS/(PNIPAAm-*co*-AAm) DNs:								
DN-AAm-5%	83.9 ± 0.11	1.04 ± 0.05	1.57 ± 0.06	139.4 ± 13.7	1.19 ± 0.06	23.7 ± 2.4	86.9 ± 1.9	4.31 ± 0.48
DN-AAm-10%	83.9 ± 0.21	1.13 ± 0.06	1.54 ± 0.12	128.0 ± 20.5	1.09 ± 0.05	25.8 ± 3.5	90.8 ± 2.6	4.69 ± 0.68
DN-AAm-15%	83.5 ± 0.16	1.15 ± 0.09	1.53 ± 0.04	131.0 ± 13.1	1.08 ± 0.04	24.1 ± 4.2	89.9 ± 3.1	4.39 ± 0.80
Cartilage								
Porcine Cartilage	76.5 ± 2.12	-	-	-	1.04 ± 0.35	30.6 ± 6.5	77.8 ± 9.9	7.03 ± 2.37

EWC = equilibrium water content, E = elastic modulus, σ = stress, ε = strain, U_t = compressive toughness (deformation energy)